Terms and Conditions of Use of Digitised Theses from Trinity College Library Dublin

Copyright statement

All material supplied by Trinity College Library is protected by copyright (under the Copyright and Related Rights Act, 2000 as amended) and other relevant Intellectual Property Rights. By accessing and using a Digitised Thesis from Trinity College Library you acknowledge that all Intellectual Property Rights in any Works supplied are the sole and exclusive property of the copyright and/or other IPR holder. Specific copyright holders may not be explicitly identified. Use of materials from other sources within a thesis should not be construed as a claim over them.

A non-exclusive, non-transferable licence is hereby granted to those using or reproducing, in whole or in part, the material for valid purposes, providing the copyright owners are acknowledged using the normal conventions. Where specific permission to use material is required, this is identified and such permission must be sought from the copyright holder or agency cited.

Liability statement

By using a Digitised Thesis, I accept that Trinity College Dublin bears no legal responsibility for the accuracy, legality or comprehensiveness of materials contained within the thesis, and that Trinity College Dublin accepts no liability for indirect, consequential, or incidental, damages or losses arising from use of the thesis for whatever reason. Information located in a thesis may be subject to specific use constraints, details of which may not be explicitly described. It is the responsibility of potential and actual users to be aware of such constraints and to abide by them. By making use of material from a digitised thesis, you accept these copyright and disclaimer provisions. Where it is brought to the attention of Trinity College Library that there may be a breach of copyright or other restraint, it is the policy to withdraw or take down access to a thesis while the issue is being resolved.

Access Agreement

By using a Digitised Thesis from Trinity College Library you are bound by the following Terms & Conditions. Please read them carefully.

I have read and I understand the following statement: All material supplied via a Digitised Thesis from Trinity College Library is protected by copyright and other intellectual property rights, and duplication or sale of all or part of any of a thesis is not permitted, except that material may be duplicated by you for your research use or for educational purposes in electronic or print form providing the copyright owners are acknowledged using the normal conventions. You must obtain permission for any other use. Electronic or print copies may not be offered, whether for sale or otherwise to anyone. This copy has been supplied on the understanding that it is copyright material and that no quotation from the thesis may be published without proper acknowledgement.

Static-Light-Light Baryons
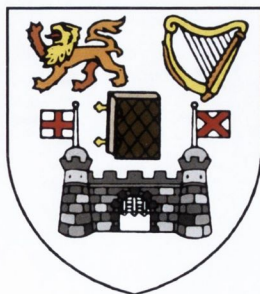# A Spectroscopic Study Using Distillation

by

Finnian Mc Elroy

B.A. (Mod.)

A Thesis submitted to
The University of Dublin
for the degree of

Doctor of Philosophy

School of Mathematics
University of Dublin
Trinity College

April, 2013

Declaration

This thesis has not been submitted as an exercise for a degree at any other University. Except where otherwise stated, the work described herein has been carried out by the author alone. This thesis may be borrowed or copied upon request with the permission of the Librarian, University of Dublin, Trinity College. The copyright belongs jointly to the University of Dublin and Finnian Mc Elroy.
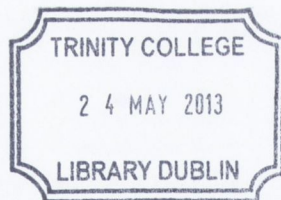
Signature of Author ....

Finnian Mc Elroy

April, 2013

Static-Light-Light Baryons
A Spectroscopic Study Using Distillation

Finnian Mc Elroy B.A. (Mod.)

We perform the first study of static-light-light baryon spectroscopy using distillation on an $N_f = 3$ dynamical, anisotropic lattice with an anisotropy $\xi = 3.5$. Baryon interpolating field operators that transform according to the irreducible representations of the symmetry group O_h of the rotationally invariant spatial lattice are constructed. Simulations are carried out at a single lattice spacing of $a_s = 0.12$fm. Simulations of both isospin-0 and isospin-1 static-light-light baryons are performed. The bare strange quark mass value is set at $a_t m_0 = -0.0734$. Two-point correlation functions are measured and fitted to with a single exponential. Ground state masses are determined for each channel.

Summary

Over the last decade, hadron spectroscopy in lattice QCD has graduated from calculating single rows of the quark propagation matrix to calculating all elements of the quark propagation matrix - the so-called all-to-all propagator. On a spatially symmetric anisotropic lattice of spatial extent N_x and temporal extent N_t the quark propagation matrix has rank $4 \times 3 \times N_x^3 \times N_t$, where 4 represents the number of components in a Dirac field and 3 represents the number of colours. Calculating all elements of this matrix requires $144 \times N_x^6 \times N_t^2$ matrix inversions - a formidable task. The relatively new method of distillation enables access to all elements of the quark propagation matrix at a much more affordable cost. This project is the first study of distillation on the bottom baryon spectrum. Simulations are performed on an $N_f = 3$ dynamical, anisotropic lattice. The heavy quark is treated in the static limit of Heavy Quark Effective Theory (HQET). Baryon interpolating field operators that transform as irreducible representations of the spatial lattice symmetry group O_h are constructed. This includes both positive parity and negative parity operators. Two-point correlation functions are measured. A variational analysis is briefly tested. Ground state effective masses are determined by fitting the correlation function to a single exponential. Mass splittings are calculated. Only one experimentally determined mass splitting exists for comparison. That is the Σ_b, Λ_b splitting. Results for this splitting are compared with other lattice work. Results are compared more generally with other lattice work.

Acknowledgements

To my family.

Contents

List of Figures

List of Tables

Chapter 1

Introduction

According to the Standard Model of particle physics, quarks emerge as a basic building block of matter. Quarks interact via the strong interaction. The theory describing the strong force is Quantum Chromodynamics. The strong force between quarks increases with increasing distance. For this reason, quarks are not seen in isolation but are confined into bound states known as hadrons. There are six varieties of quark: up (u), down (d), charm (c), strange (s), top (t) and bottom (b). The u, d and s quarks are light in comparison to the c, t, and b quarks. The u, d and s quarks lie below the QCD scale $\Lambda_{QCD} = 200$MeV.

Quark Models [1] predict eight baryons containing one bottom quark. Their properties are given in Table 1.1. They can be described by total spin J, parity P, isospin I and the total spin of the light quark pair s_l. The up or down quarks are denoted q, s denotes the strange quark and b denotes the bottom quark. For isodoublets and isotriplets the lower and lowest observed masses are quoted.

The Λ_b baryon was the first b-baryon to receive mass measurement [2, 3, 4]. Since 2007 the masses of Σ_b, Σ_b^*, Ω_b and Ξ_b have been experimentally determined by the D0 and CDF experiments at Fermilab [5, 6, 7, 8]. The bottom meson sector has been studied extensively in recent years, at the dedicated b-factories, BELLE and BaBar. Recent years have seen precise measurements of CKM matrix elements describing the flavour changing processes involving b-mesons. At Fermilab, orbitally excited B_1, B_2^*, B_{s1} and B_{s2}^* mesons have been observed. Heavy hadron b-physics research is

Baryon	Quark Content	J^P	I	s_l	Experimental Mass (Mev)
Λ_b	qqb	$\frac{1}{2}^+$	0	0	$5,620.2(1.6)$
Σ_b	qqb	$\frac{1}{2}^+$	1	1	$5,807.8(2.7)$
Σ_b^*	qqb	$\frac{3}{2}^+$	1	1	$5,829.0(3.4)$
Ω_b	ssb	$\frac{1}{2}^+$	0	1	$6,071(40)$
Ω_b^*	ssb	$\frac{3}{2}^+$	0	1	Not Measured
Ξ_b	qsb	$\frac{1}{2}^+$	$\frac{1}{2}$	0	$5,790.5(2.7)$
Ξ_b'	qsb	$\frac{1}{2}^+$	$\frac{1}{2}$	1	Not Measured
Ξ_b^*	qsb	$\frac{3}{2}^+$	$\frac{1}{2}$	1	Not Measured

Table 1.1: Experimentally determined masses for bottom baryons.

currently very rich with the PANDA experiment, the LHCb, ATLAS and CMS likely to produce data relevant for mapping the b-hadron spectrum.

Lattice QCD provides an alternative arena for studying the hadron spectrum. *Ab initio* calculations of the mass spectrum are possible on the lattice. Spectroscopy results from lattice QCD are as numerous as those from experiment. Both the charm and bottom meson sectors are rich research areas. Algorithmic improvements over the last few years have led to highly excited state mass determinations for heavy quark mesons. Over the last decade hadron spectroscopy in lattice QCD has graduated from calculating single rows of the quark propagation matrix to calculating all elements of the quark propagation matrix - the so-called all-to-all propagator. On a spatially symmetric anisotropic lattice of spatial extent N_x and temporal extent N_t the quark propagation matrix has rank $4 \times 3 \times N_x^3 \times N_t$, where 4 represents the number of components in a Dirac field and 3 represents the number of colours. Calculating all elements of this matrix requires $144 \times N_x^6 \times N_t^2$ matrix inversions - a formidable task. The relatively new method of distillation enables access to all elements of the quark propagation matrix at a much more affordable cost. This project includes the use of distillation for the first time in static-light-light baryon spectroscopy on anisotropic lattices. The aim of this project is to determine the mass spectrum of singly-bottom baryons. Mass splittings for previously unmeasured states are calculated. In addition,

mass splittings that have previously been calculated on the lattice are measured for the first time using distillation. Baryons with the quark content of the Λ_b and the Σ_b are studied. All the experimentally determined mass splittings for the singly-bottom baryons have already been computed on the lattice [9, 10, 11, 12, 13, 14, 15]. These are in agreement with experiment.

Chapter 2

Lattice Basics

2.1 QCD

In continuum QCD, a quantum field $\psi(\vec{x}, t)$ has an infinite number of degrees of freedom, labelled by the space-time coordinate $(\vec{x}, t)$, as well as discrete indices for colour and spin. Space-time can be discretized by introducing a hypercubic lattice of discrete points. The lattice sites are described by a four-vector x with components

$$x_\mu = n_\mu a_\mu, \qquad n_\mu = 0, ..., N - 1. \tag{2.1}$$

where n_μ is an integer, a_μ is the lattice spacing in the μth direction and $L = N_\mu a_\mu$ is the lattice extent in the μth direction. Momenta occur in discrete units

$$p_\mu = \frac{2\pi n_\mu}{N_\mu a_\mu}, \quad \text{where} \quad n_\mu = -N_\mu/2 + 1, -N_\mu/2 + 2, ..., N_\mu/2. \tag{2.2}$$

The lattice introduces a momentum cut-off. The largest allowed momentum is π/a and the lattice provides an ultra-violet regulator for QCD. The shortest wavelength in the μth direction is $2a_\mu$. Wavelengths less than twice the lattice spacing are eliminated from the theory.

Integrals in the path-integral representation of QCD become finite-dimensional when a lattice is introduced. The vacuum expectation value of an operator $\mathcal{O}(\psi, \overline{\psi}, U)$ is given by

$$\langle \mathcal{O} \rangle = \frac{\int [d\psi][d\overline{\psi}][dU] \mathcal{O}(\psi, \overline{\psi}, U) e^{-S}}{\int [d\psi][d\overline{\psi}][dU] e^{-S}}, \tag{2.3}$$

12

where S is the action,

$$S = \int \mathcal{L}(\psi(x), \overline{\psi}(x), U(x)) d^4 x, \tag{2.4}$$

and $\mathcal{L}(\psi(x), \overline{\psi}(x), U(x))$ is the Lagrangian density. The fields $\psi(x)$ and $U(x)$ which describe quark and gluons respectively, will be introduced later in this chapter. A Wick rotation from Minkowski space to Euclidean space has been performed. In Minkowski space, there is an oscillating phase factor e^{iS}. In Euclidean space, the factor e^{-S} can be interpreted as a real weight allowing importance sampling to be used to estimate this integral.

2.2 Gauge Invariance

The continuum QCD Lagrangian possesses an $SU(3)$ gauge invariance. Quarks and antiquarks possess colour charge. There are three different colours - red, green and blue. The three different colour fields can be written as a three-component column vector as follows

$$\psi = \begin{pmatrix} \psi_1 \\ \psi_2 \\ \psi_3 \end{pmatrix}. \tag{2.5}$$

These fields transform locally as follows

$$\psi(x) \quad \rightarrow \quad G(x)\psi(x), \tag{2.6a}$$

$$\overline{\psi}(x) \quad \rightarrow \quad \overline{\psi}(x)G^{-1}(x), \tag{2.6b}$$

where

$$G(x) = \exp\left[i\alpha^a(x)t^a(x)\right]. \tag{2.6c}$$

$G(x)$ is an element in the fundamental representation of $SU(3)$, $\alpha^a(x)$ is an arbitrary function of x and $t^a(x)$ are hermitian generators of $SU(3)$.

The derivative $\partial_\mu \psi(x)$ of a field $\psi(x)$ is defined as follows

$$\partial_\mu \psi(x) = \lim_{\epsilon \to 0} \frac{1}{\epsilon}[\psi(x + \epsilon a_\mu) - \psi(x)]. \tag{2.7}$$

This derivative transforms differently to $\psi(x)$ under the local transformations as shown below

$$\partial_\mu \psi(x) \rightarrow \lim_{\epsilon \to 0} \frac{1}{\epsilon}[G(x + \epsilon a_\mu)\psi(x + \epsilon a_\mu) - G(x)\psi(x)] \neq G(x)\partial_\mu\psi(x). \qquad (2.8)$$

The covariant derivative $D_\mu\psi(x)$ of a field $\psi(x)$ is defined as follows

$$D_\mu\psi(x) = \partial_\mu\psi(x) - igA_\mu(x)\psi(x), \qquad (2.9)$$

where the vector field $A_\mu(x)$ lies in the Lie algebra of $SU(3)$. The vector field $A_\mu(x)$ can be written as follows

$$A_\mu(x) = \sum_{b=1}^{8} A_\mu^b(x)\frac{\lambda^b}{2}, \qquad (2.10)$$

where $A^b(x)$ are real-valued functions and the λ^b are the 3x3 Gell-Mann matrices given in the Appendix. The Gell-Mann matrices act as generators for the non-Abelian group $SU(3)$. The Gell-Mann matrices obey the commutation relations

$$[\lambda^a, \lambda^b] = 2i \sum_{c=1}^{8} f_{abc}\lambda^c, \qquad (2.11)$$

where f_{abc} are antisymmetric structure constants. $D_\mu\psi(x)$ follows the same transformation law as $\psi(x)$. Under the local transformation of equations (2.6)

$$D_\mu\psi(x) \rightarrow G(x)D_\mu\psi(x). \qquad (2.12)$$

The lattice covariant derivative applied to a quark field is

$$\nabla_\mu\psi(x) = \frac{1}{2a_\mu}[U_\mu(x)\psi(x + \hat{\mu}) - U_\mu^\dagger(x - \hat{\mu})\psi(x - \hat{\mu})]. \qquad (2.13)$$

The link variables are parallel transporters between neighbouring lattice sites. They are the path-ordered product of the exponential of the vector field $A_\mu(x)$ defined as follows

$$U_\mu(x) = \mathcal{P}\exp[i \int_x^{x+\hat{\mu}} g_0 A_\mu(y)\, dy], \qquad (2.14)$$

where g_0 is the bare coupling constant and path-ordering denoted by $\mathcal{P}$ involves ordering the matrices with $A_\mu(x)$ to the right of and $A_\mu(x + \hat{\mu})$ to the left of the

product. The links are elements of the fundamental representation of the gauge group. They transform under a gauge transformation as follows

$$U_\mu(x) \to G(x)U_\mu(x)G^\dagger(x + a_\mu\hat{\mu}), \quad G(x) \in SU(3). \tag{2.15}$$

The path-ordered product of links along a path P connecting site x and site y is called a Wilson line and is denoted $W_P(x, y)$. Under gauge transformations the Wilson line transforms as follows

$$W_P(x, y) \to G(x)W_P(x, y)G^\dagger(y). \tag{2.16}$$

The trace of a Wilson line over a closed path is called a Wilson loop. The Wilson loop is gauge invariant as shown below using the cyclic property of traces

$$\begin{aligned}
\text{Tr}[W_P(x, x)] &\to \text{Tr}[G(x)W_P(x, x)G^\dagger(x)] \\
&= \text{Tr}[W_P(x, x)G^\dagger(x)G(x)] \\
&= \text{Tr}[W_P(x, x)].
\end{aligned} \tag{2.17}$$

2.3 Group Integration

The links $U_\mu(x)$ can be written as follows

$$U_\mu(x) = e^{i\phi_\mu(x)}, \tag{2.18}$$

where $\phi_\mu(x)$ is an element of the Lie-algebra of $SU(3)$. $\phi_\mu(x)$ is written in terms of the generators $T^a = \frac{\lambda^a}{2}$ of the group in the fundamental representation as follows

$$\phi_\mu(x) = \sum_{a=1}^{8} \phi_\mu^a(x)T^a. \tag{2.19}$$

The generators T^a satisfy

$$[T^a, T^b] = i\sum_c f_{abc}T^c, \tag{2.20}$$

with the same structure constants f_{abc} as in equation (2.11). The integration measure dU for the gauge fields in equation (2.3) must be gauge-invariant. The Haar measure

dU guarantees that gauge invariance is respected. The Haar measure dU on a compact group G has the two defining properties of invariance and normalization. Invariance can be stated mathematically as follows

$$\int_G f(U)dU = \int_G f(WU)dU = \int_G f(UW)dU \quad \text{for all } W \in G. \tag{2.21}$$

Normalization is given by

$$\int_G dU = 1. \tag{2.22}$$

In this study the compact group G is $SU(3)$.

2.4 Naive Fermions

The naive Euclidean lattice fermion action for a single flavour is

$$S_F = a^4 \sum_{x,y} \overline{\psi}(x) M_{xy} \psi(y), \tag{2.23}$$

where

$$M_{xy} = [\sum_{\mu} \gamma_\mu \nabla_\mu + m]\delta^4_{xy}, \tag{2.24}$$

a is the lattice spacing, ∇_μ is defined in equation (2.13) with $U_\mu(x) = 1$ for free fermions and the sum over colour and Dirac indices is implicit. The two-point function is defined as follows

$$\langle \psi_\alpha(x)\overline{\psi}_\beta(y) \rangle = \frac{\int D\overline{\psi} D\psi \, \psi_\alpha(x)\overline{\psi}_\beta(y)e^{-S_F}}{\int D\overline{\psi} D\psi \, e^{-S_F}}, \tag{2.25}$$

where the integration measure $D\overline{\psi}D\psi$ is given by

$$D\overline{\psi}D\psi = \prod_{\alpha,u} d\overline{\psi}_\alpha(u) \prod_{\beta,v} d\psi_\beta(v). \tag{2.26}$$

The two-point function momentum space representation is

$$\langle \psi_\alpha(x)\overline{\psi}_\beta(y) \rangle = \int_{-\pi/a}^{\pi/a} \frac{d^4p}{(2\pi)^4} \frac{[m - i\sum_\mu \gamma_\mu \sin(ap_\mu)/a]_{\alpha\beta}}{m^2 + \sum_\mu \sin^2(ap_\mu)/a^2} e^{ip(x-y)},$$

$$= \int_{-\pi/a}^{\pi/a} \frac{d^4p}{(2\pi)^4} [S(p)]_{\alpha\beta} e^{ip(x-y)}, \tag{2.27}$$

16

where

$$S(p) = \frac{[m - i\sum_\mu \gamma_\mu \sin(ap_\mu)/a]}{m^2 + \sum_\mu \sin^2(ap_\mu)/a^2}. \tag{2.28}$$

Near $p_\mu = 0$ or $\pm\pi/a$ for $\mu \in \{0, 1, 2, 3\}$, $\sin(ap_\mu)$ can be approximated by ap_μ to $\mathcal{O}(a)^2$. The propagator is then given by

$$S(p) = \frac{m - i\sum_\mu \gamma_\mu p_\mu}{m^2 + p^2} + \mathcal{O}(a^2). \tag{2.29}$$

The propagator has a pole at $m^2 + p^2 = 0$. These poles exist at sixteen regions in the Brillouin zone $-\pi/a < p_\mu < \pi/a$. One is near $p_0 = p_1 = p_2 = p_3 = 0$ which describes the Dirac particle. The other fifteen poles correspond to high momentum excitations near $p_\mu = 0$ or $\pm\pi/a$ for $\mu \in \{0, 1, 2, 3\}$. These fifteen excitations are known as doublers. They are lattice artefacts.

The naive Euclidean lattice fermion action is invariant under the transformation

$$\psi(x) \to e^{i\theta}\psi(x), \tag{2.30}$$

$$\overline{\psi}(x) \to \overline{\psi}(x)e^{-i\theta}. \tag{2.31}$$

When the mass $m = 0$, this action has a chiral symmetry

$$\psi(x) \to e^{i\theta\gamma_5}\psi(x), \tag{2.32}$$

$$\overline{\psi}(x) \to \overline{\psi}(x)e^{i\theta\gamma_5}. \tag{2.33}$$

2.5 Wilson Term

One solution to the doubling problem is to add a Wilson term to the naive fermion action. At finite lattice spacing, the Wilson term raises the mass of the doublers to the order of the inverse lattice spacing. This removes the effects of doubling. The Wilson action is given below

$$S_F^W = S_F - \frac{a^5 r}{2}\sum_{x,\mu}\overline{\psi}(x)\Delta_\mu\psi(x), \tag{2.34}$$

where

$$\Delta_\mu\psi(x) = \frac{1}{a_\mu^2}[\psi(x + \hat{\mu}) + \psi(x - \hat{\mu}) - 2\psi(x)], \tag{2.35}$$

and r is the Wilson parameter. For non-zero values of r, the doublers mass is increased. This action can be expressed as follows

$$S_F^W = \sum_{x,y} \overline{\psi}(x) M^W(x,y) \psi(y), \tag{2.36}$$

where

$$M^W(x,y) = (a^4 m + 4a^3 r)\delta_{xy}^4 - \frac{a^3}{2} \sum_\mu [(r - \gamma_\mu)\delta_{y,x+\hat{\mu}}^4 + (r + \gamma_\mu)\delta_{y,x-\hat{\mu}}^4]. \tag{2.37}$$

This gives the same two-point function as in equation (2.27) when the mass m is replaced with $m(p)$ as follows

$$m(p) \to m + \frac{2r}{a} \sum_\mu \sin^2(p_\mu a/2). \tag{2.38}$$

The argument of the sine function has half the periodicity of the other sine functions in the propagator. Near $p_\mu = \pi/a$, $m(p) \simeq m + \frac{2r}{a}$. As $a \to 0$ $m(p)$ diverges. This divergence lifts the masses of the fifteen doublers for fixed nonzero r to $\mathcal{O}(1/a)$. At finite lattice spacing the doublers have a non-zero mass even for $m = 0$. The Wilson term breaks chiral symmetry [16]. This induces an additive renormalization to the quark mass. The quark mass is also multiplicatively renormalized. A fine-tuning of the bare quark mass to its critical value is necessary in order to obtain a vanishing renormalized quark mass. The additive mass renormalization can lead to a negative value for the bare quark mass. The quark mass in this project is negative. The Nielson-Ninomiya no-go theorem [17] precludes the possibility of constructing a fermion action which respects locality, hermiticity, translational invariance, chirality and remains undoubled.

Chapter 3

Simulation Techniques

3.1   Lattice Actions

In this study we perform simulations on an $N_f = 3$ dynamical, anisotropic lattice. In hadron spectroscopy, fine resolution is required when fitting to the effective masses of two-point correlation functions of a creation operator $\mathcal{O}$. Correlation functions can be expanded as a series of exponential terms - an exponential term for each state to which the operator $\mathcal{O}$ couples . The exponential associated with the ground state decays slowest. Exponential terms associated with excited states decay faster. Therefore on later timeslices the ground state has a greater relative contribution to the value of the correlation function. This means that ground state masses must be extracted at later timeslices. Correlation functions also become noisier on later timeslices with signal-to-noise ratios typically degrading exponentially with time [19]. This permits only a narrow time window in which ground state mass extraction can be well-accomplished. Anisotropic lattices with a finer lattice spacing in the temporal direction provide a means of maximizing the amount of information obtainable from correlation functions by allowing fitting over a greater number of timeslices. This is especially important for a treatment of the static quark since the signal for the static quark degrades into noise faster than for light quarks [20]. Errors of $\mathcal{O}(a_t m_Q)$ in the temporal direction relating to the heavy quark can be reduced by simulating on the anisotropic lattice. Anisotropic lattices have been used with much success in hadron

spectroscopy [21]. Decreasing the lattice spacing in only the temporal direction is computationally less expensive than decreasing it in all four directions. Hypercubic symmetry is broken by the anisotropic lattice. The anisotropic lattice introduces two new parameters: the fermion and gluon anisotropies denoted ξ_f and ξ_g, respectively. These parameters are non-perturbatively tuned so that in the continuum limit full Lorentz symmetry is restored.

3.1.1 Gauge Action

The gauge action is a Symanzik-improved action with tree-level tadpole-improved coefficients [22]:

$$
\begin{aligned}
S_G^\xi[U] \;=\; & \frac{\beta}{\gamma_g N_C}\Big\{\big[\frac{5}{3u_s^4}\Omega_{sp}(x) - \frac{1}{12u_s^6}\Omega_{sr}(x)\big] \\
& + \gamma_g^2\big[\frac{4}{3u_s^2 u_t^2}\Omega_{stp}(x) - \frac{1}{12u_s^4 u_t^2}\Omega_{str}(x)\big]\Big\},
\end{aligned}
\tag{3.1}
$$

where $\beta = 2N_C/g^2$, g is the QCD coupling, $N_C = 3$ is the number of colours, γ_g is the bare gauge anisotropy, u_s and u_t are the spatial and temporal tadpole factors, $\Omega_C = \sum_C (1/3)\mathrm{ReTr}(1 - W_C)$, where W_C denotes the path-ordered product of link variables along a closed contour C. The Symanzik improvement program applied to a lattice action involves systematically including additional terms to the action in order to accelerate the rate of convergence to the continuum limit [23]. Here improvement is achieved by summing linear combinations of different plaquettes weighted with the correct coefficients. The action has a leading discretization error of $\mathcal{O}(\alpha_s^4, a_t^2, g^2 a_s^2)$. The action is designed for lattices with large anisotropies where $a_t \ll a_s$. It was first used in glueball simulations [24]. The procedure for evaluating the tadpole factors is discussed in a later section on tadpole improvement.

The various sums over plaquettes and rectangular loops are given below

$$
\Omega_{sp}(x) = \sum_x \sum_{i>j} \frac{1}{3}\mathrm{ReTr}[1 - U_i(x)U_j(x+\hat{\imath})U_i^\dagger(x+\hat{\jmath})U_j^\dagger(x)],
\tag{3.2}
$$

$$
\Omega_{sr}(x) = \sum_x \sum_{i\neq j} \frac{1}{3}\mathrm{ReTr}[1 - U_i(x)U_i(x+\hat{\imath})U_j(x+2\hat{\imath})U_i^\dagger(x+\hat{\imath}+\hat{\jmath})U_i^\dagger(x+\hat{\jmath})U_j^\dagger(x)],
\tag{3.3}
$$

$$
\Omega_{stp}(x) = \sum_x \sum_i \frac{1}{3}\mathrm{ReTr}[1 - U_t(x)U_i(x+\hat{t})U_t^\dagger(x+\hat{\imath})U_i^\dagger(x)],
\tag{3.4}
$$

20

$$\Omega_{str}(x) = \sum_x \sum_i \frac{1}{3} \mathrm{ReTr}[1 - U_i(x)U_i(x+\hat{\imath})U_t(x+2\hat{\imath})U_i^\dagger(x+\hat{\imath}+\hat{t})U_i^\dagger(x+\hat{t})U_t^\dagger(x)], \quad (3.5)$$

where x is the lattice coordinate, i, j are spatial indices, $\hat{\imath}$ and $\hat{\jmath}$ are unit vectors in the spatial directions, $\hat{t}$ is a unit vector in the time direction and $U_\mu(x)$ is the parallel transporter from site x to $x + \hat{\mu}$.
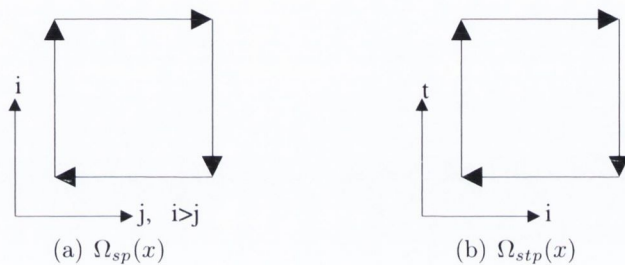
Figure 3-1: Spatial and temporal plaquettes in the gauge action.
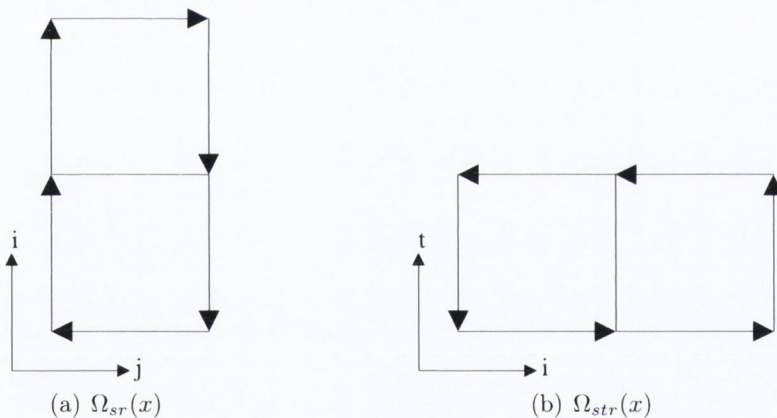
Figure 3-2: Spatial and temporal rectangular plaquettes in the gauge action.

3.1.2 Light-Quark Action

The covariant first- and second-order lattice derivatives ∇_μ and Δ_μ are defined by application to a quark field $\psi(x)$ as follows

$$\nabla_\mu \psi(x) = \frac{1}{2a_\mu}[U_\mu(x)\psi(x+\hat{\mu}) - U_\mu^\dagger(x-\hat{\mu})\psi(x-\hat{\mu})], \quad (3.6)$$

$$\Delta_\mu \psi(x) = \frac{1}{a_\mu^2}[U_\mu(x)\psi(x+\hat{\mu}) + U_\mu^\dagger(x-\hat{\mu})\psi(x-\hat{\mu}) - 2\psi(x)]. \quad (3.7)$$

21

In this notation, $U_\mu(x)$ is the parallel transporter from x to $x + \hat\mu$ and $U_\mu^\dagger(x - \hat\mu)$ is the parallel transporter from x to $x - \hat\mu$.

The field tensor $F_{\mu\nu}$ is defined by

$$F_{\mu\nu}(x) = \frac{-i}{2a^2}[Q_{\mu\nu}(x) - Q_{\mu\nu}^\dagger(x)], \tag{3.8}$$

where $Q_{\mu\nu}(x)$ is defined as follows

$$\begin{aligned} Q_{\mu\nu}(x) =& \frac{1}{4}[U_\mu(x)U_\nu(x + \hat\mu)U_\mu^\dagger(x + \hat\nu)U_\nu^\dagger(x) \\ &+ U_\nu(x)U_\mu^\dagger(x - \hat\mu + \hat\nu)U_\nu^\dagger(x - \hat\mu)U_\mu(x - \hat\mu) \\ &+ U_\mu^\dagger(x - \hat\mu)U_\nu^\dagger(x - \hat\mu - \hat\nu)U_\mu(x - \hat\mu - \hat\nu)U_\nu(x - \hat\nu) \\ &+ U_\nu^\dagger(x - \hat\nu)U_\mu(x - \hat\nu)U_\nu(x + \hat\mu - \hat\nu)U_\mu^\dagger(x)]. \end{aligned} \tag{3.9}$$

(a) $Q_{\mu\nu}(x)$ (b) $Q_{\mu\nu}^\dagger(x)$
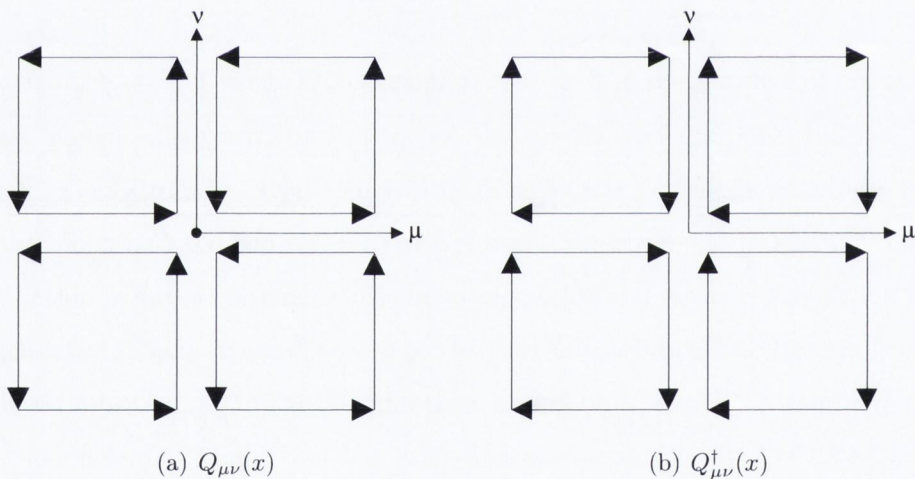
Figure 3-3: Anticlockwise and clockwise clover terms.

In the light quark sector an anisotropic clover fermion action is used [25]. It is given by

$$S_F^\xi[U, \overline\psi, \psi] = a_s^3 a_t \sum_x \overline\psi(x)\mathcal{Q}\psi(x), \tag{3.10}$$

where

$$\mathcal{Q} = [m_0 + \nu_t W_t + \nu_s W_s - \frac{a_s}{2}(c_t \sigma_{st} F^{st} + \sum_{s<s'} c_s \sigma_{ss'} F^{ss'})], \tag{3.11}$$

22

$\sigma_{\mu\nu} = (1/2)[\gamma_\mu, \gamma_\nu]$ and the $r = 1$ Wilson operator is given by

$$W_\mu = \nabla_\mu - \frac{a_\mu}{2} \gamma_\mu \Delta_\mu. \tag{3.12}$$

The following quantities with a hat are all dimensionless; $\hat{\psi} = a_s^{\frac{3}{2}} \psi$, $\hat{m}_0 = a_t m_0$, $\hat{\nabla}_\mu = a_\mu \nabla_\mu$, $\hat{\Delta}_\mu = a_\mu^2 \Delta_\mu$, $\hat{F}_{\mu\nu} = a_\mu a_\nu F_{\mu\nu}$ and $\hat{W}_\mu = \hat{\nabla}_\mu - \frac{1}{2} \gamma_\mu \hat{\Delta}_\mu$. The action can be rewritten as follows

$$S_F^\xi[U, \hat{\bar{\psi}}, \hat{\psi}] = \sum_x \hat{\bar{\psi}}(x) \hat{Q} \hat{\psi}, \tag{3.13}$$

where

$$\hat{Q} = \frac{1}{a_t} \Big\{ a_t \hat{m}_0 + \nu_t \hat{W}_t + \frac{\nu_s}{\xi_0} \sum_s \hat{W}_s$$
$$- \frac{1}{2} [c_t \sum_s \sigma_{ts} \hat{F}_{ts} + \frac{c_s}{\xi_0} \sum_{s<s'} \sigma_{ss'} \hat{F}_{ss'}] \Big\}. \tag{3.14}$$

The ratio of the bare fermion anisotropy to the bare gauge anisotropy is denoted ν. Tuning of both quantities ν_s and ν_t is not necessary. A rescaling of the fields requires only one such quantity to be tuned to ensure the anisotropic lattice obeys relativity. Setting $\nu_s = 1$ and tuning ν_t is called ν_t-tuning. Here, we employ ν_s-tuning where we set $\nu_t = 1$. The clover coefficients are set to their tree-level tadpole-improved values

$$c_s = \frac{\nu}{\tilde{u}_s^3}, \qquad c_t = \frac{1}{2}(\nu + \frac{1}{\xi}) \frac{1}{\tilde{u}_t \tilde{u}_s^2}; \tag{3.15}$$

where $\tilde{u}_s$ and $\tilde{u}_t$ are the tadpole factors for the smeared fermion fields. The tadpole factors are explained further in equations (3.29) and (3.30). The anisotropy $\xi = a_s/a_t$ is set to equal 3.5. For a spatial lattice spacing of order 0.1fm an anisotropy of $\xi = 3.5$ gives a temporal lattice spacing with the required fineness for hadron spectroscopy. Three-dimensional stout-link smeared gauge fields [24] are used in the fermion action with smearing weight $\rho = 0.2$ and $n_\rho = 10$ iterations. The parameters ρ and n_ρ are explained in (3.61). The gauge anisotropy γ_g and the fermion anisotropy γ_f are defined as follows

$$\gamma_g = \xi_0, \qquad \gamma_f = \frac{\xi_0}{\nu}. \tag{3.16}$$

The action can be reparameterized in terms of the bare gauge and fermion anisotropies as follows

$$S_F^{\xi}[U, \hat{\bar{\psi}}, \hat{\psi}] = \sum_x \hat{\bar{\psi}}(x) \hat{\mathcal{Q}} \hat{\psi}, \qquad (3.17)$$

where

$$\hat{\mathcal{Q}} = \frac{1}{\tilde{u}_t} \{ \tilde{u}_t \hat{m}_0 + \hat{W}_t + \frac{1}{\gamma_f} \sum_s \hat{W}_s$$

$$- \frac{1}{2} [\frac{1}{2} (\frac{\gamma_g}{\gamma_f} + \frac{1}{\xi}) \frac{1}{\tilde{u}_t \tilde{u}_s^2} \sum_s \sigma_{ts} \hat{F}_{ts} + \frac{1}{\gamma_f} \frac{1}{\tilde{u}_s^3} \sum_{s<s'} \sigma_{ss'} \hat{F}_{ss'}] \}. \qquad (3.18)$$

At $\beta = 1.5$, the tadpole factors are

$$u_s = 0.7336, \quad u_t = 1, \qquad \tilde{u}_s = 0.9267, \quad \tilde{u}_t = 1.$$

Critical values for γ_g^* and γ_f^* are found by imposing the renormalization conditions $\{\xi_g, \xi_f, M_t\} = \{3.5, 3.5, 0\}$ in equations (3.42). Since the gauge and fermion anisotropies show a mild quark mass dependence they are fixed at their critical values

$$\gamma_g^* = 4.3, \quad \gamma_f^* = 3.4. \qquad (3.19)$$

The critical value of the input quark mass is $\hat{m}_0 = -0.0854$. Simulations are run with an input quark mass $\hat{m}_0 = -0.0743$. Further details of tuning are given in [22]. The clover terms have the following values

$$c_s = 1.589, \quad c_t = 0.903. \qquad (3.20)$$

All lattice parameters are summarized in Table 5.1.

3.1.3   Sheikholeslami-Wohlert Term

Symanzik's improvement programme applied to ϕ^4-theory was successful in ensuring all "off-shell" Green's functions have a faster approach to the continuum limit [23]. Luscher and Weisz proposed an improvement scheme for the case of pure Yang Mills Theory that demands the improvement of all "on-shell" quantities i.e. low-lying

energy states with small momentum relative to the cutoff [26]. Based on these approaches, Sheikholeslami and Wohlert designed $\mathcal{O}(a)$- and $\mathcal{O}(a^2)$-improved fermion actions. With off-shell improvement, all parameters in the improved action must be fixed order-by-order in perturbation theory. For on-shell improvement, general local covariant transformations known as isospectral transformations that preserve the spectrum of low-lying observables are applied to the improved action. Upon applying such a transformation certain parameters appear explicitly free. The remaining parameters must be fixed order-by-order in perturbation theory as in the off-shell case.

A brief description of the Sheikholeslami and Wohlert approach is given here [27]. For $\mathcal{O}(a)$-improvement, all operators of at most dimension five that are invariant under discrete rotations, parity transformations and charge conjugation transformations are considered. Four such linearly independent operators exist, they are as follows

$$
\begin{aligned}
\mathcal{O}_0(x) &= \overline{\psi}(x)\psi(x) \text{ - dim 3,} \\
\mathcal{O}_1(x) &= \overline{\psi}(x)\gamma_\mu \nabla_\mu \psi(x) \text{ - dim 4,} \\
\mathcal{O}_2(x) &= \overline{\psi}(x)[\sum_\mu \Delta_\mu^2 - \frac{i}{2a^2}\sigma_{\mu\nu}P_{\mu\nu}]\psi(x) \text{ - dim 5,} \\
\mathcal{O}_3(x) &= \frac{i}{2a^2}\overline{\psi}(x)\sigma_{\mu\nu}P_{\mu\nu}\psi(x) \text{ - dim 5,}
\end{aligned}
\tag{3.21}
$$

where

$$
\begin{aligned}
P_{\mu\nu} = \frac{1}{4}[&U_\mu(x)U_\nu(x+\hat{\mu})U_\mu^\dagger(x+\hat{\nu})U_\nu^\dagger(x) \\
&- U_\nu^\dagger(x-\hat{\nu})U_\mu^\dagger(x-\hat{\mu}-\hat{\nu})U_\nu(x-\hat{\mu}-\hat{\nu})U_\mu(x-\hat{\mu}) \\
&+ U_\nu(x)U_\mu^\dagger(x-\hat{\mu}+\hat{\nu})U_\nu^\dagger(x-\hat{\mu})U_\mu(x-\hat{\mu}) \\
&- U_\mu(x)U_\nu^\dagger(x+\hat{\mu}-\hat{\nu})U_\mu^\dagger(x-\hat{\nu})U_\nu(x-\hat{\nu})].
\end{aligned}
\tag{3.22}
$$

Sheikholeslami and Wohlert applied an isospectral transformation to the action comprising the above operators each with an arbitrary coefficient. They showed that the coefficient of the $\mathcal{O}_2$ operator is redundant. This operator with its associated coefficient C_{SW} can be added to the naive fermion action to give $\mathcal{O}(a)$-improvement. Alternatively, the operator $\mathcal{O}_3$ with its associated coefficient C_{SW} can be added to

the Wilson fermion action to give $\mathcal{O}(a)$-improvement. More recently, the anisotropic clover-improved Wilson fermion action that is used in this project was obtained via an isospectral transformation from the naive fermion action. This action is described in work by Chen [28]. This improvement was carried out at the classical level. A full quantum treatment gives the same results when renormalization of the gauge coupling and the bare anisotropy is included.
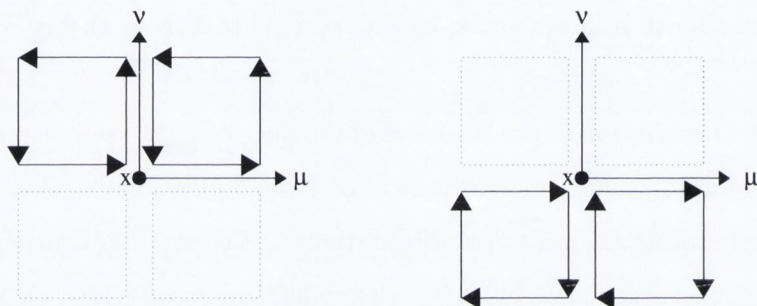
(a) Anticlockwise plaquettes.   (b) Clockwise plaquettes.

Figure 3-4: Anticlockwise and clockwise contributions to $P_{\mu\nu}(x)$.

3.1.4 Static-Quark Action

The static-quark lattice action used in this work is given by

$$S_{stat} = a_s^3 \sum_x \overline{h}(x)[h(x) - U_t^\dagger(x - \hat{t})h(x - \hat{t})]. \tag{3.23}$$

It was first proposed by Eichten and Hill in [29]. It has already been used successfully in the study of static-light mesons [21]. In position space the static-quark propagator from a space-time point $(\vec{x}, x_0)$ to a point $(\vec{y}, y_0)$ is given by

$$G(\vec{x}, x_0; \vec{y}, y_0) = \Theta(y_0 - x_0)\delta(\vec{x} - \vec{y})U_t(y_0 - \hat{t}, \vec{y})....U_t(x_0, \vec{x})P_+, \tag{3.24}$$

where $P_+ = (1/2)(1 + \gamma_0)$ is a projection operator, Θ is the Heaviside step function defined in the Appendix and $\hat{t}$ is the unit vector in the time direction. The static quark propagator is relatively straightforward to compute. One significant disadvantage of the static quark propagator is that the signal degenerates into noise quite early.

3.1.5 Sommer Scale

The Sommer scale [30] r_0 defined through the force $F(r)$ between a static quark and anti-quark separated by a distance r is given by $r_0^2 F(r_0) = 1.65$. The static quark potential is used to determine the Sommer parameter r_0 via

$$r^2 \frac{\partial V(r)}{\partial r}\Big|_{r=r_0} = 1.65. \tag{3.25}$$

One method to extract the static potential $V(r)$ between an infintely heavy quark and anti-quark, separated by a distance r in a spatial direction, is to measure the average value of the Wilson loop

$$
\begin{aligned}
\langle W(r,t) \rangle &= \langle Tr[U_k(\vec{y},0)U_k(\vec{y}+\hat{k},0)...U_k(\vec{y}+r\hat{k},0) \\
&\quad U_0(\vec{y}+r\hat{k},0)U_0(\vec{y}+r\hat{k},1)...U_0(\vec{y}+r\hat{k},t-1) \\
&\quad U_k^\dagger(\vec{y}+r\hat{k},t)U_k^\dagger(\vec{y}+(r-1)\hat{k},t)...U_k^\dagger(\vec{y},t) \\
&\quad U_0^\dagger(\vec{y},t-1)U_0^\dagger(\vec{y},1)...U_0^\dagger(\vec{y},0)]\rangle \\
&= C(r)e^{-V(r)t} + \text{(excited states)}, \tag{3.26}
\end{aligned}
$$

where $\langle .. \rangle$ denotes the average over space points $\vec{y}$ and spatial directions $\hat{k}$ and $C(r)$ is the overlap with the ground state [31]. The static potential $V(r)$ is obtained by taking ratios of Wilson loops. This method suffers excited state contamination. A variational analysis of a five-by-five matrix $C_{ij}(r,t)$ comprising operators with a better overlap with the ground state was performed [25]. For these operators, the straight path of gauge-links in the spatial direction is replaced with a sum of smeared paths. These paths are rotationally invariant about the inter-source axis and pass through the midpoint between the color sources. They may contain staples. Unsmeared straight paths are used for propagation of the static source through time. A range of space separations r spanning r_0 was used as well as a range of time separations t.

The static potential is fit to the Cornell potential [32] given by

$$V(r) = V_0 - \frac{\alpha}{r} + \sigma r, \tag{3.27}$$

where α is the Coulomb coefficient, σ is the string tension and V_0 is the lattice self energy. Best-fit parameters for the parameters V_0, α and σ are determined to calculate the Sommer scale in lattice units via $r_0/a_s = \sqrt{(1.65 - \alpha)/\sigma}$.

3.2 Tadpole Improvement

Tadpole improvement [33] consists of removing the tadpole contributions to gauge links. The lattice gauge link is defined via an expansion in its continuum analog $A_\mu(x)$ as follows

$$U_\mu(x) = e^{ia_\mu g A_\mu(x)} = 1 + ia_\mu g A_\mu(x) + \frac{(ia_\mu g A_\mu(x))^2}{2!} + ..., \tag{3.28}$$

where a_μ is the lattice spacing in the μth direction, g is the coupling and $A_\mu(x)$ is the gauge field. At first sight, it appears as though the higher order terms will be sufficiently suppressed in powers of ag. However, the contraction of the A_μ's produces ultraviolet divergences. These are known as tadpoles. These tadpoles are not sufficiently suppressed by the remaining factors a and g. In a smooth gauge, the link operator can be factored into low momentum (infrared) modes and high momentum (ultraviolet) modes. Substituting U_μ with U_μ/u removes the UV divergences contained in the tadpole factor u.

Tadpole factors appear in both the gauge and fermion actions. In the gauge action, the gauge links are unsmeared giving the two tadpole factors u_s and u_t, where the subscripts s and t denote space and time, respectively. In the fermion action, the gauge links are stout-smeared giving the two tadpole factors $\tilde{u}_s$ and $\tilde{u}_t$.

For large anisotropy ξ, small temporal lattice spacings that suppress the tadpoles associated with gauge links in the time direction can be reached. In this case, tadpole improvement is not necessary in the time direction and u_t can be set equal to unity. In this calculation, $u_t = \tilde{u}_t = 1$ and u_s and $\tilde{u}_s$ are measured from the mean field value of the spatial plaquette as follows

$$u_s = \langle \frac{1}{3} \mathrm{Tr} U_{plaq} \rangle^{\frac{1}{4}}, \tag{3.29}$$

$$\tilde{u}_s = \langle \frac{1}{3} \mathrm{Tr} \tilde{U}_{plaq} \rangle^{\frac{1}{4}}, \tag{3.30}$$

where U_{plaq} is defined by any one of the four terms in equation (3.9). The perturbative expansion of u_s to one-loop order is given by

$$\begin{aligned} \tilde{u}_s &= 1 - \frac{g^2 C_F}{16\pi^2} k_s \\ &= 1 - c^{(1)} g^2, \end{aligned} \tag{3.31}$$

28

where $c^{(1)}$ is the one-loop perturbative value of the tadpole factor [34].

The smeared and unsmeared tadpole factors are parameterized as follows

$$u = \sum_{n=1}^{3} \frac{1 + a_n g^{2n}}{1 + b_n g^{2n}}, \tag{3.32}$$

with $g^2 = 6/\beta$ and the constraint $a_1 - b_1 = c^{(1)}$, where $c^{(1)}$ is the one-loop perturbative value of the tadpole factor. An interpolation over a range of values of g^2 was carried out. The tadpole factors for this parameterization at $\beta = 1.5$ are as follows

$$u_s = 0.7336, \qquad \tilde{u}_s = 0.9267. \tag{3.33}$$

3.3 Tuning

3.3.1 Gauge Anisotropy

On an anisotropic lattice there are two static-quark potentials. These are denoted $V_t(\vec{r})$ and $V_s(\vec{r})$ and are called the "regular" and "sideways" potential, respectively. In the sideways potential, the heavy quark and anti-quark propagate in one of the spatial directions. In this calculation, the sideways potential is used to determine the renormalized gauge anisotropy denoted ξ_g. There are two types of sideways potentials: one where the quarks are separated along a spatial direction and one where the quarks are separated along a time direction. A comparison between these two potentials can be used to determine ξ_g. Solving for t, the equation

$$V_s(y a_s) = V_s(t a_t), \tag{3.34}$$

for a given y, gives the renormalised anisotropy ξ_g, via $t = \xi_g y$. In the asymptotic limit of large x, the Wilson loop W_{ss} can be described in terms of the static quark potential as follows

$$W_{ss}(x, y) \sim \exp[-x a_s V_s(y a_s)]. \tag{3.35}$$

The potential V_s is a lattice potential and differs from the the continuum static-quark potential V by a term V_0, where V_0 is the self energy of the heavy quarks [35]. The

self-energy V_0 is independent of x and y and depends only on the lattice spacing a_s. Ratios of Wilson loops can be used to extract the continuum contribution to the lattice potential [36].

The potentials can be extracted from the ratios of Wilson loops. The ratios below were measured

$$R_{ss}(x,y) = \frac{W_{ss}(x,y)}{W_{ss}(x+1,y)}, \tag{3.36}$$

$$R_{st}(x,t) = \frac{W_{st}(x,t)}{W_{st}(x+1,t)}. \tag{3.37}$$

For large x, $R_{ss}(x,y)$ asymptotically approaches $\exp[-a_s V_s(ya_s)]$ and $R_{st}(x,t)$ asymptotically approaches $\exp[-a_s V_s(ta_t)]$. These methods are described in [37]. The anisotropy ξ_g was determined by minimizing

$$L(\xi_g) = \sum_{x,y} \frac{(R_{ss}(x,y) - R_{st}(x,\xi_g y))^2}{(\Delta R_s)^2 + (\Delta R_t)^2}, \tag{3.38}$$

where ΔR_s and ΔR_t are the statistical errors of R_{ss} and R_{st}.

3.3.2 Renormalization Conditions

The renormalized anisotropies ξ_g and ξ_f as well as the partially conserved axial current (PCAC) quark mass M_t are parameterized in terms of the bare gauge anisotropy γ_g, the bare fermion anisotropy γ_f and the bare quark mass m_0. A linear parameterization is given as follows

$$\xi_g(\gamma_g, \gamma_f, m_0) = a_0 + a_1\gamma_g + a_2\gamma_f + a_3 m_0, \tag{3.39}$$

$$\xi_f(\gamma_g, \gamma_f, m_0) = b_0 + b_1\gamma_g + b_2\gamma_f + b_3 m_0, \tag{3.40}$$

$$M_t(\gamma_g, \gamma_f, m_0) = c_0 + c_1\gamma_g + c_2\gamma_f + c_3 m_0. \tag{3.41}$$

This parameterization was obtained by simulating at fixed β and various values of γ_g, γ_f and m_0. M_t and ξ_g were measured on $12^3 \times 32$ volumes while ξ_f was measured on $12^3 \times 96$ volumes.

Critical values γ_g^*, γ_f^* and m_0^* as functions of input quark mass m_q are found by imposing the following renormalization conditions

$$\xi_g(\gamma_g^*, \gamma_f^*, m_0^*) \ = \ \xi, \tag{3.42a}$$

$$\xi_f(\gamma_g^*, \gamma_f^*, m_0^*) \ = \ \xi, \tag{3.42b}$$

$$M_t(\gamma_g^*, \gamma_f^*, m_0^*) \ = \ m_q. \tag{3.42c}$$

3.4 Heavy Quark Effective Theory

Two length scales emerge in the study of heavy-light-light baryons: a short-distance scale determined by the Compton wavelength $\lambda_Q \sim 1/m_Q$ of the heavy quark and a long-distance hadronic scale $R_{had} \sim 1/\Lambda_{QCD}$ associated with the light degrees of freedom. The mass scales for a heavy-light system are as follows

$$m_L \lesssim \Lambda_{QCD} \ll m_Q, \tag{3.43}$$

where m_L is the mass of the light quarks, Λ_{QCD} is the QCD scale and m_Q is the heavy quark mass [38]. The Compton wavelength of the heavy quark is much smaller than the hadronic scale for a heavy-light system. The length scales for heavy-light systems on a lattice are as follows

$$1/m_Q \ll a \ll 1/\Lambda_{QCD} \lesssim 1/m_L. \tag{3.44}$$

It is not practical to construct lattices with $am_Q \leq 1$.

Typical momentum transfer in interactions between the heavy quark and the light degrees of freedom is of the order of the QCD scale. A heavy quark bound inside a hadron moves with the velocity v_μ of the hadron up to corrections of $\mathcal{O}(\Lambda_{QCD}/m_Q)$. Since $\Lambda_{QCD}/m_Q \ll 1$ this allows for a non-relativistic treatment of the heavy quark. Heavy quark effective theory (HQET) provides such a non-relativistic framework in which to treat the heavy quark. HQET separates the short-distance and long-distance physics. The heavy degrees of freedom associated with short-distance physics are identified in the generating functional and integrated out [39]. The heavy quark action is expanded in a power series in $1/m_Q$.

31

The generating functional of the continuum QCD Green's functions is given by

$$Z(\eta, \overline{\eta}, \lambda)) = \int [\, dQ][\, d\overline{Q}][\, d\phi_\lambda] \exp[iS + iS_\lambda + i \int d^4x(\overline{\eta}Q + \overline{Q}\eta + \phi_\lambda\lambda)], \quad (3.45)$$

where ϕ_λ denotes both the light quarks q and the gluons A_μ. S_λ is the QCD action with light quarks and the heavy quark action is given by

$$S = \int d^4x \overline{Q}(i\not{D} - m_Q)Q. \quad (3.46)$$

It should be noted that this calculation is performed in Minkowski space with the tensor $g^{\mu\nu}$ given in the Appendix. The "upper" components ϕ and "lower" components χ of the heavy quark Q can be projected as follows

$$\phi = \frac{1}{2}(1 + \not{v})Q, \qquad \not{v}\phi = \phi, \quad (3.47)$$

$$\chi = \frac{1}{2}(1 - \not{v})Q, \qquad \not{v}\chi = -\chi. \quad (3.48)$$

The transverse part $D_\mu^\perp$ of the covariant derivative D_μ is given by

$$D_\mu^\perp = D_\mu - v_\mu v_\nu D_\rho g^{\nu\rho}, \quad (3.49)$$

with $g^{\rho\mu}v_\rho D_\mu^\perp = 0$. Interactions with the light degrees of freedom alter the heavy quark velocity on the scale of Λ_{QCD}/m_Q. The heavy quark is nearly on-shell. HQET is an approximation of QCD in the kinetic regime where the heavy quark field can be parameterized in terms of a solution to the Dirac equation of a free particle with velocity v. The heavy quark components are parameterized as follows

$$\phi = e^{-im_Q(v\cdot x)}h_v, \qquad \chi = e^{-im_Q(v\cdot x)}H_v. \quad (3.50)$$

In terms of this parameterization, the heavy quark action is given by

$$\begin{aligned} S_v &= \int d^4x [\overline{h}_v i(v \cdot D)h_v - \overline{H}_v\{i(v \cdot D) + 2m_Q\}H_v \\ &\quad + \overline{h}_v i\not{D}^\perp H_v + \overline{H}_v i\not{D}^\perp h_v]. \end{aligned} \quad (3.51)$$

The small component fields H_v appear in the action with a mass term of $2m_Q$. A mass contribution of m_Q arises from differentiating the field χ in the reparamterized action. The second mass contribution of m_Q is the usual mass term in the action.

The small component fields correspond to short-distance virtual processes. These fields are integrated out in the action. The H_v propagator is expanded in a power series in $1/m_Q$. The HQET action to order $1/m_Q$ is given by

$$S_v = \int d^4x[\overline{h}_v i(v \cdot D)h_v + K_v + M_v + \mathcal{O}(\frac{1}{m_Q^2})], \qquad (3.52)$$

where

$$K_v = \frac{1}{2m_Q}\overline{h}_v D^\mu (g_{\mu\nu} - v_\mu v_\nu)D^\nu h_v, \qquad (3.53)$$

$$M_v = \frac{g}{4m_Q}\overline{h}_v \sigma^{\mu\nu} F_{\mu\nu} h_v. \qquad (3.54)$$

Both the "kinetic" term K_v and the "Pauli" term M_v are order $1/m_Q$ terms. The kinetic term describes the off-shell motion of the heavy quark. The Pauli term corresponds to the chromo-magnetic coupling of the heavy-quark with the gluon field. In the infinite mass limit, the HQET action is given by

$$S_\infty = \int d^4x[\overline{h}_v i(v \cdot D)h_v]. \qquad (3.55)$$

In this limit, the terms that describe the corrections to the heavy quark velocity vanish and the heavy quark moves with the same velocity as the hadron. In the rest frame of the hadron, i.e. where $v_\mu = (1, 0, 0, 0)$ the heavy quark is static. This action has an $SU(2)$ spin symmetry associated with heavy quark spin conservation. The static action contains no mass term and so the action possesses a flavour symmetry. For N_h heavy quarks with the same velocity v, the HQET static action possesses an $SU(2N_h)$ spin-flavour symmetry [40]. The mass splitting between the lowest lying $J = 3/2$ Σ_b^* state and lowest lying $J = 1/2$ Σ_b state, where J denotes total angular momentum, is about ten percent of the mass of Σ_b. In the static approximation of HQET the masses of Σ_b^* and Σ_b become degenerate due to spin symmetry. In the literature [41] this is taken as a possible indicator to suggest that the $\mathcal{O}(1/m_Q)$ correction to the static approximation is at the ten percent level.

3.5 Spectroscopy Methods

3.5.1 Correlators

The zero-momentum correlation function $C(t)$ for a hadron interpolating operator $\mathcal{O}(\vec{x}, t)$ is defined as follows

$$C(t) = \sum_{\vec{x}} \langle 0|\mathcal{O}(\vec{x}, t)\mathcal{O}^{\dagger}(\vec{0}, 0)|0\rangle. \tag{3.56}$$

Inserting a complete set of zero-momentum energy-eigenstates $\{|n\rangle\}$ of the Hamiltonian gives

$$C(t) = \sum_{n} \frac{1}{2E_n}|\langle 0|\mathcal{O}|n\rangle|^2 e^{-E_n t}. \tag{3.57}$$

In a finite-volume, the spectrum is discrete and the operator $\mathcal{O}(\vec{x}, t)$ has a non-zero coupling to all states $\{|n\rangle\}$ that share its quantum numbers. Correlation functions can be analysed to extract excited state energies. At large time separations t, the correlation function is dominated by the contribution of its ground state. The effective mass at time t denoted $m_{eff}(t)$ is defined as follows

$$m_{eff}(t) = \ln\left[\frac{C(t)}{C(t+1)}\right]. \tag{3.58}$$

At large times, $m_{eff}(t) \sim E_0$ where the lowest mass state E_0 is called the ground state.

3.5.2 Distillation

The basic quantity in the construction of correlation functions involving fermion fields is the fermion propagator given by

$$[M^{-1}]_{i,j}^{\alpha,\beta}(x, y) = \frac{1}{\mathcal{Z}} \int D\psi D\overline{\psi} \psi_i^{\alpha}(x)\overline{\psi}_j^{\beta}(y)e^{-\overline{\psi}M\psi}, \tag{3.59}$$

where i, j label quark flavour, α, β label quark spin and M is the fermion matrix appearing in the fermion action. Historically, access to a limited number of rows of this high-dimensional matrix has been possible to give point-to-all propagators. Here the propagator from a small number of sites on the lattice to all other sites is

evaluated. Calculating a limited number of rows saves dramatically on computing resources. More recently, all-to-all propagators have been utilised [42]. In this approach, a spectral sum of the physically important low-lying eigenmodes is formed to estimate the propagator. Random noise is also used to estimate the propagator. The spectral sum and random noise estimates of the propagator are combined in a hybrid algorithm.

Traditionally, smearing has been used to expose at earlier timeslices the asymptotic behaviour of correlation functions. This is necessary since signal-to-noise ratios diminish at larger time separations rendering large time information redundant. Smearing acts as a filter and retains the long-range modes. For the purposes of extracting low-energy masses the short-range modes are deemed unwanted and referred to as contamination. These short-range modes can be significantly removed by the application of smearing to the quark field. Smearing consists of redefining the quark fields in terms of a local distribution of quark fields. Jacobi smearing [43] involves iteratively applying the lattice Laplacian to the quark fields. The lattice Laplacian is defined as follows

$$\nabla^2_{xy}(t) = -6\delta_{xy} + \sum_{j=1}^{3}(U_j(x,t)\delta_{x+\hat{j},y} + U_j^\dagger(x-\hat{j},t)\delta_{x-\hat{j},y}), \tag{3.60}$$

where the gauge fields $U_j(x,t)$ have been constructed from gauge-covariant smeared gauge fields. The Jacobi smearing operator is defined as follows

$$J_{\rho,n_\rho}(t) = \left(1 + \frac{\rho\nabla^2(t)}{n_\rho}\right)^{n_\rho}, \tag{3.61}$$

where ρ is the smearing parameter and n_ρ is the parameter denoting the number of smearing hits. These two parameters are tuned to optimize excited state contamination reduction. The Jacobi smearing algorithm selects the lower eigenmodes of the lattice Laplace operator. Contributions from higher eigenmodes are suppressed.

A smearing operator can be defined by a projection operator onto the space of the first M eigenvectors of the gauge covariant lattice Laplace operator $\nabla^2(t)$. The lattice Laplace operator has rank $N = N_c \times N_x^3$ where N_c is the number of colors and N_x^3 is the spatial volume of the lattice. The distillation operator [44] has rank

$M << N$. The distillation operator on timeslice t denoted $\square_d(t)$ is given by

$$\square_d(t) = \sum_{k=1}^{M} v_t^k \otimes v_t^{\dagger k}, \tag{3.62}$$

where v_t^k is the kth eigenvector of ∇_t^2 calculated with background spatial gauge fields at time t. Since the rank $M << N$, distillation is not prohibitively expensive and all elements of the propagation matrix can be computed. A displaced static-light-light baryon annihilation operator is given by

$$\chi_{t'}^B = \epsilon^{abc} Q_{t'}^a (C\Gamma)^{\alpha_1 \alpha_2} \left(\mathcal{D}_1 \square \psi_{1,t'} \right)_{\alpha_1}^b \left(\mathcal{D}_2 \square \psi_{2,t'} \right)_{\alpha_2}^c, \tag{3.63}$$

where there is a contraction over color indices a, b and c as well as a summation over spin indices α_1 and α_2. Q denotes the heavy quark field, $\psi_{1,2}$ denote the light quark fields. $C\Gamma$ is a spin matrix for the light quarks; its role will be explained in the next chapter. $\mathcal{D}_{1,2}$ is a gauge-covariant displacement operator defined as follows

$$\mathcal{D}_{1,2}(x) = \sum_i C_{1,2}^i \mathcal{P}(x,y)\delta_{x,y} \tag{3.64}$$

where $\mathcal{P}(x,y)$ is a gauge-covariant product of links connecting sites x and y, $\delta_{x,y}$ is a delta function and the coefficients $C_{1,2}^i$ are complex numbers. The static-light-light correlation function is given by

$$
\begin{aligned}
C_{t',t} &= \langle \chi_{t'}^B \overline{\chi}_t^B \rangle \tag{3.65}\\
&= \epsilon^{abc}\epsilon^{def}(C\Gamma)^{\alpha_1\alpha_2}(C\Gamma)^{\beta_1\beta_2}\\
&\quad \langle Q_{t'}^a \left(\mathcal{D}_1 v_i v_i^\dagger \psi\right)_{\alpha_1,t'}^b \left(\mathcal{D}_2 v_j v_j^\dagger \psi\right)_{\alpha_2,t'}^c Q_t^d \left(\overline{\psi} v_{\overline{j}} v_{\overline{j}}^\dagger \mathcal{D}_2\right)_{\beta_2,t}^f \left(\overline{\psi} v_{\overline{i}} v_{\overline{i}}^\dagger \mathcal{D}_1\right)_{\beta_1,t}^e \rangle\\
&= \epsilon^{abc}\epsilon^{def}(C\Gamma)^{\alpha_1\alpha_2}(C\Gamma)^{\beta_1\beta_2}\\
&\quad \langle Q_{t'}^a \left(\mathcal{D}_1 v_i v_i^\dagger \psi\right)_{\alpha_1,t'}^b \left(\mathcal{D}_2 v_j v_j^\dagger \psi\right)_{\alpha_2,t'}^c Q_t^d \left(\overline{\psi} v_{\overline{j}} v_{\overline{j}}^\dagger \mathcal{D}_2\right)_{\beta_2,t}^f \left(\overline{\psi} v_{\overline{i}} v_{\overline{i}}^\dagger \mathcal{D}_1\right)_{\beta_1,t}^e \rangle\\
&\quad + \epsilon^{abc}\epsilon^{def}(C\Gamma)^{\alpha_1\alpha_2}(C\Gamma)^{\beta_1\beta_2}\\
&\quad \langle Q_{t'}^a \left(\mathcal{D}_1 v_i v_i^\dagger \psi\right)_{\alpha_1,t'}^b \left(\mathcal{D}_2 v_j v_j^\dagger \psi\right)_{\alpha_2,t'}^c Q_t^d \left(\overline{\psi} v_{\overline{j}} v_{\overline{j}}^\dagger \mathcal{D}_2\right)_{\beta_2,t}^f \left(\overline{\psi} v_{\overline{i}} v_{\overline{i}}^\dagger \mathcal{D}_1\right)_{\beta_1,t}^e \rangle\\
&= \epsilon^{abc}\epsilon^{def}(C\Gamma)^{\alpha_1\alpha_2}(C\Gamma)^{\beta_1\beta_2}\\
&\quad \langle Q_{t'}^a Q_t^d \left(\mathcal{D}_1 v_i \mathcal{D}_2 v_j\right) \left(v_i^\dagger \psi_{\alpha_1,t'}^b \overline{\psi}_{\beta_1,t}^e v_{\overline{i}}\right) \left(v_j^\dagger \psi_{\alpha_2,t'}^c \overline{\psi}_{\beta_2,t}^f v_{\overline{j}}\right) \left(v_{\overline{j}}^\dagger \mathcal{D}_2 v_{\overline{i}}^\dagger \mathcal{D}_1\right) \rangle\\
&\quad - \epsilon^{abc}\epsilon^{def}(C\Gamma)^{\alpha_1\alpha_2}(C\Gamma)^{\beta_1\beta_2}\\
&\quad \langle Q_{t'}^a Q_t^d \left(\mathcal{D}_1 v_i \mathcal{D}_2 v_j\right) \left(v_i^\dagger \psi_{\alpha_1,t'}^b \overline{\psi}_{\beta_2,t}^f v_{\overline{j}}\right) \left(v_j^\dagger \psi_{\alpha_2,t'}^c \overline{\psi}_{\beta_1,t}^e v_{\overline{i}}\right) \left(v_{\overline{j}}^\dagger \mathcal{D}_2 v_{\overline{i}}^\dagger \mathcal{D}_1\right) \rangle.
\end{aligned}
$$

Wick's theorem is used to factorize the correlation function into products of quark propagators [45]. The horizontal brackets in equation (3.65) linking two quark fields are contraction symbols. In brief, each contraction of two quark fields in equation (3.65) results in a quark propagator. The minus sign arises due to the Grassmann nature of quarks fields. Quark fields are Grassmann variables and are antisymmetric under interchange as shown below

$$\psi_1 \psi_2 = -\psi_2 \psi_1. \tag{3.66}$$

The static-light-light correlation function factorizes into the product of three terms as follows

$$C_{(t',t)} = P_{(t',t)}^{(c,d)} \Phi_{t'}^{(i,j,c)} \tau_{(t',t)}^{(i,\bar{i})} \tau_{(t',t)}^{(j,\bar{j})} \Phi_t^{*(\bar{i},\bar{j},d)} - P_{(t',t)}^{cd} \Phi_{t'}^{(i,j,c)} \tau_{(t',t)}^{(i,\bar{j})} \tau_{(t',t)}^{(j,\bar{i})} \Phi_t^{*(\bar{i},\bar{j},d)}, \tag{3.67}$$

where

$$\Phi_t^{ijc\alpha\beta} = \epsilon^{abc} \left(\mathcal{D}_1 v_t^i\right)^a \left(\mathcal{D}_2 v_t^j\right)^b (C\Gamma)^{\alpha\beta}, \tag{3.68}$$

$$\tau_{t't}^{\alpha\beta} = V_{t'}^{\dagger} \left(M^{-1}\right)_{t't}^{\alpha\beta} V_t, \tag{3.69}$$

and $P^{(c,d)}(t',t)$ is a Wilson line connecting the source at time t with the sink at time t'. The Wilson line is the heavy quark contribution to the correlation function. Both Φ and τ are square matrices of dimension $4M$. Φ contains all the information on the creation operator. τ is known as the perambulator. τ contains the information on quark propagation. All elements of τ can be computed at a reasonable computational cost. Distillation has been utilised successfully in excited light meson spectroscopy [46, 47].

Chapter 4

Group Theory

4.1   Octahedral Group

The continuum Hamiltonian is invariant under rotations in $SO(3)$. The Hamiltonian of a spatially isotropic lattice is invariant under rotations of the cubic group O. This group comprises the twenty four rotations that map a cube onto itself. In the continuum it is possible to construct spatially extended baryon interpolating field operators that belong to the $(2L + 1)$ - dimensional irreducible representations of $SO(3)$, where L denotes orbital angular momentum. In the continuum L is a well-defined quantity. On a spatially isotropic lattice, it is possible to construct spatially extended baryon interpolating field operators that belong to the irreducible representations of O. O has five conjugacy classes and therefore five single-valued irreducible representations - see the Appendix. These irreducible representations are labelled A_1, A_2, E, T_1 and T_2: they have dimensions 1, 1, 2, 3 and 3, respectively. Unlike the continuum case, each irreducible representation does not coincide with a distinct quantity L. A technique known as subduction can be used to infer the continuum orbital angular momentum content of lattice baryon interpolating field operators.

The direct product of the cubic group O with the two-element group $\{\mathbb{1}, \mathcal{P}\}$, consisting of the identity transformation $\mathbb{1}$ and the spatial inversion transformation $\mathcal{P}$, gives the Octahedral group denoted O_h. All lattice operators naturally possess

invariance under O. Since the Hamiltonian does not possess definite symmetry under spatial inversion $\mathcal{P}$, lattice operators are not guaranteed to possess any symmetry under spatial inversion. Care must be taken to ensure that lattice operators possess definite parity P. This can be achieved in a straightforward manner by considering transformations under the larger group O_h. The octahedral group has 10 single-valued irreducible representations denoted A_{1g}, A_{1u}, A_{2g}, A_{2u}, E_g, E_u, T_{1g}, T_{1u}, T_{2g} and T_{2u}: they have dimensions 1, 1, 1, 1, 2, 2, 3, 3, 3, and 3, respectively. The subscript g denotes gerade or even under spatial inversion and u denotes ungerade or odd under spatial inversion.

In this chapter, it will be shown how to construct lattice baryon interpolating field operators that belong to irreducible representations of O_h. The process of subduction will be explained. These operators have fixed isospin I, fixed parity P and fixed spin S.

4.1.1 Projections into Irreducible Representations

In HQET the heavy quark is static. This quark does not contribute to the group theory except to define the origin of the baryon interpolating field operator. The positions of the light quarks are taken as being relative to the position of the heavy quark. Rotations under O are considered as rotations about the heavy quark point. Spatial inversion is considered as reflection through the heavy quark point. A general baryon interpolating field operator, that is to say, an operator with zero, one or both light quarks displaced from the origin can be described by the diquark consisting of its two light quarks. A schematic representation of a spatially extended diquark with one light quark at position $\vec{r}_1$, the other light quark at position $\vec{r}_2$ and the heavy quark at the origin is given in Figure 4-1.
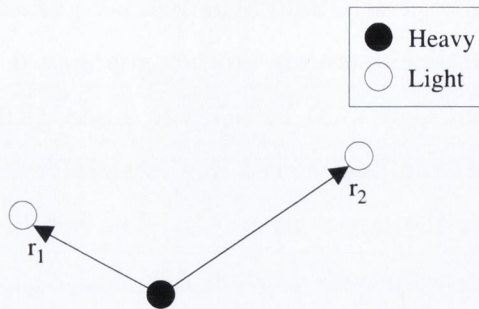
Figure 4-1: Spatially extended diquark.

Each transformation in O_h is assigned a number ranging from 1 to 48. One diquark is selected and denoted e_1. Transformation i applied to diquark e_1 produces diquark e_i where i varies from 1 to 48. If no transformation in O_h leaves this diquark invariant, a set of 48 diquarks - each with a distinct spatial orientation - is formed. In this case, e_i can be specified by a 48-d vector with one in the ith position and zeroes elsewhere. Each transformation i beginning with transformation 1 is applied in sequence to diquark e_2 to produce a permutation of the 48 quantities e_i. This process is repeated for diquark e_3 and so on. In this manner, a 48-d reducible representation M of O_h is formed. The diquarks act as basis vectors while the representative matrices are given by the permutation matrices.

The multiplicity of the irreducible representation r for the reducible representation M is given by

$$m^r = \frac{1}{g} \sum_k n_k \chi_k^r \chi_k^M, \tag{4.1}$$

where there are n_k elements in class k, χ_k^r is the character of the irreducible representation r for class k, χ_k^M is the character of the representation M for class k and g is the order of O_h [21]. The definition of the character of a group element within a representation of the group is given in the Appendix. The rotation angles associated with the conjugacy classes are given in Table 4.1. The character table for O_h is given in Table 4.2 [18].

	C_1	C_2	C_3	C_4	C_5	C_6	C_7	C_8	C_9	C_{10}
	0	$\frac{2\pi}{3}$	$\frac{\pi}{2}$	$\frac{\pi}{4}$	$\frac{\pi}{2}$	0	$\frac{2\pi}{3}$	$\frac{\pi}{2}$	$\frac{\pi}{4}$	$\frac{\pi}{2}$

Table 4.1: Rotation angles in conjugacy classes of O_h.

	C_1	C_2	C_3	C_4	C_5	C_6	C_7	C_8	C_9	C_{10}
A_{1g}	1	1	1	1	1	1	1	1	1	1
A_{1u}	1	1	1	1	1	-1	-1	-1	-1	-1
A_{2g}	1	1	1	-1	-1	1	1	1	-1	-1
A_{2u}	1	1	1	-1	-1	-1	-1	-1	1	1
E_g	2	-1	2	0	0	2	-1	2	0	0
E_u	2	-1	2	0	0	-2	1	-2	0	0
T_{1g}	3	0	-1	1	-1	3	0	-1	1	-1
T_{1u}	3	0	-1	1	-1	-3	0	1	-1	1
T_{2g}	3	0	-1	-1	1	3	0	-1	-1	1
T_{2u}	3	0	-1	-1	1	-3	0	1	1	-1

Table 4.2: Character table for O_h.

An application of equation (4.1) shows that the decomposition of the 48-dimensional reducible representation of O_h into irreducible representations of O_h contains each irreducible representation of O_h with the multiplicity for the irreducible representation being given by the dimension of the irreducible representation.

The following projection operator

$$P^\mu = \sum_g \chi^\mu(g)M(g), \qquad (4.2)$$

projects a basis vector for representation M into the irreducible representation μ where $\chi^\mu(g)$ is the character of an irreducible representation matrix for element g in O_h.

4.1.2 Subduced Representation

The method of subduction is used to uncover the continuum orbital angular momentum content of operators belonging to spatial irreducible representations of O_h. A formal definition of subduction is given in the Appendix. A subduced representation of O_h, labelled by continuum spin L, is formed by selecting the irreducible representative matrices of $SO(3) \times \{\mathbb{1}, \mathcal{P}\}$ that correspond to the 48 elements of O_h $\subset SO(3) \times \{\mathbb{1}, \mathcal{P}\}$. This representation is in general reducible. There is a two-to-one homomorphism from $SU(2)$ to the continuum Hamiltonian symmetry group $SO(3)$. The traces of $SU(2)$ matrices for spin L and rotation angle θ are given by

$$\chi_\theta^L = \frac{\sin[(L+1/2)\theta]}{\sin[\theta/2]}. \tag{4.3}$$

The multiplicity of an irreducible representation r of O_h for the subduced representation of O_h with continuum spin label L is given by

$$m_L^r = \frac{1}{g} \sum_k n_k \chi_k^r \chi_k^L, \tag{4.4}$$

where there are n_k elements in class k, χ_k^r is the character of irreducible representation r for class k, χ_k^L is the character of the subduced representation with continuum spin L for class k and g is the order of the group [48].

The decomposition of the subduced representation of O_h with continuum spin L into the irreducible representations of O_h, for spins from $L = 0$ to $L = 5$, is given in Table 4.3.

L	Λ
0	$A_{1g} \oplus A_{1u}$
1	$T_{1g} \oplus T_{1u}$
2	$E_g \oplus E_u \oplus T_{2g} \oplus T_{2u}$
3	$A_{2g} \oplus A_{2u} \oplus T_{1g} \oplus T_{1u} \oplus T_{2g} \oplus T_{2u}$
4	$A_{1g} \oplus A_{1u} \oplus E_g \oplus E_u \oplus T_{1g} \oplus T_{1u} \oplus T_{2g} \oplus T_{2u}$
5	$E_g \oplus E_u \oplus T_{1g} \oplus T_{1u} \oplus T_{1g} \oplus T_{1u} \oplus T_{2g} \oplus T_{2u}$

Table 4.3: The subduction of $SO(3) \times \{\mathbb{1}, \mathcal{P}\}$ to the irreducible representation Λ of O_h for integer L.

A continuum operator that couples to a state with definite angular momentum L decomposes with an identifiable pattern into different irreducible representations of O_h when it is restricted to the lattice. If a state appears across the same pattern of irreducible representations it can be assigned the continuum angular momentum label L. An operator from any of these irreducible representations must couple with a non-vanishing coefficient to a continuum state denoted by L. Operators transforming according to a given irreducible representation couple to a tower of states. The tower of states for each irreducible representation is given in Table 4.4.

A_{1g}	$0, 4, 6..$
A_{1u}	$0, 4, 6..$
A_{2g}	$3, 6..$
A_{2u}	$3, 6..$
E_g	$2, 4, 5..$
E_u	$2, 4, 5..$
T_{1g}	$1, 3, 4, 5..$
T_{1u}	$1, 3, 4, 5..$
T_{2g}	$2, 3, 4, 5..$
T_{2u}	$2, 3, 4, 5..$

Table 4.4: Allowed values of L for each irreducible representation of O_h.

4.2 Pauli Exclusion Principle

The Pauli Exclusion Principle requires all baryon interpolating field operators to be antisymmetric under interchange of its indistinguishable particles - namely its two light degrees of freedom. Each light quark has a colour index, a flavour index, a spin index as well as a spatial coordinate. Before considering symmetries under O_h, an elemental baryon interpolating field operator with appropriate colour, flavour, spin and spatial symmetry must be designed, see the quark model section of [4]. There is a total of four ways in which to combine the light degrees of freedom to attain an overall antisymmetry. In each case colour contraction of the heavy quark with the

two light degrees of freedom is taken at the heavy quark point. Antisymmetrization in colour space is achieved with the Levi-Civita tensor. This produces a colour-singlet quantity. The different symmetry combinations are given in Table 4.5 where A denotes an antisymmetric channel and S denotes a symmetric channel.

Colour	Flavour	Spin	Space
A	A	A	S
A	A	S	A
A	S	S	S
A	S	A	A

Table 4.5: Symmetries allowed by the Pauli Exclusion Principle.

4.2.1 Flavour

The light quarks come in two different flavours - up (u) and down (d). Strange quarks are not simulated in this project. Isospin zero baryon interpolating field operators correspond to the antisymmetric flavor-space channel. Isospin one baryon interpolating field operators correspond to the symmetric flavor-space channel. The results are summarized in Table 4.6.

$I = 0$	$\frac{1}{\sqrt{2}}(ud - du)$
$I = 1$	$uu, \frac{1}{\sqrt{2}}(ud + du), dd$

Table 4.6: Flavour symmetries.

4.2.2 Displacement

In order to maintain gauge invariance, path-dependent gauge links are used to displace the light quarks. In the general case each light quark has a distinct spatial displacement from the heavy quark point. The combined symmetries are explicit in

the most general elemental field operator given below

$$
\begin{aligned}
B(\vec{x}) \quad &= \{\epsilon^{abc} Q^a(\vec{x}) [q^\alpha_{f_1}(\vec{y}) P(\vec{y},\vec{x})]^b C_{\alpha\beta} \Gamma_{\beta\delta} [q^\delta_{f_2}(\vec{z}) P(\vec{z},\vec{x})]^c \\
&\pm \epsilon^{abc} Q^a(\vec{x}) [q^\alpha_{f_2}(\vec{y}) P(\vec{y},\vec{x})]^b C_{\alpha\beta} \Gamma_{\beta\delta} [q^\delta_{f_1}(\vec{z}) P(\vec{z},\vec{x})]^c\} \\
&\pm \{\epsilon^{abc} Q^a(\vec{x}) [q^\alpha_{f_1}(\vec{z}) P(\vec{z},\vec{x})]^b C_{\alpha\beta} \Gamma_{\beta\delta} [q^\delta_{f_2}(\vec{y}) P(\vec{y},\vec{x})]^c \\
&\pm \epsilon^{abc} Q^a(\vec{x}) [q^\alpha_{f_2}(\vec{z}) P(\vec{z},\vec{x})]^b C_{\alpha\beta} \Gamma_{\beta\delta} [q^\delta_{f_1}(\vec{y}) P(\vec{y},\vec{x})]^c\},
\end{aligned}
\tag{4.5}
$$

where f_1 denotes the flavour of light quark one, α denotes the spin of light quark one, $P(\vec{y},\vec{x})$ is the path-dependent gauge link (with two suppressed colour indices) that displaces a quark from point $\vec{x}$ to point $\vec{y}$, ϵ^{abc} is the Levi-Civita tensor with explicit colour indices, C is the charge conjugation matrix and Γ is a combination of gamma matrices. The combination of $\pm$ signs as well as spin matrix Γ is chosen to satisfy the Pauli Exclusion Principle.

4.2.3 Spin

The four Euclidean gamma matrices satisfy the anticommutation relation below

$$
\{\Gamma_\mu, \Gamma_\nu\} = 2\delta_{\mu\nu} \mathrm{x} I_{4\times 4} \qquad \text{(Dirac algebra)}, \tag{4.6}
$$

where $\mu \in [0,1,2,3]$. This identity is basis-independent. There is an additional matrix Γ_5. It satisfies the following basis-independent identities

$$
(\Gamma_5)^2 \;=\; I_{4\times 4}, \tag{4.7}
$$

$$
(\Gamma_5)^\dagger \;=\; \Gamma_5, \tag{4.8}
$$

$$
\{\Gamma_5, \Gamma_\mu\} \;=\; 0, \tag{4.9}
$$

where $I_{4\times 4}$ is the 4-dimensional identity matrix.

In Euclidean space Γ_5 is defined as follows

$$
\Gamma_5 \;=\; i\Gamma_0 \Gamma_1 \Gamma_2 \Gamma_3. \tag{4.10}
$$

In HQET, the heavy quark spin decouples. The two spin-1/2 light quarks combine to form either an $S = 0$ or an $S = 1$ baryon interpolating field operator. The choice of gamma matrix determines the spin.

The charge conjugation matrix C satisfies the following representation-independent identities

$$CT_\mu C^{-1} = -\Gamma_\mu^T, \qquad \mu \in \{0,1,2,3\}, \tag{4.11}$$

$$CT_5 C^{-1} = \Gamma_5^T. \tag{4.12}$$

The basis used in this work is the Dirac basis. In the Dirac basis the charge conjugation matrix has the following definition

$$C = i\Gamma_2\Gamma_0. \tag{4.13}$$

The definition of the Euclidean metric tensor $\delta^{\mu\nu}$ and the representation of the gamma matrices are given in the Appendix.

4.2.4 Spin Irreducible Representation

Each element $g \in O_h$ can be assigned a matrix $R(g)$ such that

$$R(g)e_i = \pm e_j, \tag{4.14}$$

where e_i is a unit vector in the ith direction and $i,j \in \{1,2,3\}$. The set of matrices $R(g)$ has the following property

$$R(g_1 g_2) = R(g_1)R(g_2), \tag{4.15}$$

for $g_1, g_2 \in O_h$, thus providing a matrix representation for O_h. The characters of these matrices show that this representation is a T_{1u} irreducible representation of O_h. The T_{1u} irreducible representation of O_h is called the vector representation of O_h. The set of matrices $\{\Gamma_5\Gamma_1, \Gamma_5\Gamma_2, \Gamma_5\Gamma_3\}$ also forms a basis for a T_{1u} irreducible representation of O_h. The set $\{\Gamma_1, \Gamma_2, \Gamma_3\}$ transform as a T_{1g} irreducible representation of O_h. Any element of $\{I, \Gamma_0, \Gamma_5, \Gamma_0\Gamma_5\}$ can be used to construct an $S = 0$ operator which transforms as either an A_{1g} or A_{1u} irreducible representation of O_h. The results are summarized in Table 4.7.

46

	Spin	Parity	Symmetry
$C\Gamma_0$	0	$-$	S
$C\Gamma_5, C\Gamma_0\Gamma_5$	0	$+$	A
C	0	$-$	A
$C\Gamma_1, C\Gamma_2, C\Gamma_3$	1	$+$	S
$C\Gamma_5\Gamma_1, C\Gamma_5\Gamma_2, C\Gamma_5\Gamma_3$	1	$-$	A
$C\Gamma_0\Gamma_1\Gamma_5, C\Gamma_0\Gamma_2\Gamma_5, C\Gamma_0\Gamma_3\Gamma_5$	1	$-$	S

Table 4.7: Properties of gamma matrices.

4.3   Parity

In 4-dimensional Euclidean space the parity transformation denoted by $\mathcal{P}$, maps $(t, \vec{x}) \rightarrow (t, -\vec{x})$. For a quantum field $\psi(t, \vec{x})$ the parity transformation is as follows

$$\psi(x) \rightarrow \psi'(x) \;\; = \;\; S(\mathcal{P})\psi(\mathcal{P}x), \tag{4.16}$$

where $S(\mathcal{P})$ is a unitary operator. The transformation of a diquark is as follows

$$
\begin{aligned}
q_1^\alpha(y)C_{\alpha\beta}\Gamma_{\beta\delta}q_2^\delta(z) \;\; &\rightarrow \;\; [S(\mathcal{P})]_\lambda^\alpha q_1^\lambda(\mathcal{P}y)C_{\alpha\beta}\Gamma_{\beta\delta}[S(\mathcal{P})]_\rho^\delta q_2^\rho(\mathcal{P}z) \\
&= \;\; q_1^\lambda(\mathcal{P}y)[S(\mathcal{P})]_\lambda^\alpha C_{\alpha\beta}\Gamma_{\beta\delta}[S(\mathcal{P})]_\rho^\delta q_2^\rho(\mathcal{P}z) \\
&= \;\; q_1^\lambda(t, -\vec{y})[S(\mathcal{P})]_\lambda^\alpha C_{\alpha\beta}\Gamma_{\beta\delta}[S(\mathcal{P})]_\rho^\delta q_2^\rho(t, -\vec{z}) \\
&= \;\; q_1^\lambda(t, -\vec{y})\Lambda_{\lambda\rho}q_2^\rho(t, -\vec{z}), \tag{4.17}
\end{aligned}
$$

where $\Lambda_{\lambda\rho} = [S(\mathcal{P})]_\lambda^\alpha C_{\alpha\beta}\Gamma_{\beta\delta}[S(\mathcal{P})]_\rho^\delta$.

There are two contributions to parity. The parity contribution due to the configuration of spatial coordinates is called smearing parity. The other contribution to parity is from the spin matrix. In any basis $[C\Gamma]$ has definite parity of ± 1, i.e. $\Lambda = \pm[C\Gamma]$, where $\Gamma \in \{I, \Gamma_0, \Gamma_0\Gamma_5, \Gamma_1, \Gamma_2, \Gamma_3, \Gamma_5\Gamma_1, \Gamma_5\Gamma_2, \Gamma_5\Gamma_3, \Gamma_0\Gamma_1\Gamma_5, \Gamma_0\Gamma_2\Gamma_5, \Gamma_0\Gamma_3\Gamma_5\}$. For an operator to have well-defined total parity it must also have well-defined smearing parity i.e. smearing parity of ± 1.

The two transformations below have smearing parities of $+1$ and -1, respectively,

$$q_1^\alpha(t, \vec{y})[C\Gamma]_{\alpha\delta}q_2^\delta(t, \vec{z}) + q_1^\alpha(t, -\vec{y})[C\Gamma]_{\alpha\delta}q_2^\delta(t, -\vec{z})$$

$$\rightarrow \quad [q_1^\alpha(t, -\vec{y})\Lambda_{\alpha\delta}q_2^\delta(t, -\vec{z}) + q_1^\alpha(t, \vec{y})\Lambda_{\alpha\delta}q_2^\delta(t, \vec{z})]$$

$$= \quad (+1)[q_1^\alpha(t, \vec{y})\Lambda_{\alpha\delta}q_2^\delta(t, \vec{z}) + q_1^\alpha(t, -\vec{y})\Lambda_{\alpha\delta}q_2^\delta(t, -\vec{z})]$$

$$= \quad (+1)(\rho)[q_1^\alpha(t, \vec{y})[C\Gamma]_{\alpha\delta}q_2^\delta(t, \vec{z}) + q_1^\alpha(t, -\vec{y})[C\Gamma]_{\alpha\delta}q_2^\delta(t, -\vec{z})], \qquad (4.18)$$

$$q_1^\alpha(t, \vec{y})[C\Gamma]_{\alpha\delta}q_2^\delta(t, \vec{z}) - q_1^\alpha(t, -\vec{y})[C\Gamma]_{\alpha\delta}q_2^\delta(t, -\vec{z})$$

$$\rightarrow \quad [q_1^\alpha(t, -\vec{y})\Lambda_{\alpha\delta}q_2^\delta(t, -\vec{z}) - q_1^\alpha(t, \vec{y})\Lambda_{\alpha\delta}q_2^\delta(t, \vec{z})]$$

$$= \quad (-1)[q_1^\alpha(t, \vec{y})\Lambda_{\alpha\delta}q_2^\delta(t, \vec{z}) - q_1^\alpha(t, -\vec{y})\Lambda_{\alpha\delta}q_2^\delta(t, -\vec{z})]$$

$$= \quad (-1)(\rho)[q_1^\alpha(t, \vec{y})[C\Gamma]_{\alpha\delta}q_2^\delta(t, \vec{z}) - q_1^\alpha(t, -\vec{y})[C\Gamma]_{\alpha\delta}q_2^\delta(t, -\vec{z})], \qquad (4.19)$$

where ρ is the parity due to the spin matrix $C\Gamma$.

These two cases are summarized in the following equation

$$q_1^\alpha(t, \vec{y})[C\Gamma]_{\alpha\delta}q_2^\delta(t, \vec{z}) + (p)q_1^\alpha(t, -\vec{y})[C\Gamma]_{\alpha\delta}q_2^\delta(t, -\vec{z})$$

$$\rightarrow \quad (p)(\rho)[q_1^\alpha(t, \vec{y})[C\Gamma]_{\alpha\delta}q_2^\delta(t, \vec{z}) + (p)q_1^\alpha(t, -\vec{y})[C\Gamma]_{\alpha\delta}q_2^\delta(t, -\vec{z})], \qquad (4.20)$$

where $p = \pm 1$ is the smearing parity and ρ is the parity due to the spin matrix. The overall parity is the product of smearing parity and spin matrix parity.

4.4 Tensor Product of Spin and Spatial Irreducible Representations

Spin angular momentum and orbital angular momentum are combined by taking the tensor product of the irreducible representation of O_h associated with spin with the irreducible representation of O_h associated with spatial displacement. The identity representation is the A_{1g} irreducible representation. The tensor product of the A_{1u} irreducible representation with an irreducible representation D produces the irreducible representation corresponding to D with the opposite parity. In general the tensor product of two irreducible representations produces a reducible representation. The decomposition and projection into irreducible representations is given by

48

the methods explained earlier. The coefficients used in the projection are Clebsch-Gordan coefficients. All possible tensor products and their decompositions are given in Table A-1 and Table A-2 in the Appendix.

Chapter 5

Results

5.1 Results

All the techniques used in this work have been described in previous chapters. In this chapter, a summary will be presented of key results. The chapter begins with a section on eigenvector testing. The next section is a study on non-local baryon interpolating field operators. This is followed by a section on the quark model. This is followed by a section on effective mass fittings. Following this, there is a section on mass splittings. The next section shows a comparison of results with experiment. This is followed by a summary of, and comparison with, contemporary lattice work on the b-hadron spectrum. The chapter concludes with a brief discussion of systematic errors. To begin, the list of lattice parameters used in this work is presented in Table 5.1.

In this chapter L denotes the orbital angular momentum of the diquark, S denotes the total spin of the diquark, J denotes the total angular momentum of the diquark, I denotes the isospin of the diquark and P denotes the parity under spatial inversion of the diquark. In the static limit of HQET the static (bottom) quark does not contribute to the orbital angular momentum, the spin, the isospin or the parity of the baryon interpolating field operator. For this reason the quantum numbers and group irrep label of the baryon operator and diquark operator are interchangeable.

Parameter	Value
β	1.5
Volume	$12^3 \times 96$
Number of Configurations	49
N_f	3
$a_t m_0$	-0.0734
a_s	0.12fm
ξ	3.5
γ_g^*	4.3
γ_f^*	3.4
u_s	0.7336
u_t	1
$\tilde{u}_s$	0.9267
$\tilde{u}_t$	1
c_s	1.589
c_t	0.903
ρ	0.14
n_ρ	2

Table 5.1: Summary of all lattice parameters.

The lattice dimensions and the number of $N_f = 3$ dynamical gauge configurations are given. The bare up quark mass $a_t m_0$ is given. The ratio of spatial to temporal lattice spacings ξ as well as the anisotropies $\gamma_{g,f}$ fixed during tuning are shown. The unsmeared spatial and temporal tadpole factors in the gauge sector are given, denoted u_s and u_t, respectively. The smeared tadpole factors in the fermion sector denoted $\tilde{u}_s$ and $\tilde{u}_t$ are given. The choice of stout-link smearing parameters in the gauge action denoted ρ and n_ρ are presented. The values of the tree-level tadpole improved coefficients c_s and c_t are shown.

5.2 Eigenvector Tests

Previous work on distillation [44] has studied the dependence of 2-point correlator data on the number of eigenvectors of the Laplace operator utilized in the distillation procedure. In that work, single exponentials were fitted to correlators and effective mass plots were analysed. These plots show that excited state contamination as well as noise are sensitive to the number of eigenvectors used in the distillation process. In this work, a study was conducted on the dependence of the quality of data on the number of eigenvectors. The results from this study are given in Figures 5-1 and 5-2. Throughout this chapter, the effective mass plots presented are for fits of a single-exponential to a 2-point correlation function.
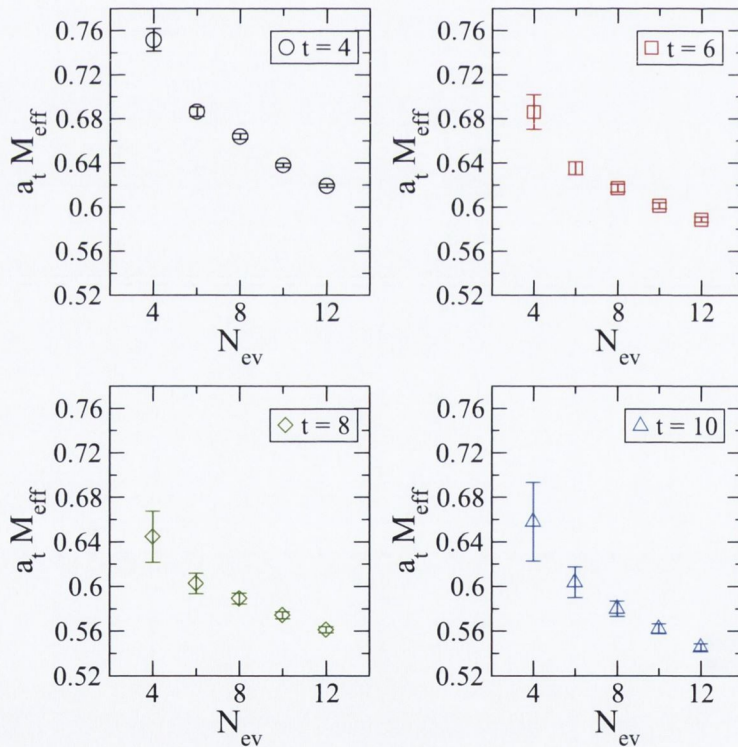

Figure 5-1: Eigenvector test for an ($L = 1$, $S = 0$, $J = 1$, $I = 0$, $P = -$) state with a T_1 operator.

Figure 5-1 has two main features. Firstly, it demonstrates that the value of the

effective mass for a particular timeslice decreases as the number of eigenvectors is increased from 4 to 12. This is seen for each of the 4 timeslices. Secondly, it demonstrates that the error in the effective mass decreases as the number of eigenvectors is increased from 4 to 12. This is observed for each of the 4 timeslices. In Figure 5-2, a plateau in the effective mass first begins to appear around timeslice $t = 11$ for both $N_{ev} = 12$ and $N_{ev} = 24$. The effective mass plot for $N_{ev} = 12$ begins to show definite signs of noise at timeslice $t = 16$. Whereas the effective mass plot for $N_{ev} = 24$ begins to show definite signs of noise at timeslice $t = 21$. Thus increasing the number of eigenvectors from 12 to 24 improves the statistical error by allowing fitting over a wider time window. All data points for the $N_{ev} = 12$ data are higher than the corresponding data points for the $N_{ev} = 24$ data up to and including timeslice $t = 15$.
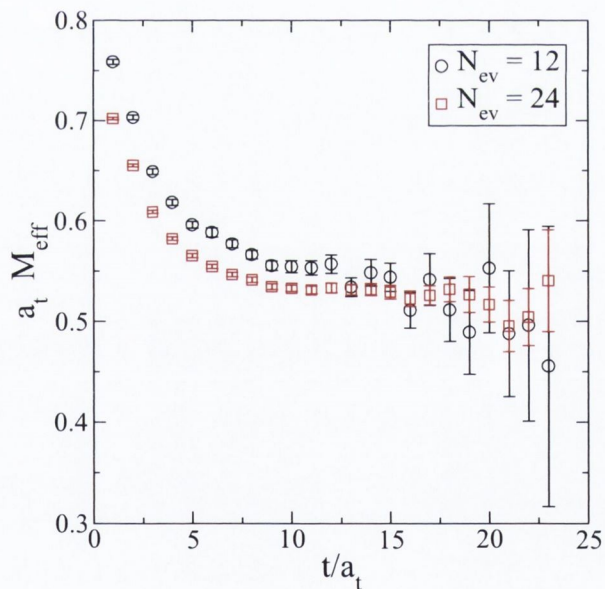

Figure 5-2: Eigenvector test for an $(L = 0, S = 0, J = 0, I = 1, P = -)$ state with an A_1 operator.

The data in Figure 5-1 was obtained using an earlier version of CHROMA [22] on a data set of 99 configurations. The data in Figure 5-2 was obtained using the most current version of CHROMA. The number of configurations used is 49.

5.3 Non-Local Operators

One-link, two-link and three-link operators were tested with 12 eigenvectors. Spin-0 operators for each of the five irreducible representations of O were tested. Both $I = 0$ and $I = 1$ as well as $P = +$ and $P = -$ operators were tested. In each case, it was seen that the effective mass plots were identical within an individual irrep. That is to say, no variation in excited state contamination was seen in moving from the simplest realization of an irrep operator to an operator with a slighlty larger radius. Figure 5-3 is one such example. This suggested that further study of the dependence of excited state contamination on the spatial configuration of the diquark was necessary. C-code was written to construct A_1 operators with both light quarks displaced from the origin and from each other. Operators with a radius of less than 8 spatial lattice units were constructed. A sample of more than 250 operators were tested. This examination used 4 eigenvectors and 5 configurations. Again, very little variation in excited state contamination was seen. These results are summarized in Figure 5-4 which displays an arbitrary sample of 6 of these operators with inclusion of the corresponding single-site operator for direct comparison. All results presented in this chapter for irreps with dimension greater than 1 were obtained by fitting a single exponential to the row-averaged correlator for the irrep. Results obtained by fitting a single exponential to an individual row of an irrep are given in the Appendix.

A small number of correlation matrices up to dimension 5 were constructed for A_1 and T_1 operators. Again both parities and both isospins were tested. These simulations were run with 24 eigenvectors and on 49 configurations. A variational analysis was performed [49, 50] . The results of one such test are plotted in Figure 5-5. No excitations were observed.
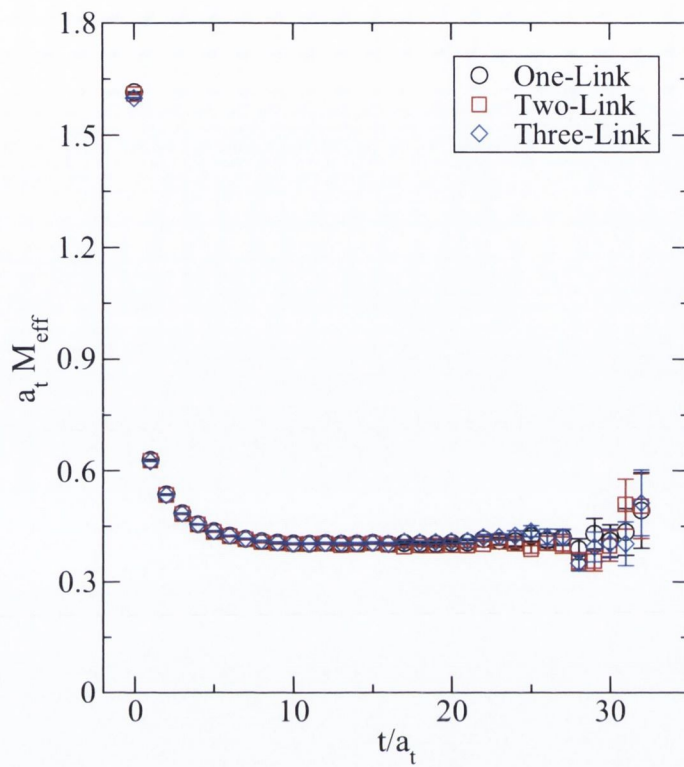
Figure 5-3: Comparison between one-link, two-link and three-link data for an ($L = 0$, $S = 0$, $J = 0$, $I = 0$, $P = -$) state.
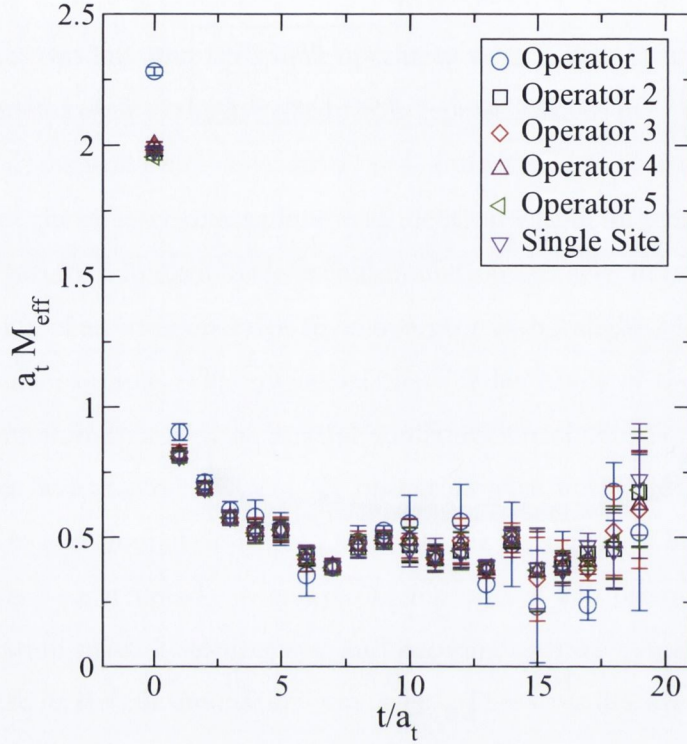
Figure 5-4: Sample of different (A_1, $I = 0$, $P = -$) operator results.

Operator	Quark 1 (x, y, z) coordinates	Quark 2 (x, y, z) coordinates
Operator 1	$(-7, -3, 0)$	$(7, 1, 1)$
Operator 2	$(-6, 0, 0)$	$(2, 0, 0)$
Operator 3	$(-4, -2, -5)$	$(1, 4, 3)$
Operator 4	$(-1, -5, 3)$	$(1, 5, 3)$
Operator 5	$(-1, -5, -3)$	$(2, 1, 2)$
Single Site	$(0, 0, 0)$	$(0, 0, 0)$

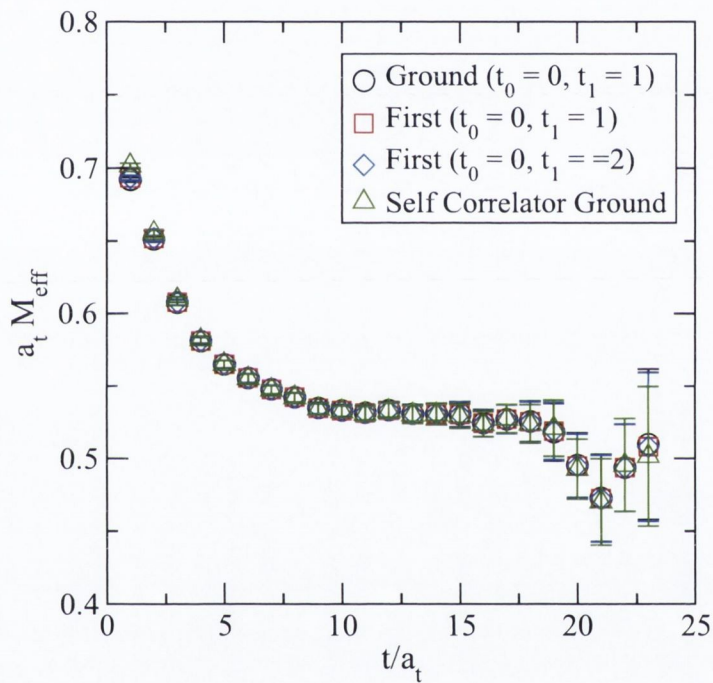Table 5.2: List of displacement operators.

Figure 5-5: Variational analysis results for a 4×4 correlation matrix optimized on timeslices ($t_0 = 0, t_1 = 1, 2$) for one-link, two-link and three-link isospin-1 operators in the A_{1u} irreducible representation of O_h.

5.4 Quark Model

The up quark denoted u is an isospin-1/2 particle with isospin projection $I_z = +1/2$. The down quark denoted d is an isospin-1/2 particle with isospin projection $I_z = -1/2$. The Λ_b^0 particle has isospin $I = 0$ with quark content udb, where b denotes a

bottom quark. The quark model [4] gives the lowest Λ_b^0 particle the quantum numbers $J = 1/2$ and $P = +$, where J and P denote total angular momentum and parity, respectively. Σ_b^+, Σ_b^0 and Σ_b^- belong to the isospin-1 triplet (uud, udb, ddb). In the quark model the lowest Σ_b particle has the quantum numbers $J = 1/2$ and $P = +$. The masses of both Λ_b and Σ_b have been measured experimentally [2, 6]. The Σ_b - Λ_b splitting has already been measured in lattice QCD. In this project, the operators that couple to the lowest lying Λ_b and Σ_b particles are designed according to the symmetries of the "good" and "bad" diquarks in [51].

5.5 Effective Mass Fittings

The effective mass plot for each operator was individually inspected. In each case, a minimum value for the lower fit timeslice parameter t_0 was chosen. This was taken to be the timeslice value at which the effective mass begins to plateau. A maximum value for the higher fit timeslice parameter t_1 was taken. This was chosen to be the timeslice beyond which fitting would be meaningless due to noise. Ground state effective mass fittings were performed for all pairs (t_0, t_1) that lie within these limits. The fits with the better values of $\chi^2_{d.o.f.}$ were selected. For each operator, these results are collated in a detailed figure which contains three subplots. The first subplot shows the effective mass. The second subplot shows the better ground state effective mass fits. The third subplot shows the corresponding set of $\chi^2_{d.o.f.}$ values.

5.5.1 A_1 Results

Four states are studied in this section. A single-site operator is defined as an operator with all three quarks living on the same lattice site. Both single-site and one-link operators were used to simulate an operator that couples to Λ_b. There was only a very slight difference in the quality of the data between these two operators. The one-link operator was selected as the Λ_b canditate for the calculation of mass splittings. The following five pages each contains a figure containing effective mass results as well as a brief description of the operator underneath.
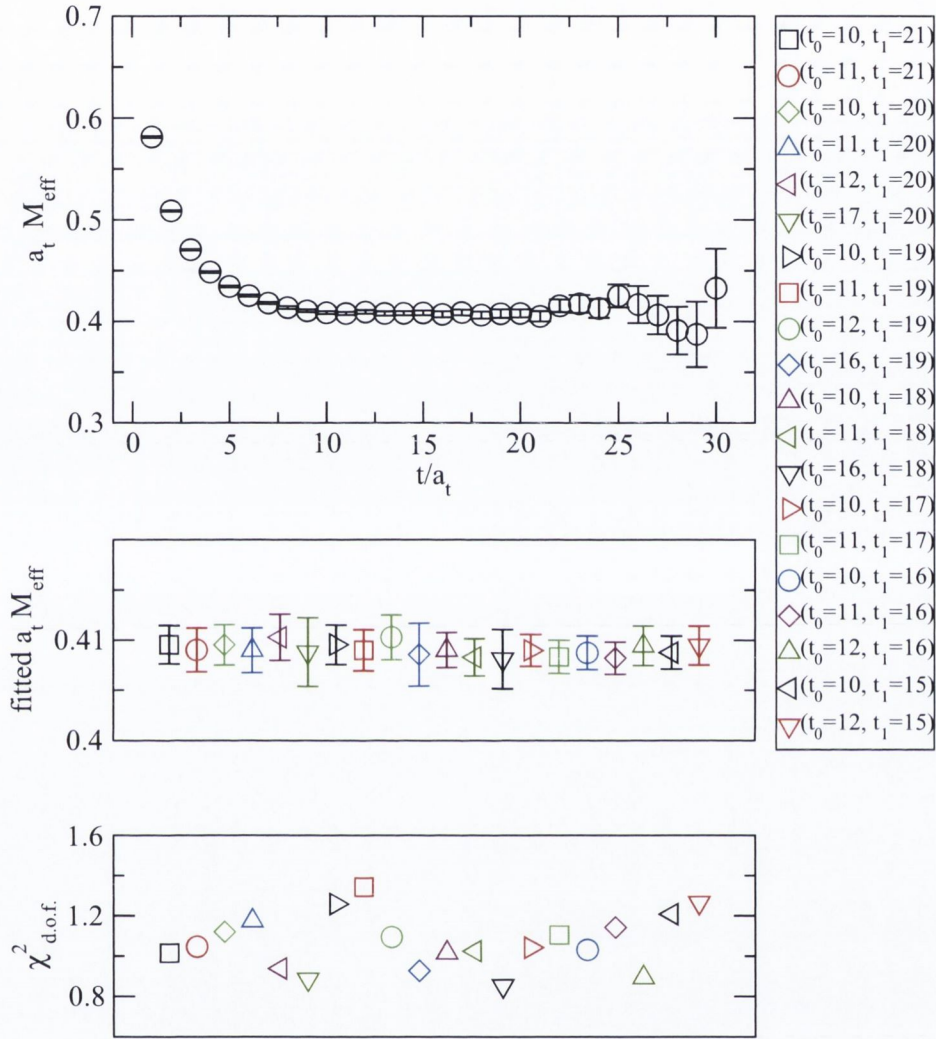
Figure 5-6: Irrep A_1: $L = 0$, $S = 0$, $J = 0$, $I = 0$, $P = +$.

This operator is constructed with the spin matrix $C\Gamma_5$. It is a single-site operator. It couples to the lowest lying Λ_b state. The mass of Λ_b has been experimentally determined.
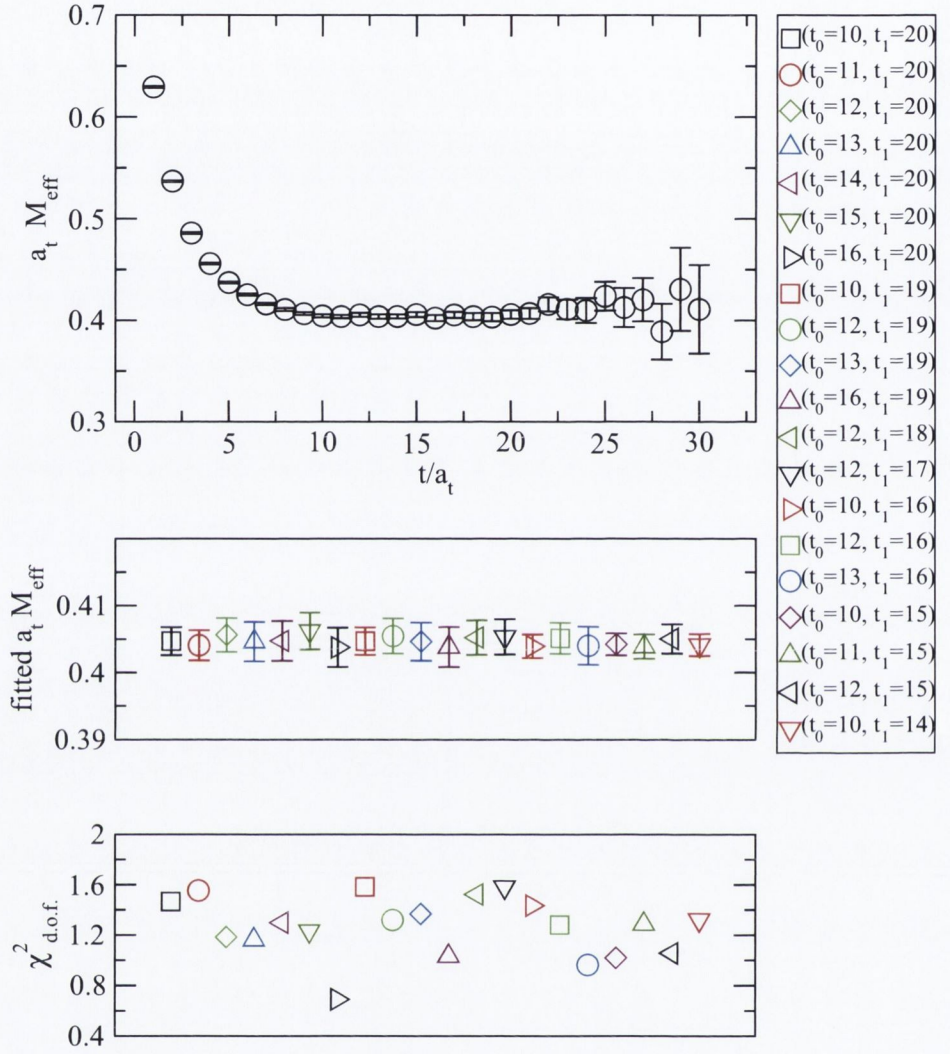
Figure 5-7: Irrep A_1: $L = 0$, $S = 0$, $J = 0$, $I = 0$, $P = +$.

This operator is constructed with the spin matrix $C\Gamma_5\Gamma_0$. It is a non-local operator. It couples to the lowest lying Λ_b state. The mass of Λ_b has been experimentally determined.
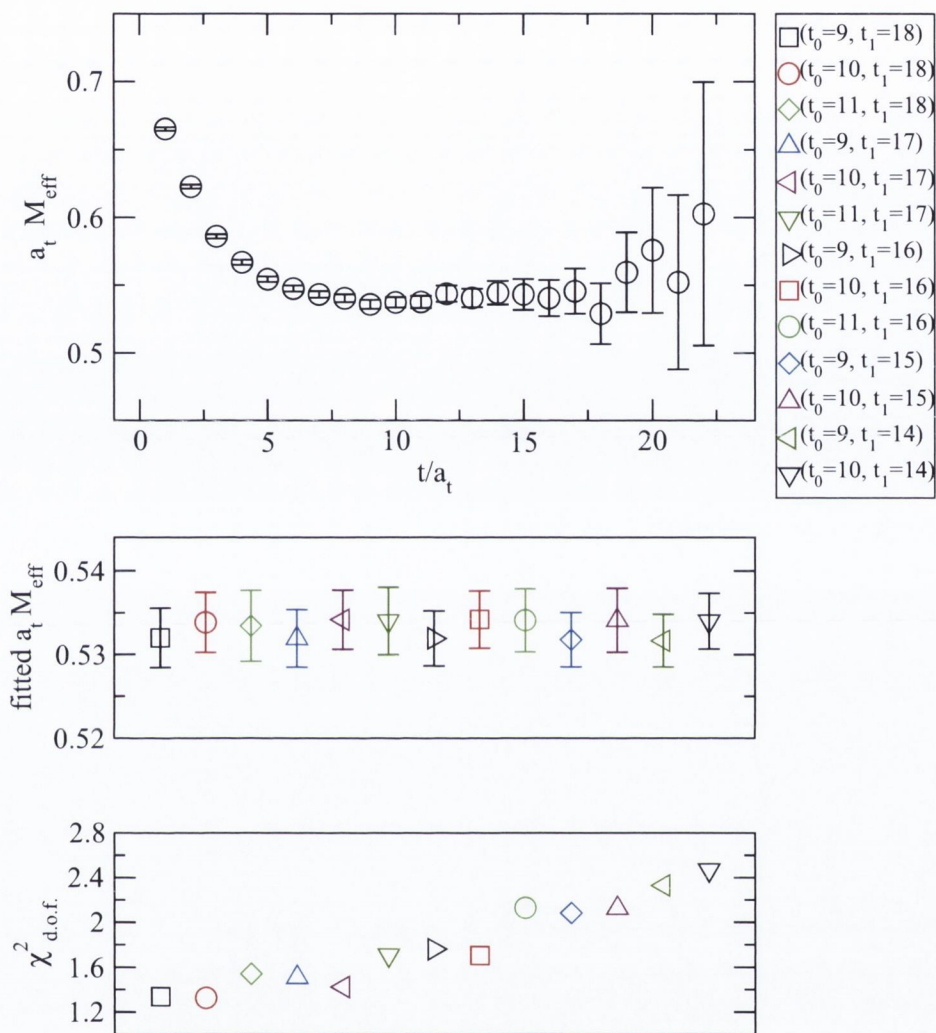
Figure 5-8: Irrep A_1: $L = 0$, $S = 0$, $J = 0$, $I = 0$, $P = -$.

This operator is constructed with the spin matrix C. It is a single-site operator.

Figure 5-9: Irrep A_1: $L = 0$, $S = 0$, $J = 0$, $I = 1$, $P = +$.

This operator is constructed with the spin matrix $C\Gamma_5\Gamma_0$. It is a non-local operator.
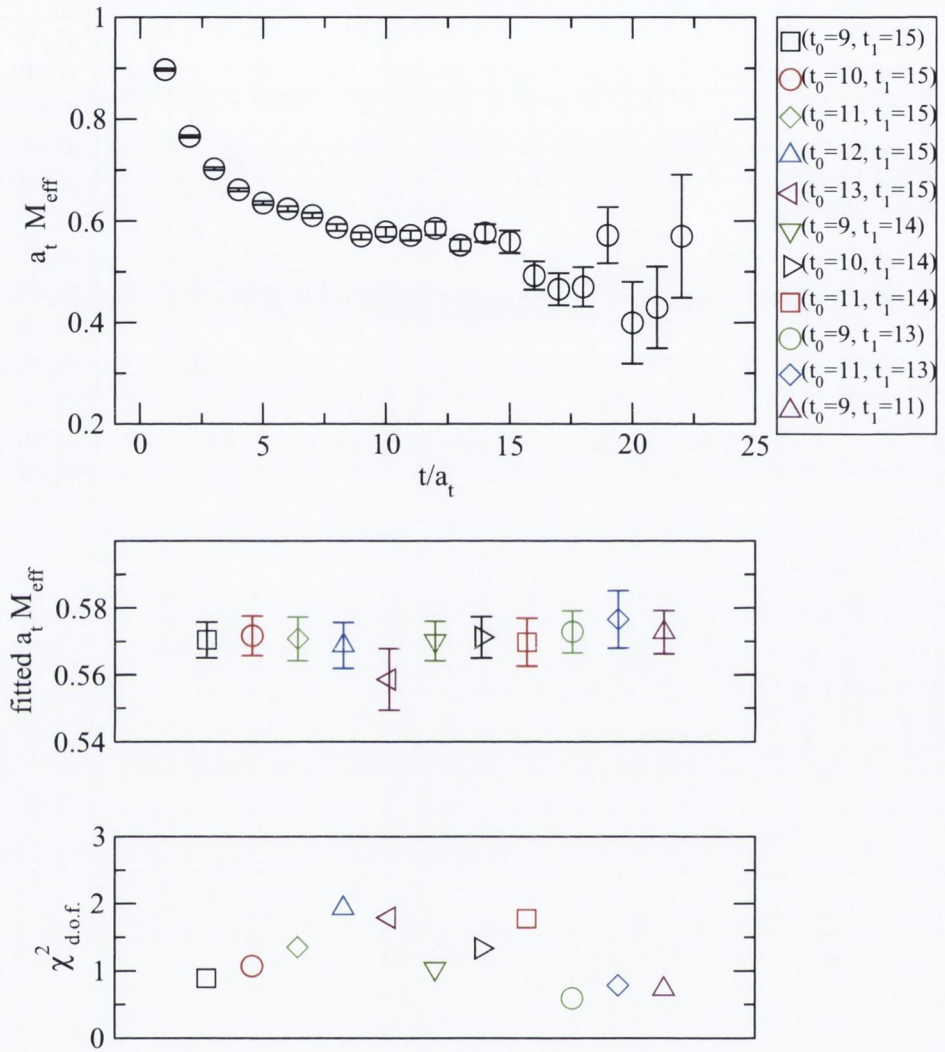
Figure 5-10: Irrep A_1: $L = 0$, $S = 0$, $J = 0$, $I = 1$, $P = -$.

This operator is constructed with the spin matrix $C\Gamma_0$. It is a non-local operator.
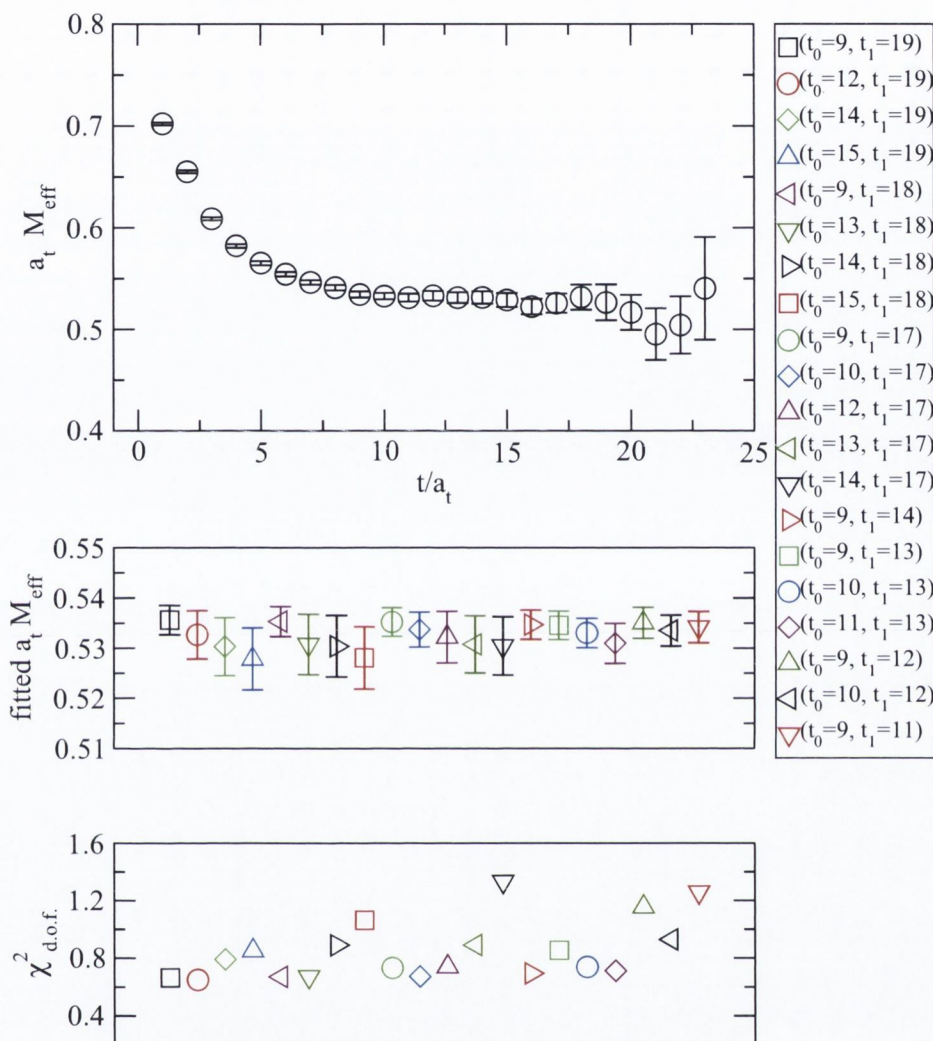
5.5.2 Spin-1 Results

This section contains results for the masses of four states. Three of these states have been measured by contemporary lattice calculations. One of these states is the lowest lying Σ_b state. The results for the T_1, $I = 0$ and $P = +$ operator are the first results for the $J = 1$, $I = 0$ and $P = +$ state.

Figure 5-11: Irrep T_1: $L = 0$, $S = 1$, $J = 1$, $I = 0$, $P = +$.

These are the row-averaged results for operators that are constructed with the spin matrices $C\Gamma_1$, $C\Gamma_2$ and $C\Gamma_3$. These results are the first results for this state.

Figure 5-12: Irrep T_1: $L = 0$, $S = 1$, $J = 1$, $I = 0$, $P = -$.

These are the row-averaged results for operators that are constructed with the spin matrices $C\Gamma_5\Gamma_1$, $C\Gamma_5\Gamma_2$ and $C\Gamma_5\Gamma_3$. These are single-site operators.
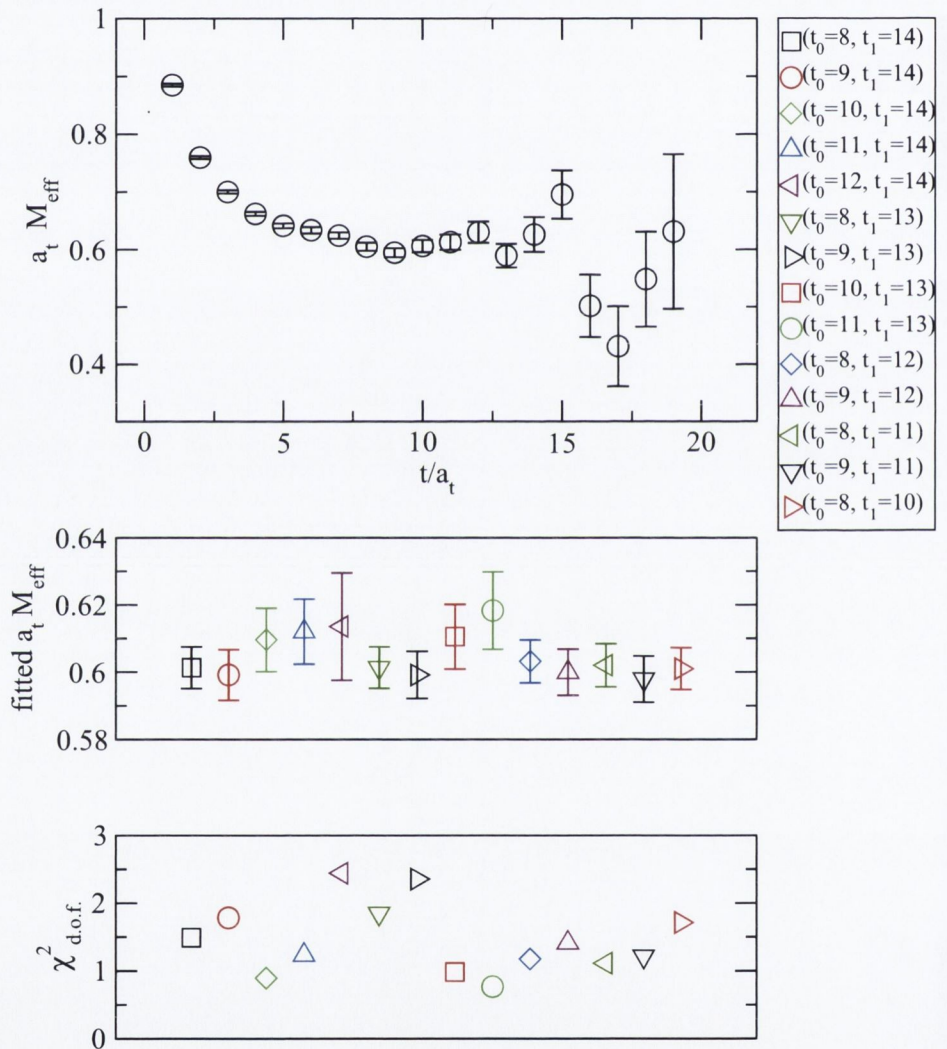
Figure 5-13: Irrep T_1: $L = 0$, $S = 1$, $J = 1$, $I = 1$, $P = +$.

These are the row-averaged results for operators that are constructed with the spin matrices $C\Gamma_1$, $C\Gamma_2$ and $C\Gamma_3$. These are single-site operators. They couple to the lowest lying Σ_b state. The mass of Σ_b has been experimentally determined.
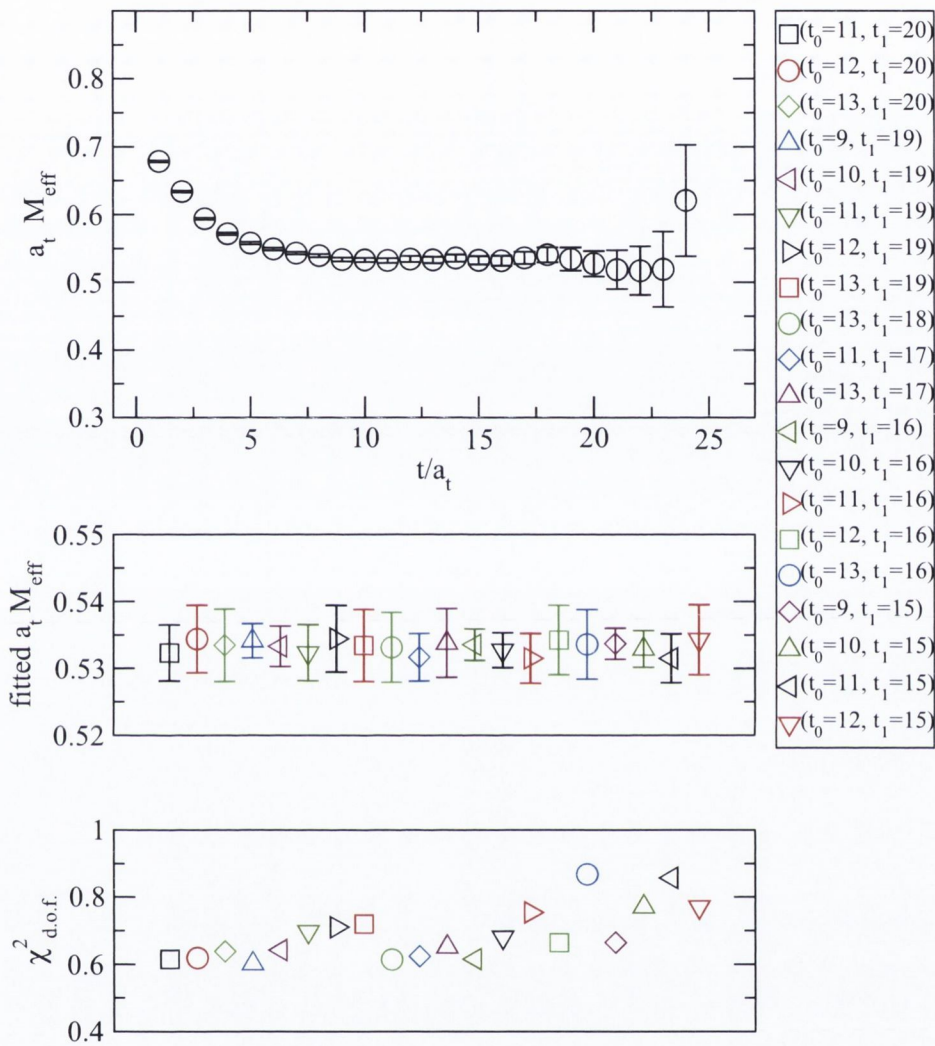
Figure 5-14: Irrep T_1: $L = 0$, $S = 1$, $J = 1$, $I = 1$, $P = -$.

These are the row-averaged results for operators that are constructed with the spin matrices $C\Gamma_0\Gamma_1\Gamma_5$, $C\Gamma_0\Gamma_2\Gamma_5$ and $C\Gamma_0\Gamma_3\Gamma_5$. These are single-site operators.

5.5.3 E Results

All the operators in this section are non-local. All the results in this section are the first results for $J = 2$ static-light-light baryons. The masses of four newly determined states are given in this section.
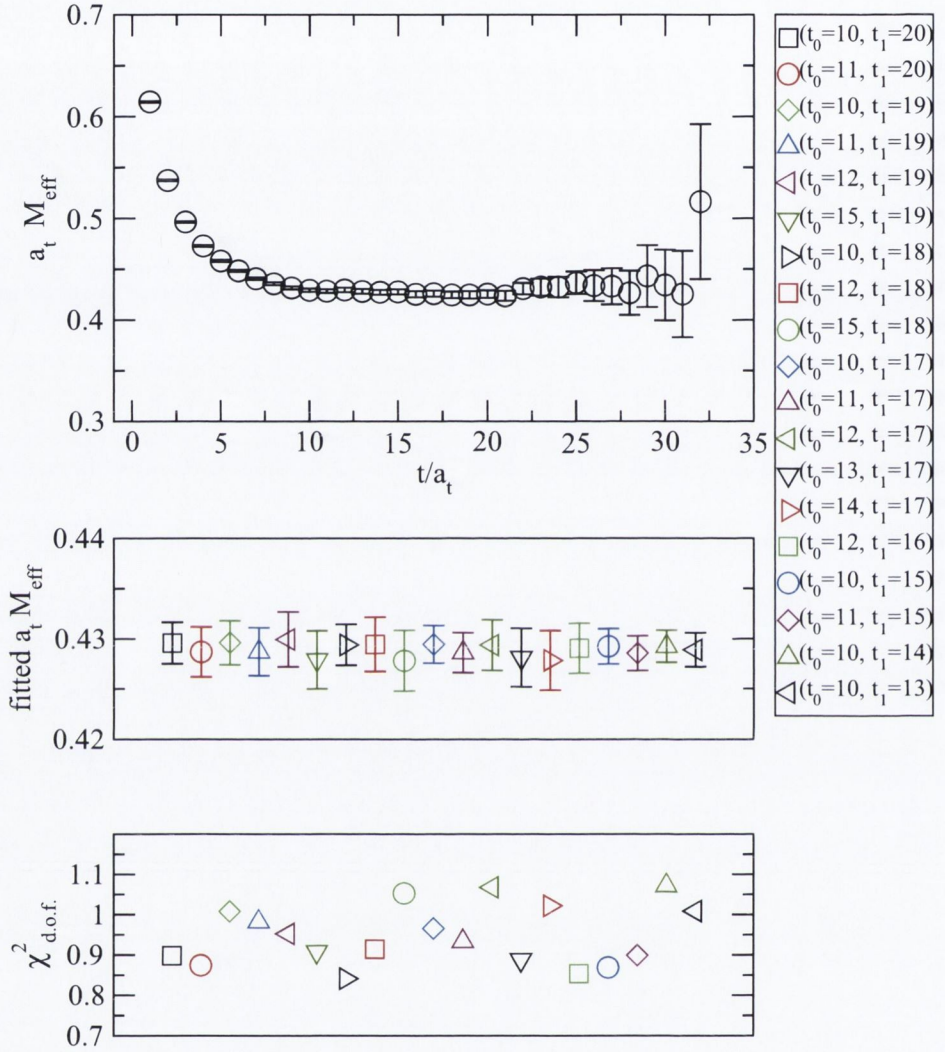

Figure 5-15: Irrep E: $L = 2$, $S = 0$, $J = 2$, $I = 0$, $P = +$.

These are the row-averaged results for operators that are constructed with the spin matrix $C\Gamma_5$.

Figure 5-16: Irrep E: $L = 2$, $S = 0$, $J = 2$, $I = 0$, $P = -$.

These are the row-averaged results for operators that are constructed with the spin matrix C.

Figure 5-17: Irrep E: $L = 2$, $S = 0$, $J = 2$, $I = 1$, $P = +$.

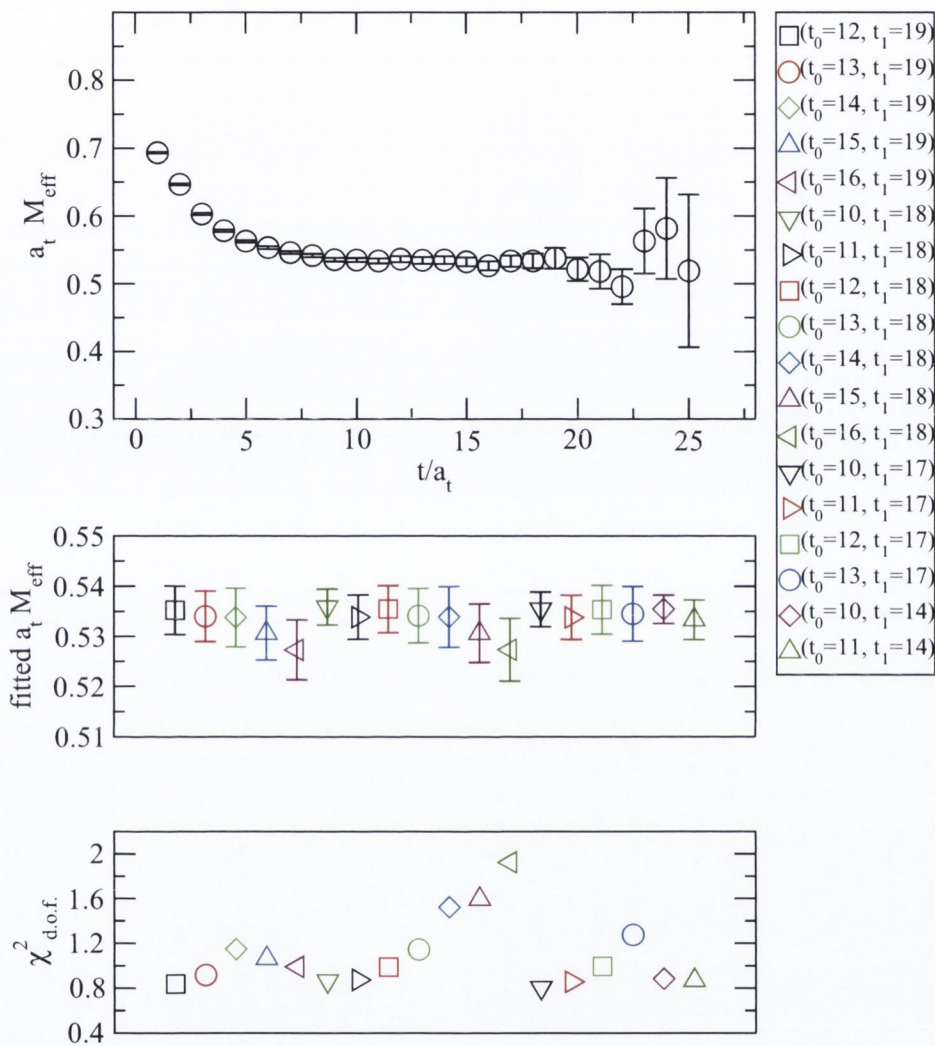These are the row-averaged results for operators that are constructed with the spin matrix $C\Gamma_5$.
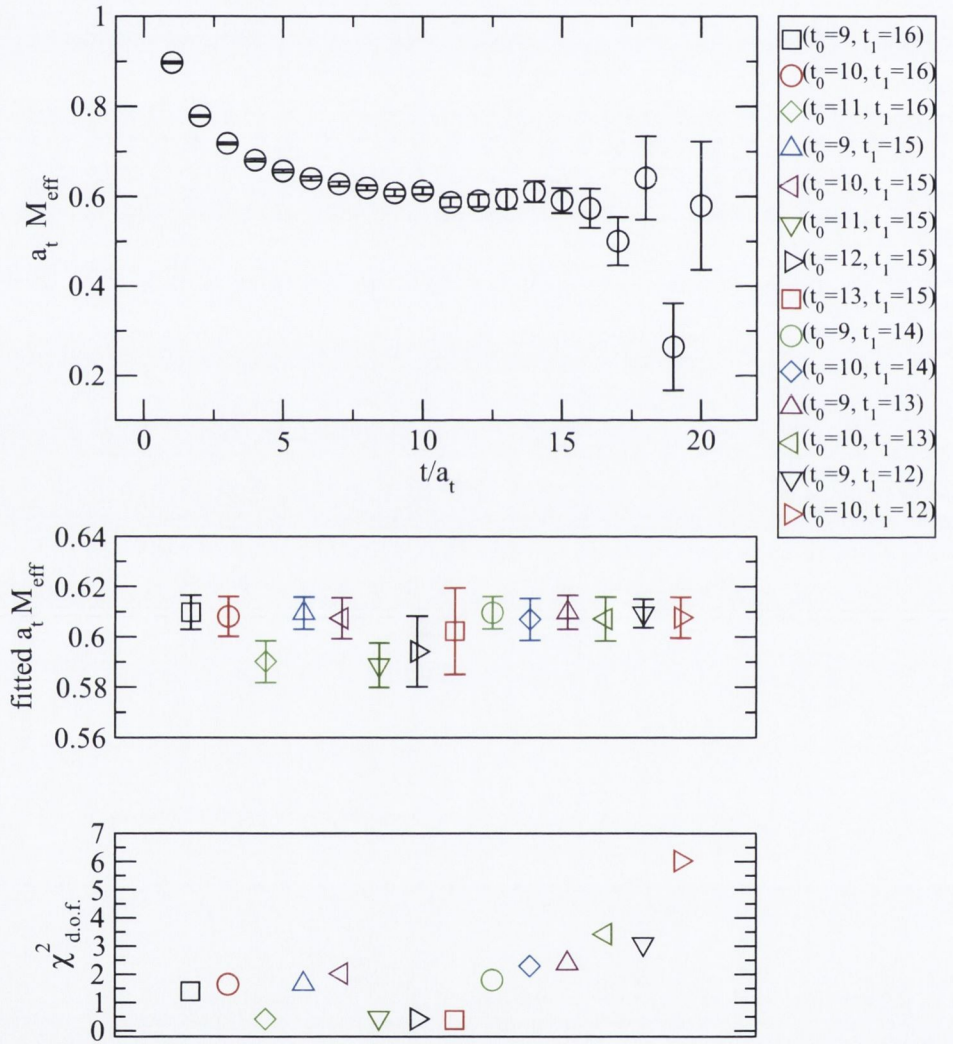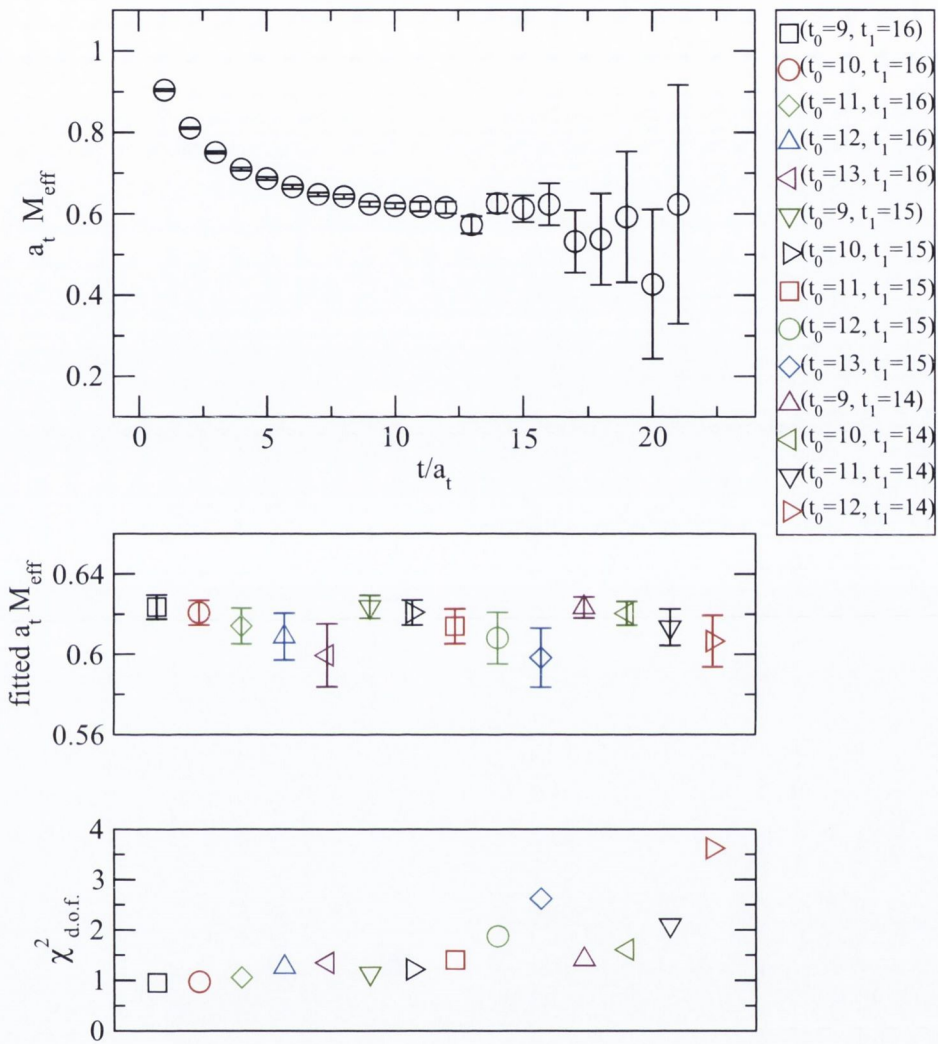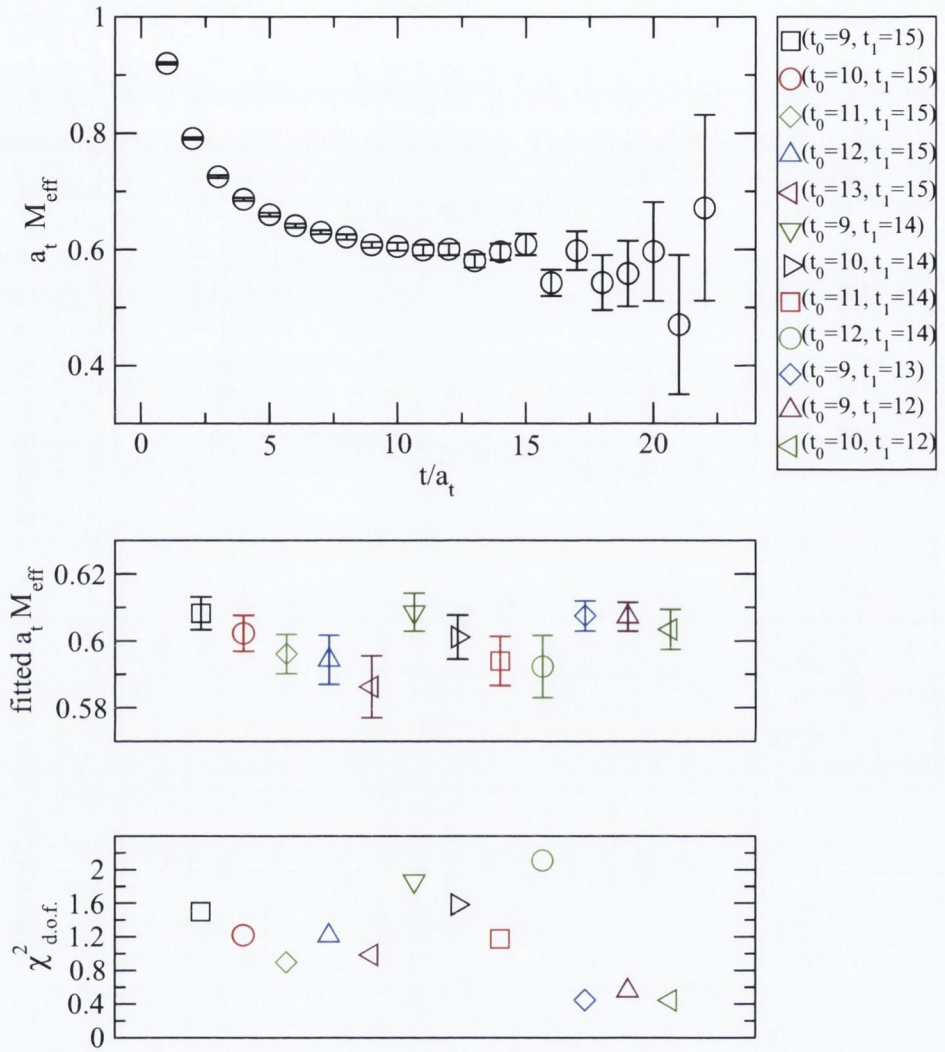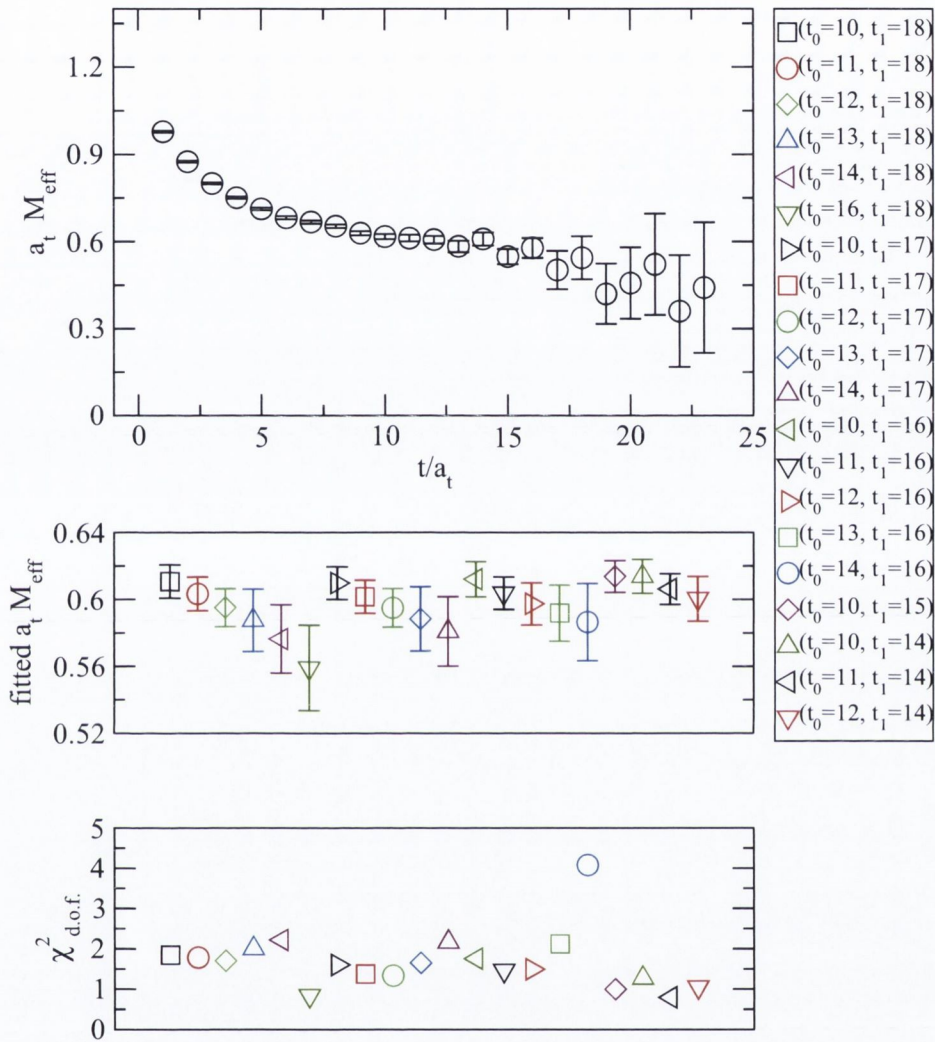
Figure 5-18: Irrep E: $L = 2$, $S = 0$, $J = 2$, $I = 1$, $P = -$.

These are the row-averaged results for operators that are constructed with the spin matrix $C\Gamma_0$.

5.5.4 Fitting Method

For each operator in Figures 5-6 to 5-18 inclusive, it is necessary to select one "best fit". Two criteria were used to select a best fit. The first criterion is that the fitted effective mass must be one of the lowest fitted effected masses for that operator. This criterion eliminates effective masses that include excited state contamination. The second criterion is to chose from the shortlist of good fits, the one with the widest time range. In each case, once the first criterion is met only two to three candidates remain for the best fit. In order to maximize statistics, the one with the wider or widest time range is chosen. Bootstrapping with 100 bootstrap samples is used to estimate the statisical error. Fitting details for the ground state effective masses are given in Table 5.3. There is a wide range in precision ranging from the one percent level to the six percent level. The range of the fit windows vary considerably from three timeslices in length to nine timeslices in length.

State (L, S, J, I, P)	Operator	Fit Range	$\chi^2_{d.o.f.}$	$a_t m$	Precision (%)
$(0, 0, 0, 0, +)$	A_1	$(13, 20)$	1.16	0.405(3)	1
$(0, 0, 0, 0, -)$	A_1	$(10, 18)$	1.33	0.53(3)	6
$(0, 1, 1, 0, +)$	T_1	$(11, 14)$	1.23	0.61(1)	2
$(0, 1, 1, 0, -)$	T_1	$(12, 19)$	0.71	0.534(5)	1
$(2, 0, 2, 0, +)$	E	$(13, 15)$	0.38	0.60(2)	3
$(2, 0, 2, 0, -)$	E	$(12, 15)$	1.87	0.61(1)	2
$(0, 0, 0, 1, +)$	A_1	$(11, 15)$	1.35	0.571(7)	1
$(0, 0, 0, 1, -)$	A_1	$(13, 17)$	0.89	0.532(5)	1
$(0, 1, 1, 1, +)$	T_1	$(13, 17)$	0.89	0.429(3)	1
$(0, 1, 1, 1, -)$	T_1	$(13, 19)$	0.92	0.534(5)	1
$(2, 0, 2, 1, +)$	E	$(11, 14)$	1.17	0.594(7)	1
$(2, 0, 2, 1, -)$	E	$(13, 17)$	1.64	0.59(2)	3

Table 5.3: Ground state fitting details for all states including $\chi^2_{d.o.f.}$ and fitting range (t_0, t_1).

5.6   Mass Splittings

All results presented thusfar have been in lattice units. In order to reconnect with the units of particle physics such as GeV an experimentally determined input is required. The mass of the Ω baryon [7] is used as experimental input to set the scale of the temporal lattice spacing in the units of particle physics [25]. The lattice measurement of Ω was $a_t m_\Omega = 0.353$. Taking the experimentally determined Ω mass of 1.672GeV gives an inverse lattice spacing of $a_t^{-1} = 4.74\text{GeV}$. In this project, there is a self energy correction present in all mass calculations. This correction is the same for all states. This means that only mass differences can successfully be measured. In the literature, mass splittings are typically quoted between pairs of states that differ in only one quantum number. This quantum number is usually either total angular momentum, isospin or parity. Results are presented in a similar fashion in this project except that total angular momentum is replaced by a group irrep label. Mass splittings are presented in Tables 5.4, 5.5 and 5.6.

In Table 5.4, mass splittings between states of different isospin are given. The pair of operators involved in the calculation of the mass splittings share the same orbital angular momentum L, spin S, parity P and total angular momentum J. All mass splittings are taken between pairs of operators belonging to the same irreducible representation of O.

States (L, S, J, I, P)	Splitting m(MeV)	Precision (%)
$(0,0,0,1,+) - (0,0,0,0,+)$	784(25)	3
$(0,0,0,0,-) - (0,0,0,1,-)$	23(15)	65
$(0,1,1,1,-) - (0,1,1,0,-)$	10(6)	60
$(0,1,1,0,+) - (0,1,1,1,+)$	869(42)	5
$(2,0,2,0,-) - (2,0,2,1,-)$	104(87)	84
$(2,0,2,0,+) - (2,0,2,1,+)$	71(58)	82

Table 5.4: Mass splittings between states with the same parity P and total angular momentum J but different isospin I.

In Table 5.5, mass splittings between states of different parity are presented. The pair of operators involved in these calculations share the same orbital angular momentum L, spin S, total angular momentum J and isospin I. All mass splittings are taken from pairs of operators belonging to the same irreducible representation of O.

States (L, S, J, I, P)	Splitting m(MeV)	Precision (%)
$(0, 0, 0, 0, -) - (0, 0, 0, 0, +)$	610(22)	4
$(0, 0, 0, 1, +) - (0, 0, 0, 1, -)$	186(29)	16
$(0, 1, 1, 0, +) - (0, 1, 1, 0, -)$	370(33)	9
$(0, 1, 1, 1, -) - (0, 1, 1, 1, +)$	500(14)	3
$(2, 0, 2, 0, -) - (2, 0, 2, 0, +)$	68(54)	79
$(2, 0, 2, 1, +) - (2, 0, 2, 1, -)$	70(60)	86

Table 5.5: Mass splittings between states with the same isospin I and total angular momentum J but different parity P.

In Table 5.6, mass splittings between pairs of operators belonging to different irreducible representations of O are presented. For a given splitting, the pair of operators share the same isospin I and parity P.

States (L, S, J, I, P)	Splitting m(MeV)	Precision (%)
$(0, 1, 1, 0, +) - (0, 0, 0, 0, +)$	979(42)	4
$(2, 0, 2, 0, +) - (0, 0, 0, 0, +)$	941(79)	8
$(0, 0, 0, 0, -) - (0, 1, 1, 0, -)$	18(13)	72
$(2, 0, 2, 0, -) - (0, 0, 0, 0, -)$	351(63)	18
$(0, 0, 0, 1, +) - (0, 1, 1, 1, +)$	674(29)	4
$(2, 0, 2, 1, +) - (0, 0, 0, 1, +)$	112(32)	29
$(0, 1, 1, 1, -) - (0, 0, 0, 1, -)$	14(9)	64
$(2, 0, 2, 1, -) - (0, 0, 0, 1, -)$	269(82)	30

Table 5.6: Mass splittings between irreducible representations of O.

5.7 Comparison with Experiment

Experimentally, the masses of Λ_b^0, Σ_b^+, Σ_b^-, Σ_b^{*+}, Σ_b^{*-}, Ξ_b^- and Ω_b^- have all been determined [5, 6, 7, 8]. The experimentally determined masses of the baryons relevant to this project are given in Table 5.7. None of the quantum numbers shown have been measured. They are quark model predictions.

State	Mass (GeV)	$I(J^P)$	Quark Content
Λ_b^0	$5{,}620.2 \pm 1.6$	$0(\frac{1}{2}^+)$	udb
Σ_b^+	$5{,}807.8 \pm 2.7$	$1(\frac{1}{2}^+)$	uub
Σ_b^-	$5{,}815.2 \pm 2.0$	$1(\frac{1}{2}^+)$	ddb
Σ_b^{*+}	$5{,}829.0 \pm 3.4$	$1(\frac{3}{2}^+)$	uub
Σ_b^{*-}	$5{,}836.4 \pm 2.8$	$1(\frac{3}{2}^+)$	ddb

Table 5.7: Experimentally determined bottom baryon masses.

As explained in Chapter 4, static-light-light baryon interpolating field operators are labelled by the irreducible representation of O_h to which the diquark belongs. The procedure for comparing these operator results with Particle Data Group (PDG) data is twofold. Firstly, the irrep label of the diquark must be translated into a continuum diquark angular momentum value. Secondly, the heavy quark spin which does not contribute in the static limit of HQET must be reintroduced. In the continuum limit, a static-light-light baryon interpolating field operator in the A_1 irrep of O_h couples to a state with zero diquark total angular momentum. Reintroducing the heavy quark spin gives a $J = \frac{1}{2}$ state. In the continuum limit, a static-light-light baryon interpolating field operator in the T_1 irrep of O_h couples to a state with unit diquark total angular momentum. Reintroducing the heavy quark spin could give a state with $J = \frac{1}{2}$ or $J = \frac{3}{2}$. Experimentally, there is a splitting on the order of 20MeV between these states.

On the lattice, it is possible to calculate the mass splitting between Σ_b and Λ_b. Such a measurement in this project gives

$$\mathrm{m}(\Sigma_b - \Lambda_b) = 110(6)\mathrm{MeV}. \tag{5.1}$$

The experimental result for this splitting is 191(4)MeV. Results for the operator that couples to Λ_b are given in Figure 5-7. Results for the operator that couples to Σ_b are given in Figure 5-13. The statistical precision in the determination of the Λ_b effective mass is one percent. The fit window includes data from eight timeslices. The statistical precision in the determination of the Σ_b effective mass is also one percent. The fit window includes data from five timeslices. Systematic errors are discussed in a later section.

5.8 Contemporary Results

There are a variety of ways of studying heavy hadron physics. Outside of lattice QCD, theoretical work includes the quark model, the QCD sum rules and the combined heavy quark and $1/N_C$ expansions. Within lattice QCD different collaborations have been studying the b-hadron spectrum using different approaches.

Non-relativistic quantum chromodynamics (NRQCD) [52] is used for bottom quark simulations in [9]. Actions are computed by CP-PACS and JLQCD [53, 54]. The gauge action is an Iwasaki action and the fermion action is a clover improved action. Results are obtained at a single lattice spacing. Eight different ensembles are used corresponding to two different strange quark masses and four different light quark masses. Simulations are performed at three values of the heavy quark bare mass allowing for an interpolation to the physical bottom mass value. Extrapolations are made for up/down quarks and interpolations are made to the physical strange quark mass. The measured value in this setup for the $\Sigma_b - \Lambda_b$ splitting is 154(26)MeV.

Another group [10] uses NRQCD to simulate the b quark. Sea and valence quarks are treated with the domain wall fermion action [55]. The gauge action is an Iwasaki gauge action [56, 57]. The gauge ensembles used are generated by the RBC and UKQCD collaborations [58]. All calculations are performed at a single lattice spacing. Spin splittings are calculated. The $\Sigma_b^* - \Sigma_b$ splitting is measured to be 25(25)MeV.

One group simulates the b quark with an improved clover heavy quark action with the Fermilab interpretation [59]. They use MILC lattice gauge configurations with $2 + 1$ dynamical sea quark flavors [60]. An improved staggered fermion action is

used for the light quarks [60]. Fine ($a \approx 0.09$fm), coarse ($a \approx 0.12$fm) and medium-coarse ($a \approx 0.15$fm) lattices are used. Mass differences are calculated from the ratio of propagators. Extrapolations to the chiral limit are made using the full QCD data points. The mass differences $\Xi_b - \Lambda_b$, $\Xi_b' - \Sigma_b$ and $\Omega_b - \Xi_b'$ agree well with the PDG data. All results are plotted in [11, 12]. Possible sources of error in these calculations include a constant mass shift due to the heavy quark or the hyper-fine structure of the singly heavy baryon.

The Bern-Graz-Regensburg BGR collaboration [13] simulates the b quark with a static quark action. Dynamical $N_f = 2$ ensembles are used. The gauge action is a one-loop improved Luscher-Weisz action for both the sea and the valence quarks. Chirally improved fermions are used for the light quarks. The signal-to-noise ratio of long distance correlations is greatly enhanced by implementing the so-called domain-decomposition improvement [61]. Both baryon mass differences and baryon-meson mass differences are calculated. Extrapolations to $m_{u/d}$ and interpolations to m_s are performed by plotting mass differences against m_π^2. Finite-a dynamical mass differences agree with experimental values. Some calculations of the $1/m_Q$ kinetic corrections are also carried out. The measured value in this setup for the $\Sigma_b - \Lambda_b$ splitting is 200(27)MeV.

Another group [14] simulates the b quark with a static quark action. Ensembles of $2 + 1$ flavor lattices are used. These are generated by the RBC and UKQCD collaborations using Iwasaki gauge actions. Domain wall propagators are computed for the light and strange quarks using various different partially quenched quark masses. The static limit of HQET is taken for the bottom quark. In this limit the $J^P = 1/2^+$ states ($\Sigma_b, \Xi_b', \Omega_b$) and the $J^P = 3/2^+$ states ($\Sigma_b^*, \Xi_b'^*, \Omega_b^*$) become degenerate. Simple linear, quadratic and cubic fits to m_π^2 give the chiral extrapolations. Mass differences are calculated at a single lattice spacing. The measured value in this setup for the $\Sigma_b - \Lambda_b$ splitting is 190(130)MeV.

Yet another group [15] simulates the b quark with a static quark action. The gauge action used is a one-loop tadpole improved gauge action generated by the MILC collaboration. The fermion action for the sea quarks is the asqtad improved

Kogut-Susskind action. Domain-wall fermions are used for the light valence quarks. Chiral extrapolations to the light quark mass are made by fitting data to m_π^2. The strange quark mass value is already near the physical point, this can be accounted for by a systematic error. Mass splittings are calculated. The measured value in this setup for the $\Sigma_b - \Lambda_b$ splitting is 274(25).

The European Twisted Mass Collaboration takes the static limit of HQET to simulate the b quark [41]. A HYP2 [62, 63, 64] static action is used for the b quark. $N_f = 2$ flavour ETMC gauge fields are used. The gauge action is tree-level symanzik improved. The fermion action is a Wilson twisted mass action. Light quarks with the same mass as the sea quarks are used for a range of pion masses. Extrapolation to the physical point is taken. Masses are determined at a single lattice spacing. This group presents the first results for negative parity states. Results agree with quark model predictions. Mass predictions from three different quark models [65, 66, 67] are given in Table 5.8. A comparison of the results from this project with the ETMC results is given in Table 5.9. The ETMC mass splittings are given in Table 5.10. The corresponding splittings measured in this project are given in Table 5.11

It is worth noting that in Table 5.8 particles are labelled by their total angular momentum J. In the static limit of HQET the static quark does not contribute to total angular momentum.

$I(J^P)$	m(MeV)[65]	m(MeV)[66]	m(MeV)[67]
$0(\frac{1}{2}^+)$	5622	5585	5624
$0(\frac{3}{2}^+)$	6189	6145	6246
$0(\frac{1}{2}^-)$	5930	5912	5890
$0(\frac{3}{2}^-)$	5947	5920	5890
$1(\frac{1}{2}^+)$	5805	5795	5789
$1(\frac{3}{2}^+)$	5834	5805	5844
$1(\frac{1}{2}^-)$	6108	6070	6039
$1(\frac{3}{2}^-)$	6076	6070	6039

Table 5.8: Various quark model mass splittings.

$I(J^P)$	(Trinlat)$a_t m$	Precision (%)	(ETMC)$a_t m$	Precision (%)
$0(0^+)$	0.405(3)	1	0.1889(85)	5
$0(0^-)$	0.534(4)	1	0.5612(318)	6
$0(1^-)$	0.534(5)	1	0.3727(175)	5
$1(0^-)$	0.532(6)	1	0.3519(440)	13
$1(1^+)$	0.429(3)	1	0.2629(84)	3
$1(1^-)$	0.534(5)	1	0.4376(162)	4

Table 5.9: Comparison between Trinlat and ETMC data.

State 1 $I(J^P)$,State 2 $I(J^P)$	Mass difference MeV	Precision (%)
$0(0^-)$, $0(0^+)$	1069(161)	15
$0(0^-)$, $0(1^-)$	818(194)	24
$0(1^-)$, $0(0^+)$	251(123)	49
$1(0^-)$, $1(1^+)$	294(182)	62
$1(1^-)$, $1(0^-)$	132(197)	149
$1(1^-)$, $1(1^+)$	426(99)	23
$1(1^+)$, $0(0^+)$	181(60)	33

Table 5.10: ETMC mass splittings.

State 1 $I(J^P)$,State 2 $I(J^P)$	Mass difference MeV	Precision (%)
$0(0^-)$, $0(0^+)$	610(22)	4
$0(0^-)$, $0(1^-)$	18(13)	72
$0(1^-)$, $0(0^+)$	609(21)	3
$1(0^-)$, $1(1^+)$	488(17)	3
$1(1^-)$, $1(0^-)$	14(9)	64
$1(1^-)$, $1(1^+)$	500(14)	3
$1(1^+)$, $0(0^+)$	110(5)	5

Table 5.11: Trinlat mass splittings.

The mass splitting between the Σ_b baryon and the Λ_b baryon has been measured by all of the lattice groups working on heavy baryons. The results from this project compare well with these results. A direct comparison is given in Table 5.12. Results by Meinel as well as results by Gottlieb and Na agree with experiment. Their results appear in plots in [10, 11, 12].

Group	m $(\Sigma_b - \Lambda_b)$(MeV)	Precision (%)
This project	110(5)	5
Detmold, Lin, Wingate	190(130)68	77
Lin, Cohen, Mathur, Orginos	274(25)	9
BGR	200(27)	14
Lewis and Woloshyn	154(26)17	20
ETMC	181(60)	33
PDG	191(4)	2

Table 5.12: Comparison of different $\Sigma_b - \Lambda_b$ lattice mass splitting calculations.

In summary, high precision calculations of ground state masses have been performed. The statistical precision in mass fittings is typically at the one percent level and at most is at the six percent level. The ordering of states calculated in this project is in agreement with contemporary lattice work, quark models and exper-

iment. The calculation of the $\Sigma_b - \Lambda_b$ splitting is 80MeV lower than experiment. Systematic errors of $\mathcal{O}(100)$MeV appear in mass splittings. Negative parity states have been calculated as well as the first $J = 2$ mass splittings.

5.9   Systematic Errors

Many sources of systematic error appear in this work including finite-volume effects, simulating at unphysical light quark masses, taking the static approximation of HQET and discretization effects. Simulations were run at a single lattice spacing and for a single quark mass. Therefore it is not possible to study the continuum limit behaviour, the dependence on the light-quark mass or possible finite-volume effects. A detailed study of the errors is beyond the scope of this project. Instead a brief description is given here.

The scaling behaviour for the anisotropic clover fermion action is $\mathcal{O}(a)^2$. Tuning removes possible $\mathcal{O}(a)$ errors. There is a leading discretization error in the Symanzik-improved gauge action with tree-level tadpole improved coefficients of $\mathcal{O}(a_s^4, a_t^2, g^2 a_s^2)$ [25]. According to HQET, the leading error to the static approximation is $\mathcal{O}(1/m_Q)$ where m_Q is the mass of the heavy quark. The statistical error in the number of gauge configurations scales as $\frac{1}{\sqrt{N}}$, where N is the number of configurations. Simulations were run on 49 configurations of gauge fields. The statistical precision of results in this project is high.

An understanding of the systematic errors involved in this project is possible by drawing a comparison with work done by the Hadron Spectrum Collaboration [22] which has performed hadron spectroscopy using the same lattices as this project. Recent work on charmonium [68] assigns an approximate scale of 40MeV to the leading-order $\mathcal{O}(a_s)$ correction to the fermion action arising from using the tree-level tadpole-improved value for c_s. However, a full study of the discretisation effects by using a non-perturbatively determined value of c_s was not conducted. A volume dependence study of light meson spectroscopy showed no significant change in results between $16^3 \times 128$ and $20^3 \times 128$ lattices [69]. A study of the light quark mass dependence of light meson spectroscopy results on quark masses down to pion masses

81

~ 400MeV was also conducted. Only a mild dependence of results on the quark mass was observed. Experimentally the $\Sigma_b^* - \Sigma_b$ splitting has been measured at 21MeV. These $J = 3/2$ and $J = 1/2$ states become degenerate in the static limit of HQET. For this reason the $\mathcal{O}(1/m_Q)$ correction is expected to be relatively small [41].

In summary, it is worth emphasising that a detailed analysis of systematic errors is beyond the scope of this project. Reference has been made to the most relevant contemporary lattice work in an attempt to quantify the systematic errors. This approach has its drawbacks insofar as systematic studies of all the sources of error incurred in this project do not exist.

Chapter 6

Concluding Remarks

The focus of this project was a complete examination of the use of distillation on an anisotropic lattice in the static limit of HQET. To this end, a knowledge was required of how to construct the most general non-local baryon interpolating field operator transforming as an irreducible representation of O_h. The measured quantity from simulations was the static-light-light correlation function. A small number of correlation matrices were also measured and analysed.

The first step in examining the spectrum of static-light-light baryons is the construction of non-local baryon interpolating field operators, as discussed in Chapter 4. This is the first time that the techniques for constructing spatially extended hadron operators have been applied to static-light-light baryons. Non-local operators were constructed, and correlation functions between a source operator at timeslice t and a sink operator at timeslice $t + dt$ were measured. In order to improve statistics, averaging over all source timeslices t was taken. Single exponentials were fitted to these correlation functions. Ground state effective masses were obtained. The effective mass plot typically shows three regions. The first region is characterized by excited state contamination. The second region shows a plateau. The third region is characterized by noise. The divide between these three regions can be quite blurred. Tests were conducted to establish how the effective mass depends on the number of eigenvectors N_{ev}. It was established that increasing the number of eigenvectors from between 4 and 24 shows a dramatic reduction in excited state contamination as well

as a reduction in noise.

Once the eigenvector dependence was understood, studies of some low dimensional ($n_{dim} < 6$) correlation functions were performed. Operators belonging to the same irreducible representation of O_h, but with different light quark field displacements were utilized. To begin, one-link, two-link and three-link operators were used to construct correlation matrices. The variational analysis of the correlation matrices showed two interesting results. Firstly, no excited states were found. Secondly, diagonalization of the correlation matrices gave the same ground state effective mass as any of the effective masses obtained from self-correlators. In a successful variational analysis optimized correlators are constructed. The optimized correlator for the ground state would give a better determination of the ground state mass than would the input correlators. Further variational analysis was performed using operators with the light quarks displaced from the static quark by ever increasing distance. Again the results were the same. This prompted the study of various elaborate operators.

Detailed studies were conducted on the dependence of the profile of the effective mass plot (obtained from single exponential fits to the correlator) with the diquark displacement vectors. C-code was written to construct different spatial configurations of diquarks with both light quarks displaced from the static quark, from each other and less than eight lattice units in radius. A sample of more than 250 such diquarks were tested on a data set of 5 configurations and with $N_{ev} = 4$. The operators in question belonged to the A_1 irreducible representation of O_h. Both isospin-0 and isospin-1 sectors were tested as well as both parities. No variation in the effective mass profile was observed. It was concluded that finding static-light-light baryon interpolating field operators suitable for variational analysis and optimization is challenging.

Determining the low-lying ground state static-light-light spectrum subsequently became the sole focus of the project. Ground state fittings to 12 different operators were carried out and ground state masses, which include a constant self-energy correction, were determined with reasonable success. Mass splittings were calculated. The range in precision between results is from the one percent level to the six percent level. Some of the results obtained in this project do not yet have a lattice counter-

part. The ETMC has measured a subset of the masses and mass splittings that lie within the scope of this project. Their results are in agreement with quark models. Some ETMC mass splittings differ in magnitude from the results presented here.

Experimentally, only one mass splitting is a suitable candidate for comparison: the Σ_b - Λ_b mass splitting. This splitting has been calculated by various lattice groups by treating the heavy quark in various lattice setups - NRQCD, HQET, clover fermions with the Fermilab interpretation. The lattice results from different collaborations are all of the same order of magnitude. Precision varies across collaborations. The Σ_b - Λ_b splitting extracted in this project is smaller than the experimental result.

In summary, some high precision measurements have been performed. In general the A_1 and the T_1 operators give a better signal than the E operators. The use of distillation on an anisotropic lattice in the static limit of HQET produces results with a high level of statistical precision. Mass predictions for the four $J = 2$ states have been made. Quantifying systematic errors has been beyond the scope of this project. Comparing results with contemporay work suggests large systematic errors arise. There are two obvious candidates for further work in this area. The first would be to simulate at a different lattice spacing in an attempt to study discretization effects. The second would be to include $\mathcal{O}(1/m_Q)$ corrections to the static approximation of HQET.

Appendix

Mathematical Definitions

The commutator of two matrices A and B is denoted $[A, B]$ and is defined as

$$[A, B] = AB - BA. \tag{A-1}$$

The Heaviside step function denoted Θ is given by

$$\Theta(\text{x}) = \begin{cases} 0 & \text{if } x < 0; \\ 1 & \text{if } x \geq 0. \end{cases} \tag{A-2}$$

The Levi-Civita tensor denoted ϵ^{abc} is defined by

$$\epsilon^{abc} = \begin{cases} 0 & \text{if any two labels are the same;} \\ 1 & \text{if a, b, c is an even permutation of 1, 2, 3;} \\ -1 & \text{if a, b, c is an odd permutation of 1, 2, 3.} \end{cases} \tag{A-3}$$

There are three even permutations of 123. They are 123, 312 and 231. There are three odd permutations of 123. They are 213, 132 and 321. An even(odd) permutation of 123 is obtained by an even(odd) number of interchanges of two of the elements in the ordered list 123.

The trace of a matrix A denoted $\text{Tr}[A]$ is the sum of the diagonal elements of A. For example, the trace of the following 2×2 matrix

$$B = \begin{pmatrix} a & b \\ c & d \end{pmatrix} \tag{A-4}$$

is given by $\text{Tr}[B] = a + d$.

The real part of the trace of a complex matrix B is denoted $\text{ReTr}[B]$.

Representation Theory

This section begins with formal definitions needed to explain the group theory.

Definition: An element T of a group G is conjugate to $S \in G$ if there exists $X \in G$ such that

$$T = XSX^{-1}. \tag{A-5}$$

From this definition it follows that S is also conjugate to T i.e. $S = X^{-1}T(X^{-1})^{-1}$.

Corollary:If S is conjugate to T and R is conjugate to T then R and S are both conjugate.

$$S = XTX^{-1} \qquad \text{(A-6)}$$

and

$$R = YTY^{-1} \qquad \text{(A-7)}$$

imply

$$R = Y(X^{-1}SX)Y^{-1} = (YX^{-1})S(XY^{-1}) = (YX^{-1})S(YX^{-1})^{-1}. \qquad \text{(A-8)}$$

Definition: A conjugacy class of a group G is a set of mutually conjugate elements of G.

Definition: A mapping f of a group G_1 onto a group G_2 is said to be homomorphic if it has the property

$$f(S)f(T) = f(ST) \qquad \text{(A-9)}$$

for all $S, T \in G_1$.

Definition: The inverse of an $n \times n$ matrix A is the $n \times n$ matrix A^{-1} such that

$$AA^{-1} = A^{-1}A = I, \qquad \text{(A-10)}$$

where the $n \times n$ identity matrix I is the matrix with ones on the diagonal and zeroes elsewhere.

Definition: An $n \times n$ matrix that does not possess an inverse is said to be singular.

Definition: An $n \times n$ matrix that does possess an inverse is said to be non-singular.

Definition: Given a group of non-singular $n \times n$ matrices $\Gamma(T)$ with matrix multiplication as the group operation, if there exists a homomorphic mapping of a group G onto this group of matrices then the group of matrices is said to form an n-dimensional representation of G.

Definition: Let Γ be an n-dimensional representation of a group G. The character of $T \in G$ in the representation Γ is denoted $\chi(T)$ and is given by

$$\chi(T) = \text{Tr}[\Gamma(T)] = \sum_{i=1}^{n} \Gamma(T)_{ii}. \qquad \text{(A-11)}$$

Theorem: Given a representation Γ of a group G, all elements in the same conjugacy class have the same character in the representation Γ [18].

Theorem: Given an n-dimensional representation Γ of a group G and an $n \times n$ matrix P there exists an n-dimensional representation Γ' defined via a similarity transformation with the representation Γ. For each $T \in G$ the matrix $\Gamma'(T)$ is defined by

$$\Gamma'(T) = P^{-1}\Gamma(T)P. \tag{A-12}$$

The representations Γ' and Γ are called equivalent.

Definition: A reducible n-dimensional representation Γ of a group G is a representation that is equivalent to a representation Γ' where the matrices $\Gamma'(T)$ are of the form

$$\Gamma'(T) = \begin{pmatrix} \Gamma_{11}(T) & \Gamma_{12}(T) \\ 0 & \Gamma_{22}(T) \end{pmatrix}, \tag{A-13}$$

for each $T \in G$, where $\Gamma_{11}(T), \Gamma_{12}(T), \Gamma_{22}(T)$ and the zero matrix 0 have dimensions $s_1 \times s_1$, $s_1 \times s_2$, $s_2 \times s_2$ and $s_2 \times s_1$, respectively. $s_1 \geq 1$ and $s_2 \geq 1$. s_1 and s_2 take the same values for all $T \in G$.

Definition: An irreducible representation of a group G is a representation that is not reducible.

Theorem: For a finite group G the number of inequivalent single-valued irreducible representations is equal to the number of conjugacy classes of G [18].

Definition: Given a representation $\Gamma(G) = \{\Gamma(g); g \in G\}$ of a group G and a subgroup $H = \{h\}$ of G, the subduced representation of $\Gamma(g)$ onto H denoted as $\Gamma^{\downarrow}(H)$ (or $[\Gamma(G) \downarrow H]$) is defined by restricting Γ to H and is given by

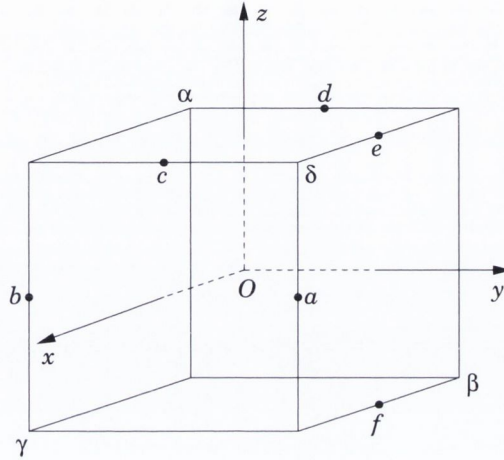$$\Gamma^{\downarrow}(H) = \{\Gamma(h); h \in H\}. \tag{A-14}$$

Cubic Group

Figure A-1: Conjugacy classes of O.

C_{np} denotes a proper rotation through $2\pi/n$ in the right-hand screw sense about the axis Op. $\mathcal{C}_1$ contains the identity operator E. $\mathcal{C}_2$ contains the eight rotations $C_{3\alpha}$, $C_{3\alpha}^{-1}$, $C_{3\beta}$, $C_{3\beta}^{-1}$, $C_{3\gamma}$, $C_{3\gamma}^{-1}$, $C_{3\delta}$ and $C_{3\delta}^{-1}$. $C_{3\alpha}^{-1}$, $C_{3\beta}^{-1}$, $C_{3\gamma}^{-1}$ and $C_{3\delta}^{-1}$ denote rotations of $-2\pi/3$ in the right-hand screw sense about the axes $O\alpha$, $O\beta$, $O\gamma$ and $O\delta$, respectively. $\mathcal{C}_3$ contains the three rotations C_{2x}, C_{2y} and C_{2z}. $\mathcal{C}_4$ contains the six rotations C_{4x}, C_{4x}^{-1}, C_{4y}, C_{4y}^{-1}, C_{4z} and C_{4z}^{-1}. C_{4x}^{-1}, C_{4y}^{-1} and C_{4z}^{-1} denote rotations through $-2\pi/4$ in the right-hand screw sense about the axes Ox, Oy and Oz, respectively. $\mathcal{C}_5$ contains the six rotations C_{2a}, C_{2b}, C_{2c}, C_{2d}, C_{2e} and C_{2f}.

$O_h = O \times \{\mathbb{1}, \mathcal{P}\}$ has ten conjugacy classes. The spatial inversion operator $\mathcal{P}$ applied to C_1, C_2, C_3, C_4 and C_5 give the conjugacy classes C_6, C_7, C_8, C_9 and C_{10}, respectively. Details of O and O_h are given in [18].

Tensor in Minkowski Space

The tensor $g^{\mu\nu}$ with $\mu, \nu \in \{0, 1, 2, 3\}$ is defined as follows

$$g = \begin{pmatrix} 1 & 0 & 0 & 0 \\ 0 & -1 & 0 & 0 \\ 0 & 0 & -1 & 0 \\ 0 & 0 & 0 & -1 \end{pmatrix}. \tag{A-15}$$

Gamma Matrices

The Euclidean metric tensor $\delta^{\mu\nu}$ with $\mu, \nu \in \{0, 1, 2, 3\}$ is defined as follows

$$\delta = \begin{pmatrix} 1 & 0 & 0 & 0 \\ 0 & 1 & 0 & 0 \\ 0 & 0 & 1 & 0 \\ 0 & 0 & 0 & 1 \end{pmatrix}. \tag{A-16}$$

The Dirac basis is given below.

$$\Gamma_0 = \begin{pmatrix} 1 & 0 & 0 & 0 \\ 0 & 1 & 0 & 0 \\ 0 & 0 & -1 & 0 \\ 0 & 0 & 0 & -1 \end{pmatrix} = \begin{pmatrix} \sigma_0 & 0 \\ 0 & -\sigma_0 \end{pmatrix}, \tag{A-17}$$

$$\text{where } \sigma_0 = \begin{pmatrix} 1 & 0 \\ 0 & 1 \end{pmatrix}. \tag{A-18}$$

$$\Gamma_1 = \begin{pmatrix} 0 & 0 & 0 & 1 \\ 0 & 0 & 1 & 0 \\ 0 & -1 & 0 & 0 \\ -1 & 0 & 0 & 0 \end{pmatrix} = \begin{pmatrix} 0 & \sigma_1 \\ -\sigma_1 & 0 \end{pmatrix}, \tag{A-19}$$

$$\text{where } \sigma_1 = \begin{pmatrix} 0 & 1 \\ 1 & 0 \end{pmatrix}. \tag{A-20}$$

$$\Gamma_2 = \begin{pmatrix} 0 & 0 & 0 & -i \\ 0 & 0 & i & 0 \\ 0 & i & 0 & 0 \\ -i & 0 & 0 & 0 \end{pmatrix} = \begin{pmatrix} 0 & \sigma_2 \\ -\sigma_2 & 0 \end{pmatrix}, \tag{A-21}$$

$$\text{where } \sigma_2 = \begin{pmatrix} 0 & -i \\ i & 0 \end{pmatrix}. \tag{A-22}$$

$$\Gamma_3 = \begin{pmatrix} 0 & 0 & 1 & 0 \\ 0 & 0 & 0 & -1 \\ -1 & 0 & 0 & 0 \\ 0 & 1 & 0 & 0 \end{pmatrix} = \begin{pmatrix} 0 & \sigma_3 \\ -\sigma_3 & 0 \end{pmatrix}, \tag{A-23}$$

$$\text{where } \sigma_3 = \begin{pmatrix} 1 & 0 \\ 0 & -1 \end{pmatrix}. \tag{A-24}$$

$$\Gamma_5 = i\Gamma_0\Gamma_1\Gamma_2\Gamma_3 = \begin{pmatrix} 0 & 0 & 1 & 0 \\ 0 & 0 & 0 & 1 \\ 1 & 0 & 0 & 0 \\ 0 & 1 & 0 & 0 \end{pmatrix} = \begin{pmatrix} 0 & 1 \\ 1 & 0 \end{pmatrix}. \tag{A-25}$$

$$C = i\gamma_2\gamma_0 = \begin{pmatrix} 0 & 0 & 0 & -1 \\ 0 & 0 & 1 & 0 \\ 0 & -1 & 0 & 0 \\ 1 & 0 & 0 & 0 \end{pmatrix} \tag{A-26}$$

Representation Matrices of O_h

$$R(E) = \begin{pmatrix} 1 & 0 & 0 \\ 0 & 1 & 0 \\ 0 & 0 & 1 \end{pmatrix}, \tag{A-27}$$

where E denotes the identity element,

$$R(C_{3\alpha}) = \begin{pmatrix} 0 & 0 & -1 \\ 1 & 0 & 0 \\ 0 & -1 & 0 \end{pmatrix}, \tag{A-28}$$

$$R(C_{3\alpha}^{-1}) = \begin{pmatrix} 0 & 1 & 0 \\ 0 & 0 & -1 \\ -1 & 0 & 0 \end{pmatrix}, \tag{A-29}$$

$$R(C_{3\beta}) = \begin{pmatrix} 0 & 0 & 1 \\ -1 & 0 & 0 \\ 0 & -1 & 0 \end{pmatrix}, \tag{A-30}$$

$$R(C_{3\beta}^{-1}) = \begin{pmatrix} 0 & -1 & 0 \\ 0 & 0 & -1 \\ 1 & 0 & 0 \end{pmatrix}, \tag{A-31}$$

$$R(C_{3\gamma}) = \begin{pmatrix} 0 & 0 & -1 \\ -1 & 0 & 0 \\ 0 & 1 & 0 \end{pmatrix}, \tag{A-32}$$

$$R(C_{3\gamma}^{-1}) = \begin{pmatrix} 0 & -1 & 0 \\ 0 & 0 & 1 \\ -1 & 0 & 0 \end{pmatrix}, \tag{A-33}$$

$$R(C_{3\delta}) = \begin{pmatrix} 0 & 0 & 1 \\ 1 & 0 & 0 \\ 0 & 1 & 0 \end{pmatrix}, \tag{A-34}$$

$$R(C_{3\delta}^{-1}) = \begin{pmatrix} 0 & 1 & 0 \\ 0 & 0 & 1 \\ 1 & 0 & 0 \end{pmatrix}, \tag{A-35}$$

$$R(C_{2x}) = \begin{pmatrix} 1 & 0 & 0 \\ 0 & -1 & 0 \\ 0 & 0 & -1 \end{pmatrix}, \tag{A-36}$$

$$R(C_{2y}) = \begin{pmatrix} -1 & 0 & 0 \\ 0 & 1 & 0 \\ 0 & 0 & -1 \end{pmatrix}, \tag{A-37}$$

$$R(C_{2z}) = \begin{pmatrix} -1 & 0 & 0 \\ 0 & -1 & 0 \\ 0 & 0 & 1 \end{pmatrix}, \tag{A-38}$$

$$R(C_{4x}) = \begin{pmatrix} 1 & 0 & 0 \\ 0 & 0 & -1 \\ 0 & 1 & 0 \end{pmatrix}, \tag{A-39}$$

$$R(C_{4x}^{-1}) = \begin{pmatrix} 1 & 0 & 0 \\ 0 & 0 & 1 \\ 0 & -1 & 0 \end{pmatrix}, \tag{A-40}$$

$$R(C_{4y}) = \begin{pmatrix} 0 & 0 & 1 \\ 0 & 1 & 0 \\ -1 & 0 & 0 \end{pmatrix}, \tag{A-41}$$

$$R(C_{4y}^{-1}) = \begin{pmatrix} 0 & 0 & -1 \\ 0 & 1 & 0 \\ 1 & 0 & 0 \end{pmatrix}, \tag{A-42}$$

$$R(C_{4z}) = \begin{pmatrix} 0 & -1 & 0 \\ 1 & 0 & 0 \\ 0 & 0 & 1 \end{pmatrix}, \tag{A-43}$$

$$R(C_{4z}^{-1}) = \begin{pmatrix} 0 & 1 & 0 \\ -1 & 0 & 0 \\ 0 & 0 & 1 \end{pmatrix}, \tag{A-44}$$

$$R(C_{2a}) = \begin{pmatrix} 0 & 1 & 0 \\ 1 & 0 & 0 \\ 0 & 0 & -1 \end{pmatrix}, \tag{A-45}$$

$$R(C_{2b}) = \begin{pmatrix} 0 & -1 & 0 \\ -1 & 0 & 0 \\ 0 & 0 & -1 \end{pmatrix}, \tag{A-46}$$

$$R(C_{2c}) = \begin{pmatrix} 0 & 0 & 1 \\ 0 & -1 & 0 \\ 1 & 0 & 0 \end{pmatrix}, \tag{A-47}$$

$$R(C_{2d}) = \begin{pmatrix} 0 & 0 & -1 \\ 0 & -1 & 0 \\ -1 & 0 & 0 \end{pmatrix}, \tag{A-48}$$

$$R(C_{2e}) = \begin{pmatrix} -1 & 0 & 0 \\ 0 & 0 & 1 \\ 0 & 1 & 0 \end{pmatrix}, \tag{A-49}$$

$$R(C_{2f}) = \begin{pmatrix} -1 & 0 & 0 \\ 0 & 0 & -1 \\ 0 & -1 & 0 \end{pmatrix}, \tag{A-50}$$

$$R(P) = \begin{pmatrix} -1 & 0 & 0 \\ 0 & -1 & 0 \\ 0 & 0 & -1 \end{pmatrix}. \tag{A-51}$$

Gell-Mann Matrices

The eight Gell-Mann matrices are given below.

$$\lambda_1 = \begin{pmatrix} 0 & 1 & 0 \\ 1 & 0 & 0 \\ 0 & 0 & 0 \end{pmatrix}, \tag{A-52}$$

$$\lambda_2 = \begin{pmatrix} 0 & -i & 0 \\ i & 0 & 0 \\ 0 & 0 & 0 \end{pmatrix}, \tag{A-53}$$

$$\lambda_3 = \begin{pmatrix} 1 & 0 & 0 \\ 0 & -1 & 0 \\ 0 & 0 & 0 \end{pmatrix}, \tag{A-54}$$

$$\lambda_4 = \begin{pmatrix} 0 & 0 & 1 \\ 0 & 0 & 0 \\ 1 & 0 & 0 \end{pmatrix}, \tag{A-55}$$

$$\lambda_5 = \begin{pmatrix} 0 & 0 & -i \\ 0 & 0 & 0 \\ i & 0 & 0 \end{pmatrix}, \tag{A-56}$$

$$\lambda_6 = \begin{pmatrix} 0 & 0 & 0 \\ 0 & 0 & 1 \\ 0 & 1 & 0 \end{pmatrix}, \tag{A-57}$$

$$\lambda_7 = \begin{pmatrix} 0 & 0 & 0 \\ 0 & 0 & -i \\ 0 & i & 0 \end{pmatrix}, \tag{A-58}$$

$$\lambda_8 = \frac{1}{\sqrt{3}} \begin{pmatrix} 1 & 0 & 0 \\ 0 & 1 & 0 \\ 0 & 0 & -2 \end{pmatrix}. \tag{A-59}$$

Irreducible Representations of O_h

Tensor Product	Irreducible Representation
$A_{1g} \otimes A_{1g}$	A_{1g}
$A_{1u} \otimes A_{1u}$	A_{1g}
$A_{1g} \otimes A_{1u}$	A_{1u}
$A_{1u} \otimes A_{1g}$	A_{1u}
$A_{1g} \otimes E_g$	E_g
$A_{1u} \otimes E_u$	E_g
$A_{1g} \otimes E_u$	E_u
$A_{1u} \otimes E_g$	E_u
$A_{1g} \otimes T_{1g}$	T_{1g}
$A_{1u} \otimes T_{1u}$	T_{1g}
$A_{1g} \otimes T_{1u}$	T_{1u}
$A_{1u} \otimes T_{1g}$	T_{1u}

Table A-1: List of spin-0 operators.

Tensor Product	Irreducible Representation
$T_{1g} \otimes A_{1g}$	T_{1g}
$T_{1u} \otimes A_{1u}$	T_{1g}
$T_{1g} \otimes A_{1u}$	T_{1u}
$T_{1u} \otimes A_{1g}$	T_{1u}

Table A-2: List of spin-1 operators.

Results for $S = 1$
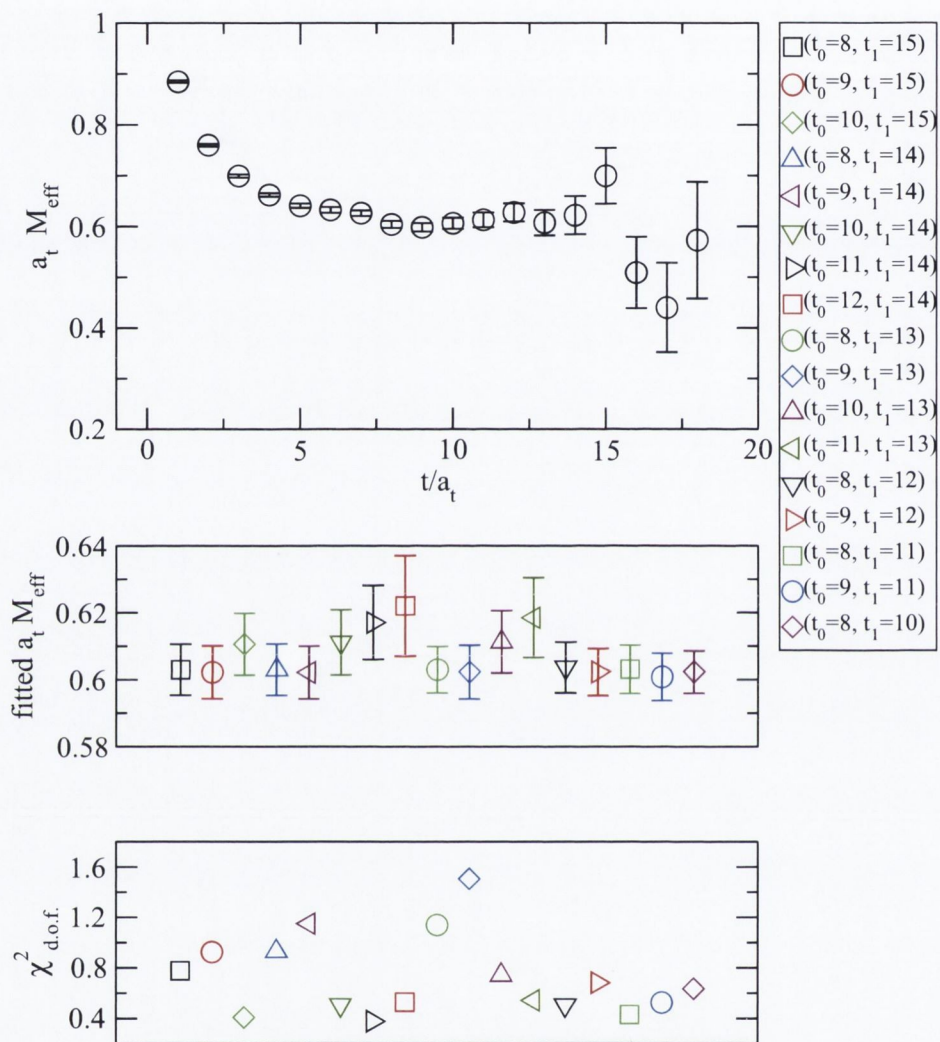
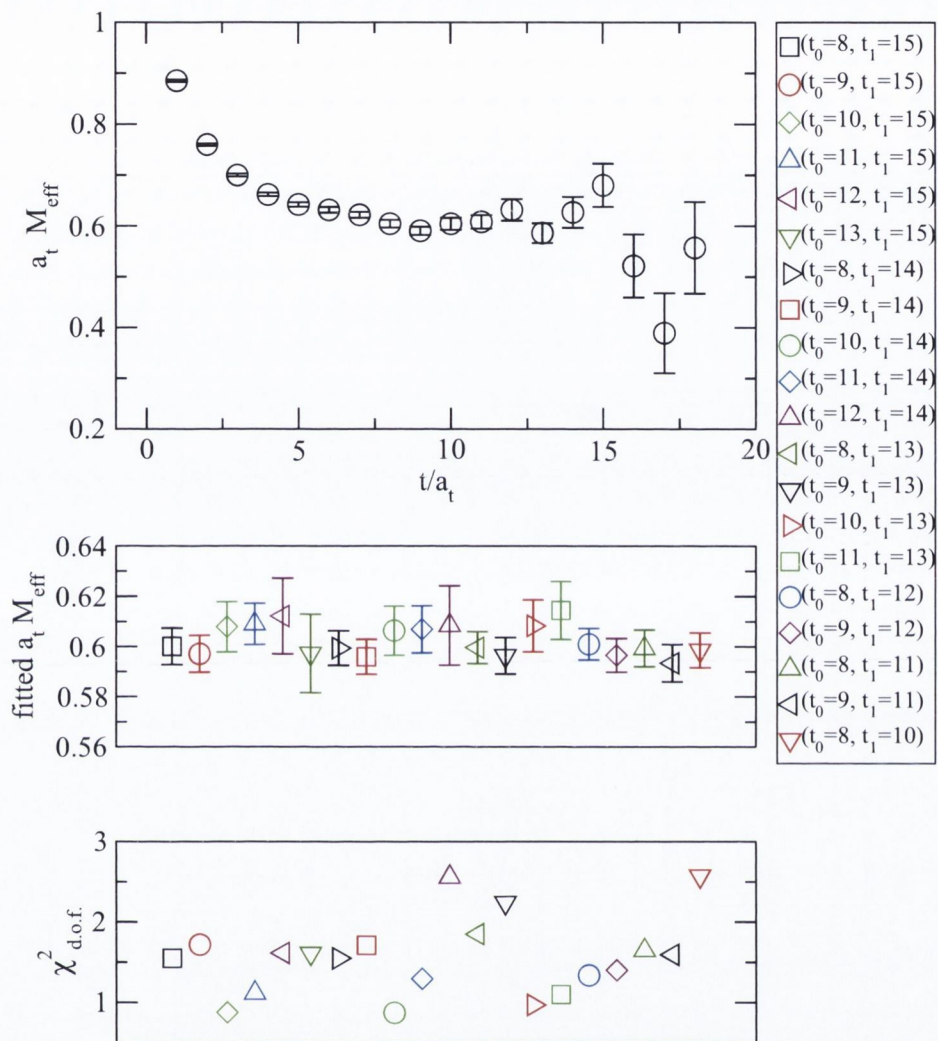Figure A-2: Irrep T_1 row 1: $L = 0$, $S = 1$, $J = 1$, $I = 0$, $P = +$.

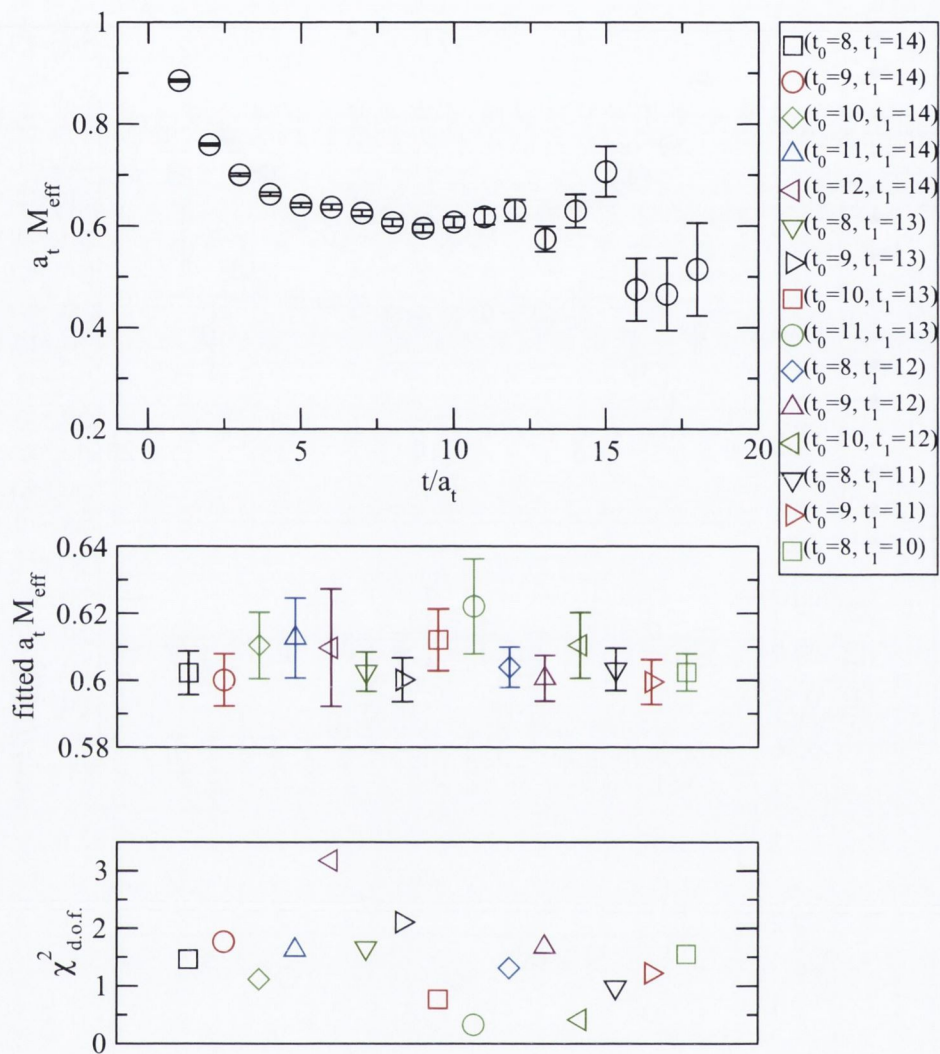Figure A-3: Irrep T_1 row 2: $L = 0$, $S = 1$, $J = 1$, $I = 0$, $P = +$.
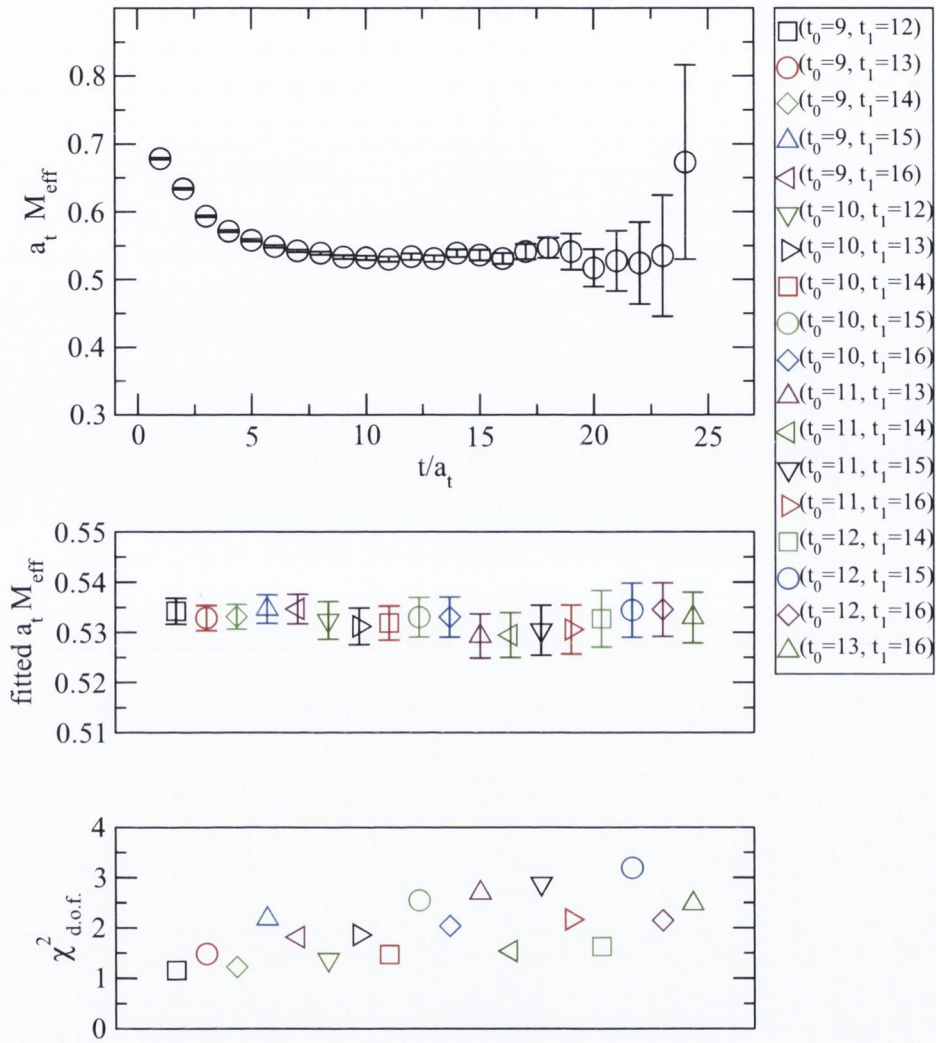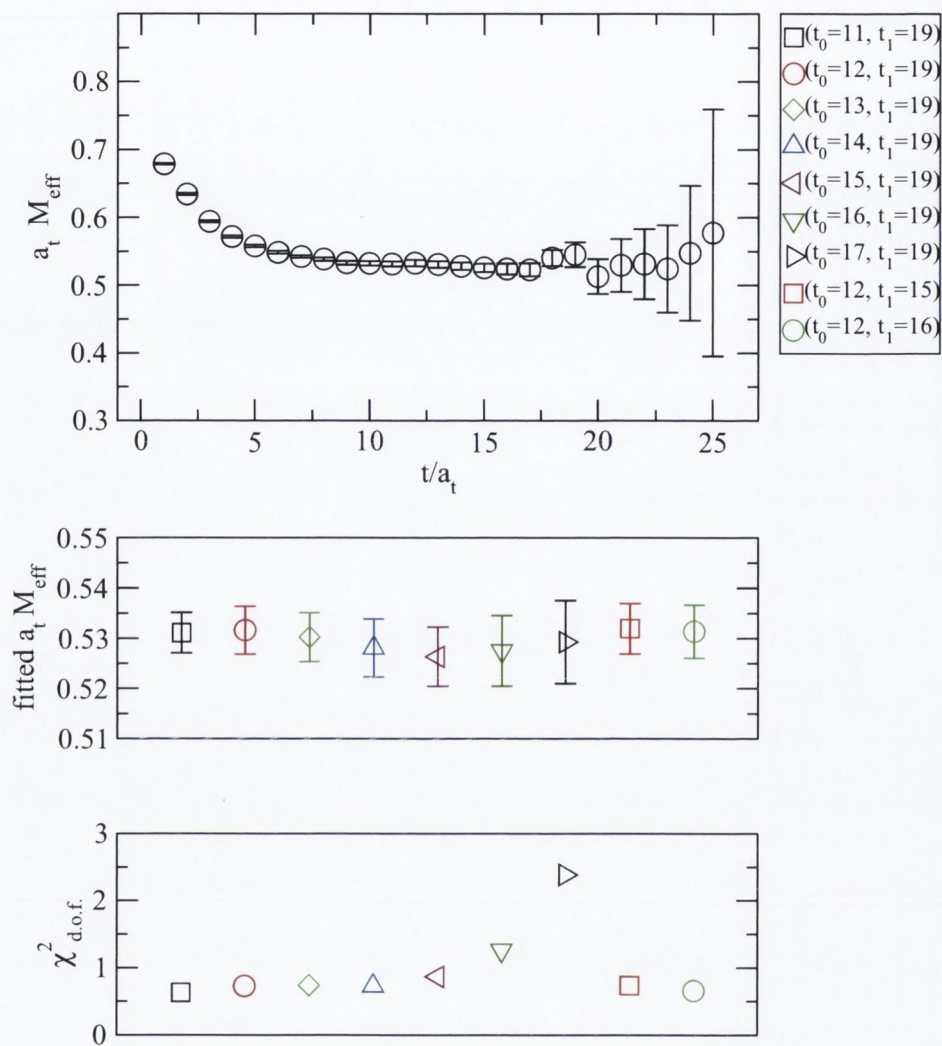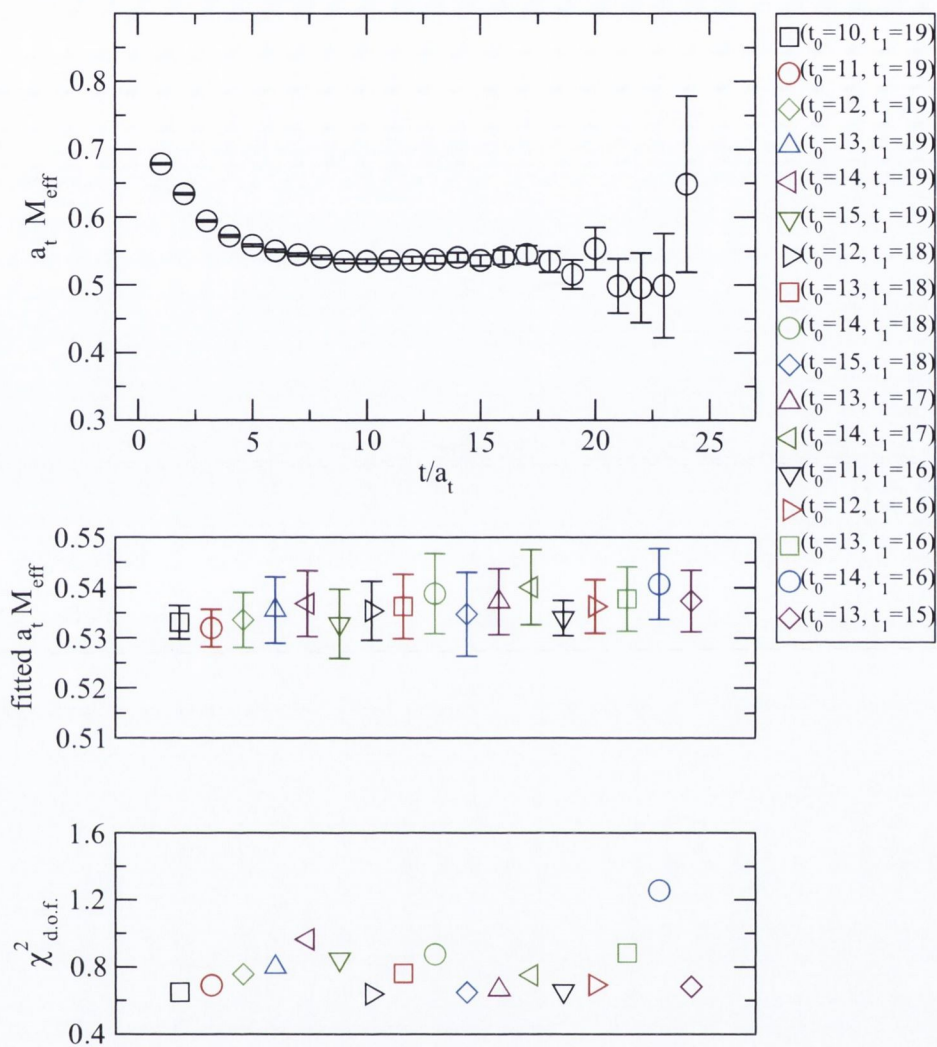
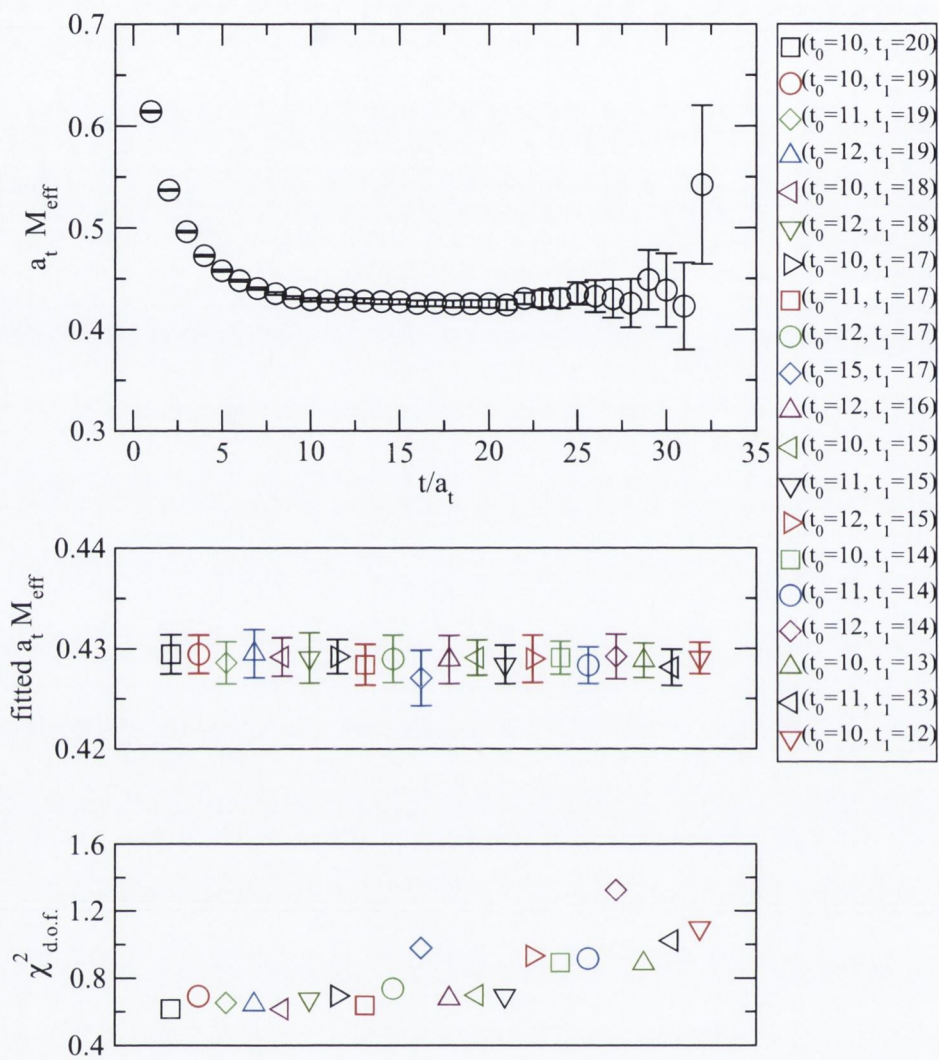Figure A-4: Irrep T_1 row 3: $L = 0$, $S = 1$, $J = 1$, $I = 0$, $P = +$.

Figure A-5: Irrep T_1 row 1: $L = 0$, $S = 1$, $J = 1$, $I = 0$, $P = -$.

Figure A-6: Irrep T_1 row 2: $L = 0$, $S = 1$, $J = 1$, $I = 0$, $P = -$.

Figure A-7: Irrep T_1 row 3: $L = 0$, $S = 1$, $J = 1$, $I = 0$, $P = -$.

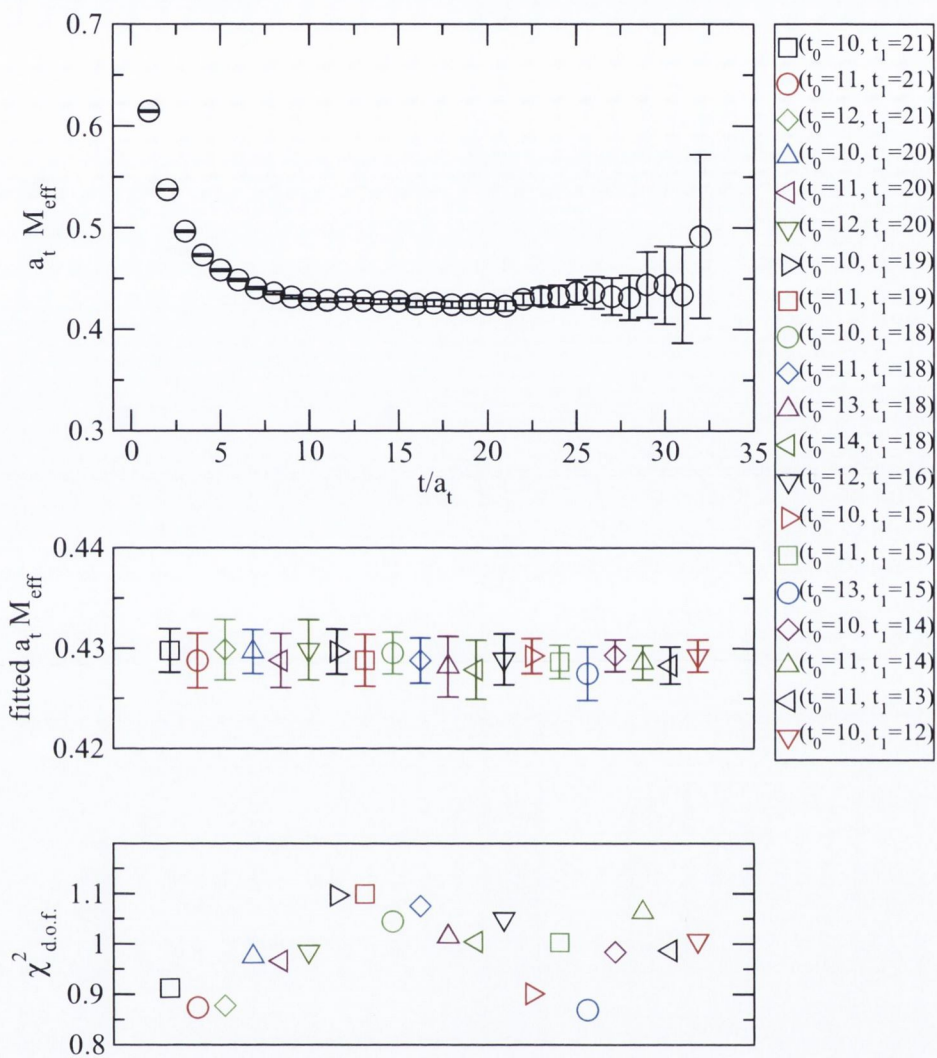Figure A-8: Irrep T_1 row 1: $L = 0$, $S = 1$, $J = 1$, $I = 1$, $P = +$.

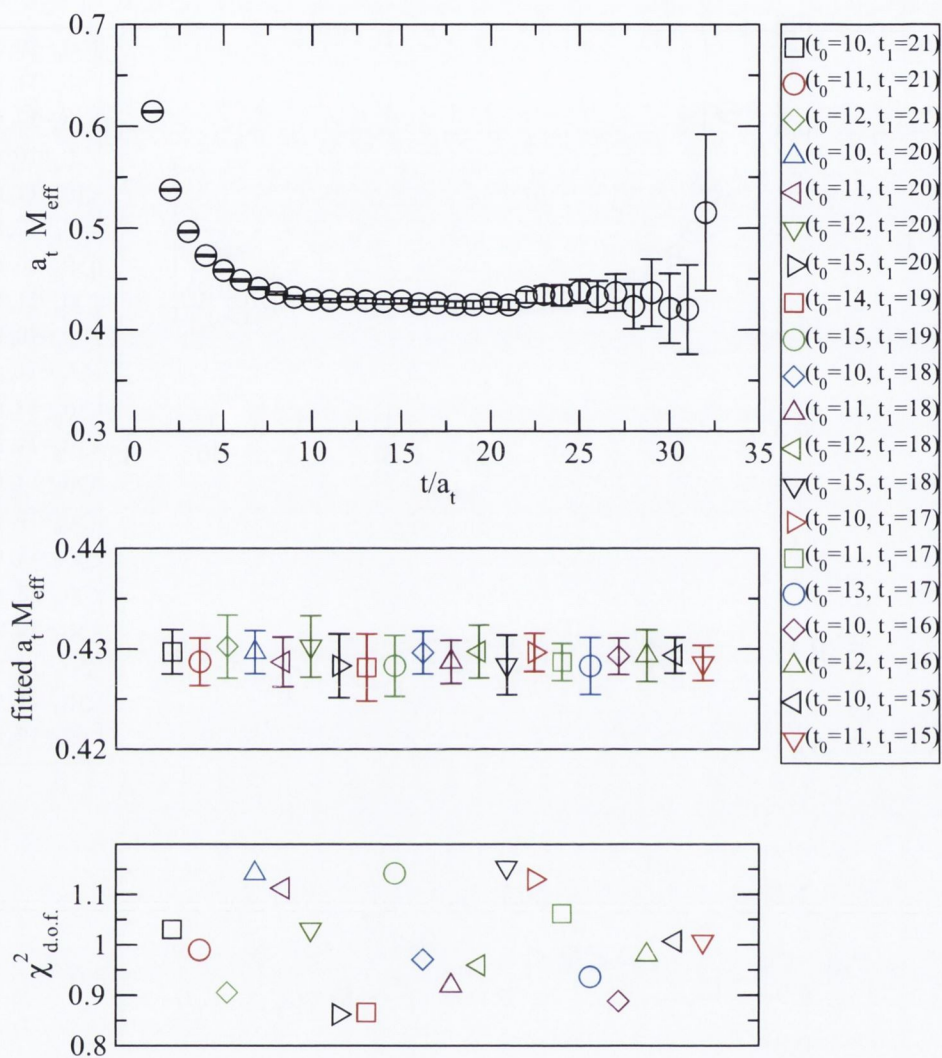Figure A-9: Irrep T_1 row 2: $L = 0$, $S = 1$, $J = 1$, $I = 1$, $P = +$.

Figure A-10: Irrep T_1 row 3: $L = 0$, $S = 1$, $J = 1$, $I = 1$, $P = +$.
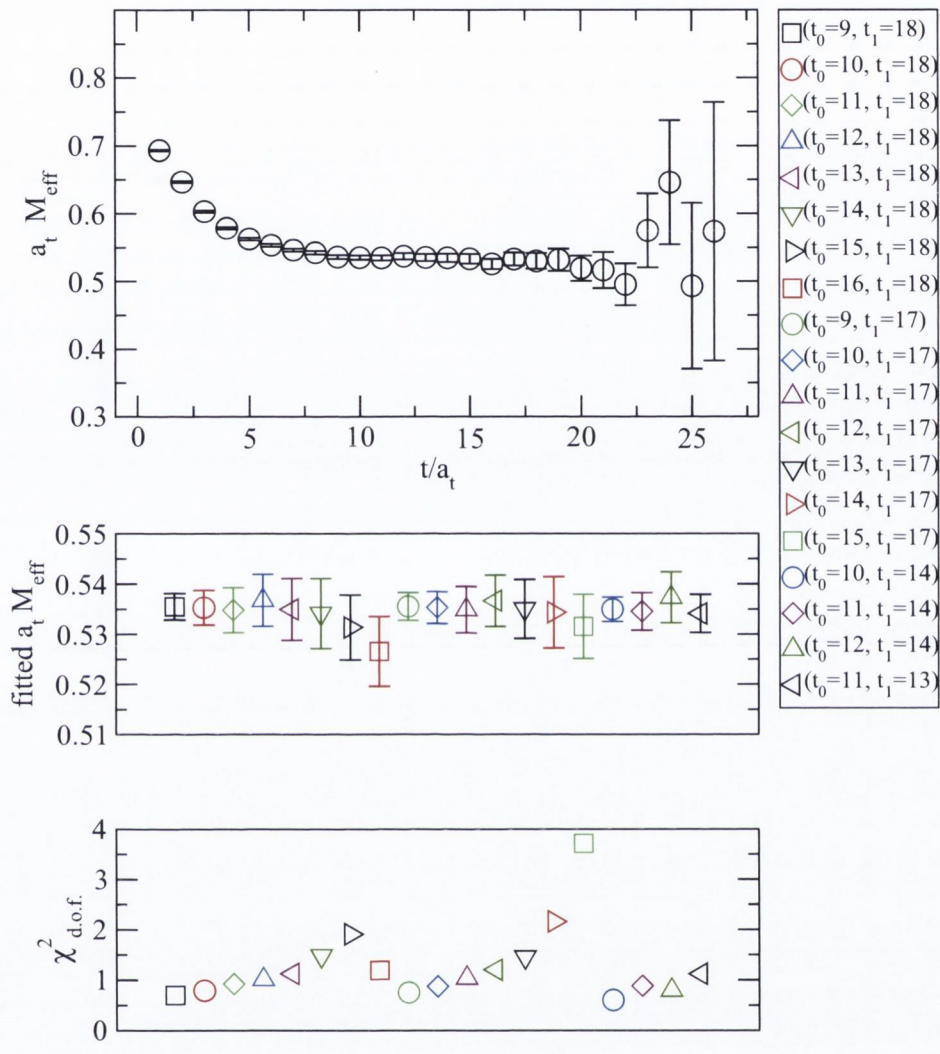
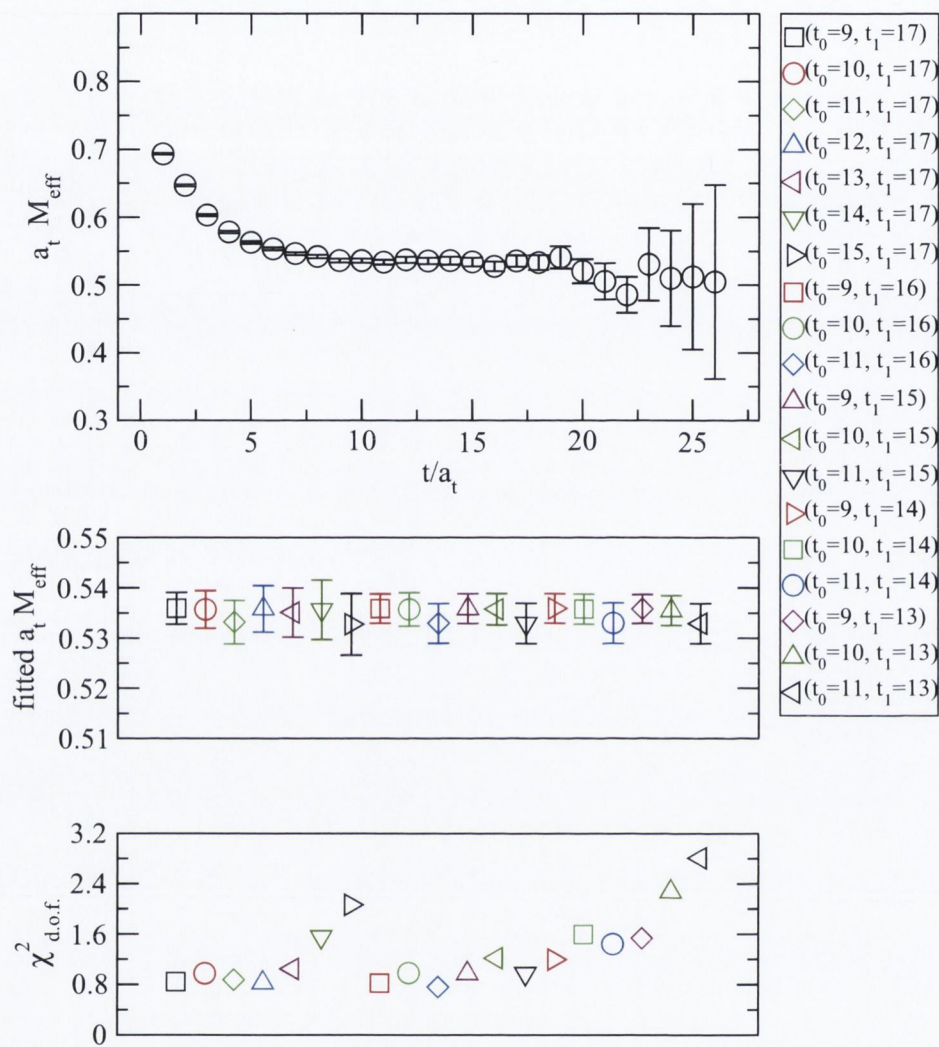Figure A-11: Irrep T_1 row 1: $L = 0$, $S = 1$, $J = 1$, $I = 1$, $P = -$.

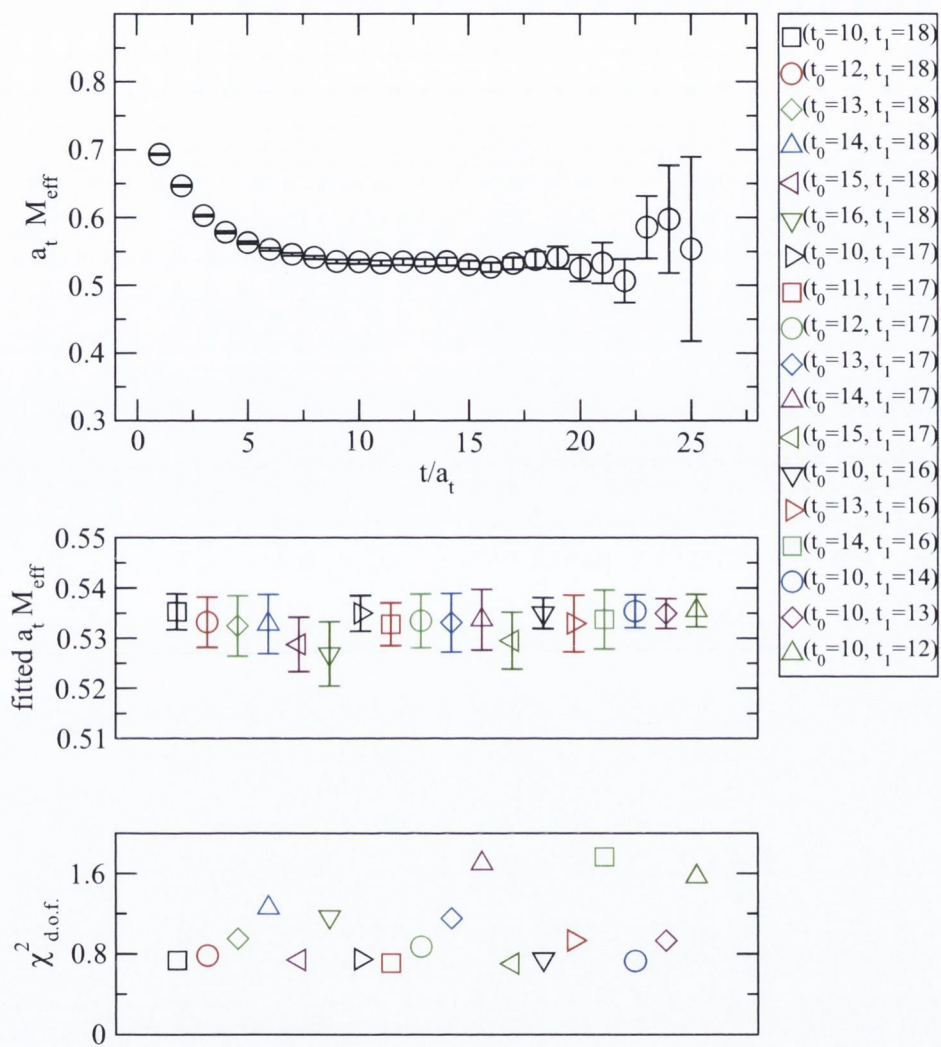Figure A-12: Irrep T_1 row 2: $L = 0$, $S = 1$, $J = 1$, $I = 1$, $P = -$.

Figure A-13: Irrep T_1 row 3: $L = 0$, $S = 1$, $J = 1$, $I = 1$, $P = -$.

Bibliography

[1] Wen-Long Lin, *Spectroscopy of Bottom Hadrons,* Chinese Journal of Physics, Vol.17, No.2. 1979.

[2] D. Buskulic et al. *Measurement of the mass of the Λ_b baryon,* Phys. Lett. B380 (1996) 442.

[3] P. Abreu et al. *Search for exclusive decays of the Λ_b baryon and measurement of its mass,* Phys. Lett. B374 (1996) 351.

[4] Particle Data Group: L Montanet et al. *Review of particle properties. Particle Data Group,* Phys. Rev. D50 (1994) 1173.

[5] D. Acosta et al. *Measurement of b hadron masses in exclusive J/Psi decays with the CDF detector,* Phys. Rev. Lett. 96:202001, hep-ex/0508022v1.

[6] CDF Collaboration: Aaltonen, et al. *First Observation of Heavy Baryons Σ_b and Σ_b^*,* Phys.Rev.Lett.99:202001,2007.

[7] CDF Collaboration: T. Aaltonen et al. *Observation of the Ω_b^- and Measurement of the Properties of the Ξ_b^-, and Ω_b^-,* Phys.Rev.D80:072003,2009.

[8] D0 Collaboration, V. Abazov et al. *Direct observation of the strange b baryon Ξ_b^-,* Phys.Rev.Lett.99:052001,2007.

[9] Randy Lewis and R. M. Woloshyn, *Bottom baryons from a dynamical lattice QCD simulation,* Phys.Rev.D79:014502,2009.

[10] S. Meinel, W. Detmold, C.J. Lin, and M. Wingate, *Bottom hadrons from lattice QCD with domain wall and NRQCD fermions,* PoS LAT2009:105, 2009.

[11] Heechang Na and Steve Gottlieb, *Charm and Bottom heavy baryon mass spectrum from lattice QCD with* $2 + 1$ *flavors*, PoS LAT2007:124,2007.

[12] Heechang Na and Steve Gottlieb, *Heavy baryon mass spectrum from lattice QCD with* $2 + 1$ *dynamical sea quark flavors*, PoS LATTICE2008:119,2008.

[13] T. Burch et al. *Excitations of single-beauty hadrons*, Phys.Rev.D79:014504,2009.

[14] W. Detmold et al. *Bottom hadron mass splittings in the static limit from 2+1 flavour lattice QCD*, Nucl.Phys.B818:17-27,2009.

[15] H. W. Lin, Cohen, Mathur and Orginos, *Bottom-Hadron Mass Splittings from Static-Quark Action on* $2 + 1$ *Flavor Lattices*, Phys.Rev.D80:054027,2009.

[16] K. G. Wilson, *Confinement of quarks*, Phys. Rev. D10, 2445 (1974).

[17] H.B. Nielson and M. Ninomiya, *Absence of Neutrinos on a Lattice. 1. Proof by Homotopy Theory*, Nucl. Phys. B185 (1981) 20.

[18] J.F. Cornwell, *Group Theory in Physics: Volume 1*.

[19] G. P. Lepage, *The Analysis of Algorithms for Lattice Field Theory*, Invited lectures given at TASI'89 Summer School, Boulder, CO, Jun 4-30, 1989. Published in Boulder ASI 1989:97-120(QCD161:T45:1989).

[20] G. P. Lepage, *Simulating heavy quarks*, Nucl. Phys. Proc. Suppl. 26 (1992) 45.

[21] J. Foley et al. *Radial and orbital excitations of static-light mesons*, Phys. Rev. D75:094503, 2007, hep-lat/0702010.

[22] R. G. Edwards, B. Joo, and H. W. Lin, *Tuning for Three-flavors of Anisotropic Clover Fermions with Stout-link Smearing*, Phys. Rev. D78:054501, 2008.

[23] K. Symanzik, *Continuum Limit and Improved Action in Lattice Theories: 1. Principles and* ϕ^4 *theory*, Nucl. Phys. B226: 187, 1983.

[24] C. Morningstar, and M. Peardon, *Efficient glueball simulation on anisotropic lattices*, Phys. Rev. D56:4043-4061, 1997. hep-lat/9704011.

[25] Huey-Wen Lin, *First results from 2+1 dynamical quark flavors on an anisotropic lattice: light-hadron spectroscopy and setting the strange-quark mass,* Phys.Rev.D79:034502,2009.

[26] M. Luscher, and P. Weisz, *On-Shell Improved Lattice Gauge Theories,* Commun. Math. Phys. 97: 59, 1985.

[27] B. Sheikholeslami, and R. Wohlert, *Improved Continuum Limit Lattice Action for QCD with Wilson Fermions,* Nucl. Phys. B259 (1985) 572.

[28] P. Chen, *Heavy Quarks on Anisotropic Lattices: The Charmonium Spectrum,* Phys. Rev. D64, 034509 (2001), hep-lat/0006019.

[29] E. Eichten B. Hill, *Renormalisation of heavy-light bilinears and f(B) for Wilson fermions,* Phys. Lett. B240, 193 1990.

[30] R. Sommer, *A New Way to Set the Energy Scale in Lattice Gauge Theories and its Application to the Static Force and α_s in SU(2) Yang–Mills Theory,* Nucl. Phys. B411:839-854, 1994, hep-lat/9310022.

[31] K. Hashimoto and T, Izubuchi, *Static $\bar{Q}$-Q Potential from $N_f = 2$ Dynamical Domain-Wall QCD,* Nucl. Phys. Proc. Suppl. 140:341-343, 2005, hep-lat/0409101.

[32] E. Eichten, K. Gottfried, T. Kinoshita, K. D. Lane, Tung-Mow Yan, *Charmonium: The Model,* Phys. Rev. D17: 3090, 1978.

[33] G.P. Lepage, and P.B. Mackenzie, *On the Viability of Lattice Perturbation Theory,* Phys. Rev. D48 (1993) 2250-2264. hep-lat/9209022.

[34] R. Horsley et al. *Perturbative determination of C_{SW} for plaquette and Symanzik gauge action and stout link clover fermions,* Phys. Rev. D78:054504, 2008, hep-lat/0807.0345.

[35] J.D. Stack, *The Heavy Quark Potential in SU(2) Lattice Gauge Theory,* Phys. Rev. D 27 (1983) 412.

[36] J. Engels, F. Karsch and T. Scheideler, *Determination of Anisotropy Coefficients for SU(3) Gauge Actions from the Integral and Matching Methods*, Nucl. Phys. B (Proc. Suppl.)63 (1998) 427, hep-lat/9905002v1.

[37] T.R. Klassen, *The Anisotropic Wilson Gauge Action*, Nucl. Phys. B533, 557 (1998), hep-lat/9803010.

[38] E. Eichten, *Heavy Quarks on the Lattice*, Nucl.Phys.Proc.Suppl. 4(1988) 170.

[39] T. Mannel, W. Roberts, and Z. Ryzak, *A Derivation of the heavy quark effective Lagrangian from QCD*, Nucl.Phys. B368:204-220, 1992.

[40] N.Neubert, *Heavy-Quark Effective Theory*, Invited talk at 20th Johns Hopkins Workshop on Current Problems in Particle Theory, 27-29 Jun 1996, hep-ph/9610385.

[41] M. Wagner, and C. Wiese, *The static-light baryon spectrum from twisted mass lattice QCD*, JHEP 1107:016,2011, hep-lat/1104.4921.

[42] J. Foley et al. *Practical all-to-all propagators for lattice QCD*, Comput. Phys. Commun. 172:145-162, 2005.

[43] C. R. Allton et al. *Gauge-Invariant Smearing and Matrix Correlators using Wilson Fermions at $\beta = 6.2$*, Phys. Rev. D47, 5128 (1993), hep-lat/9303009.

[44] M. Peardon et al. *A novel quark-field creation operator construction for hadronic physics in lattice QCD*, Phys. Rev. D80: 054506, 2009, hep-lat/0905.2160.

[45] M.E. Peskin, and D.V. Schroeder, *An Introduction to Quantum Field Theory*.

[46] J. Dudek et al. *Toward the excited meson spectrum of dynamical QCD*, Phys. Rev. D82:034508, 2010, hep-lat/1004.4930.

[47] J. Dudek et al. *Highly excited and exotic meson spectrum from dynamical lattice QCD*, Phys. Rev. Lett. 103:262001, 2009, hep-lat/0909.0200.

[48] R.C. Johnson, *Angular Momentum On A Lattice*, Phys.Lett.B114:147, 1982.

[49] C. Michael, *Adjoint Sources In Lattice Gauge Theory*, Nucl. Phys. B259 (1985) 58-76.

[50] M. Lusher, U. Wolff, *How To Calculate The Elastic Scattering Matrix In Two-Dimensional Quantum Field Theories By Numerical Simulations*, Nucl. Phys. B339 (1990) 222-252.

[51] R. L. Jaffe, *Exotica,* Talk presented at QM2004, Berkeley, CA, January 2004, and elsewhere, Phys. Rept.409:1-45, 2005, hep-ph/0409065.

[52] W.E. Caswell, and G. P. Lepage, *Effective Lagrangians for Bound State Problems in QED, QCD, and Other Field Theories*, Phys. Lett. B167 (1986) 437.

[53] T. Ishikawa et al. *2 + 1 flavor light hadron spectrum and quark masses with the $\mathcal{O}(a)$-improved Wilson-clover quark formalism*, PosLAT2006:181, 2006, hep-lat/0610050.

[54] T. Ishikawa et al. *Light quark masses from unquenched lattice QCD,* Phys. Rev. D78: 011502, 2008, hep-lat/0704.1937.

[55] D. B. Kaplan, *A Method for Simulating Chiral Fermions on the Lattice*, Phys. Lett. B288: 342-347, 1992, hep-lat/9206013.

[56] Y. Iwasaki, *Renormalization Group Analysis of Lattice Theories and Improved Lattice Action: Two-Dimensional Nonlinear O(N) Sigma Model*, Nucl. Phys. B258 (1985) 141-156.

[57] Y. Iwasaki, *Renormalization Group Analysis of Lattice Theories and Improved Lattice Action. 2. Four-dimensional Nonabelian SU(n) Gauge Model*, Univ. of Tsukuba report UTHEP-118 (1983), unpublished.

[58] C. Allton et al. *Physical Results from 2+1 Flavor Domain Wall QCD and SU(2) Chiral Perturbation Theory*, Phys. Rev. D78:114509, 2008, hep-lat/0804.0473v1.

[59] A.El-Khadra, A. Kronfeld, and P. Mackenzie, *Massive Fermions in Lattice Gauge Theory,* Phys. Rev. D55:3933-3957, 1997, hep-lat/9604004v1.

[60] C. Aubin et al. *Light hadrons with improved staggered quarks: approaching the continuum limit*, Phys. Rev. D70 (2004) 094505, hep-lat/0402030.

[61] T. Burch, and C. Hagen, *Domain decomposition improvement of quark propagator estimation*, Comput. Phys. Commun. 176(2007)137-145, hep-lat/0607029.

[62] A. Hasenfratz, and F. Knechtli, *Flavor Symmetry and the Static Potential with Hypercubic Blocking*, Phys. Rev. D64 (2001) 034504, hep-lat/0103029.

[63] M. Della Morte, S. Durr, et al. *Lattice HQET with exponentially improved statistical precision*, Phys. Lett. B581:93 2004, hep-lat/0307021.

[64] M. Della Morte, A. Shindler, and R. Sommer, *On lattice actions for static quarks*, JHEP0508:051, 2005, hep-lat/0506008.

[65] D. Ebert, R. Faustov, and V. Galkin, *Masses of excited heavy baryons in the relativistic quark-diquark picture*, Phys. Lett. B659:612-620, 2008, hep-ph/0705.2957v2.

[66] S. Capstick, and N. Isgur, *Baryons in a Relativized Quark Model with Chromodynamics*, Phys. Rev. D34 (1986) 2809.

[67] H. Garcilazo, J. Vijande, and A. Valcarce, *Faddeev study of heavy baryon spectroscopy*, J. Phys. G34: 961-976, 2007, hep-ph/0703257.

[68] L. Liu, G. Moir, M. Peardon et al. *Excited and exotic charmonium spectroscopy from lattice QCD*, JHEP 07(2012) 126, hep-ph/1204.5425v2.

[69] J. Dudek, R. Edwards, M. Peardon et al. *Toward the excited meson spectrum of dynamical QCD*, Phys. Rev. D82:034508, 2010 hep-ph/1004.4930v1.